A THEORETICAL STUDY OF CHARGED PARTICLE ENERGY LOSS, CHANNELING AND RELATED EFFECTS USING STATISTICAL AND SHELL MODEL POTENTIALS

A thesis submitted for the degree of
Doctor of Philosophy

by

V. HARI KUMAR

School of Physics
University of Hyderabad
Central University P.O.
Hyderabad - 500 046
INDIA

May 1995

C E R T I F I C A T E

This is to certify that the work contained in this thesis entitled " *A Theoretical Study Of Charged Particle Energy Loss, Channeling And Related Effects Using Statistical And Shell Model Potentials* " has been carried out by *Mr. V. Hari kumar* under my supervision for the full period prescribed under Ph.D. ordinances of the University and the same has not been submitted for the award of research degree in any University.

Place: Hyderabad — Thesis Supervisor

Date : 19-5-95 — (Prof. A. P. Pathak)

Dean

School of Physics

D E C L A R A T I O N

I hereby declare that the matter embodied in this thesis is the result of investigations carried out by me in the School of Physics, University of Hyderabad, Hyderabad - 500 046, under the supervision of Prof. A. P. Pathak.

Place: Hyderabad

Date : 19-5-95

(V. Hari kumar)

Dedicated to

Mr. K. S. Vasudevan Nair & Mrs. P. M. Vasumathy Amma

(my parents)

and

Mrs. Rema Jayaprakash

(my sister)

ACKNOWLEDGEMENTS

It is with great pleasure and deep sense of gratitude I thank **Prof. A. P. Pathak** for introducing me to the field of *Channeling.* His utmost patience and readiness to help has left me deeply indebted to him.

I also thank Prof. A. P. Pathak's family to have been very kind and affectionate towards me.

I thank Prof. N. Nath, Dr. Shyam kumar, Dr. Sanjay kumar (Kurukshetra Univerity) and Dr. D. K. Avasthi (Nuclear Science Centre, New Delhi) for their valuable guidance and encouragement in the field of ERDA experiments.

I would like to thank the Dean, School of Physics, for making all the facilities available to me.

I thank Prof. G. S. Agarwal for allowing me to use the μ - vax system.

I thank all the faculty members in school for their cooperation. The friendly cooperation extended by the non teaching staff of the school whenever I needed their help is also acknowledged.

1 am deeply indebted to my friends in the university and outside who have shared the good times and stood by me during the difficult times, for their support in more ways than one.

I gratefully acknowledge DST, UGC CSIR and IUC-DAE for the financial assistance during the tenure in which this work was carried out.

It gives me great pleasure to acknowledge the cooperation of my colleagues Mr. Rajesh Agnihotri, Mr. A. M. Siddiqui, Mr. T. Vcnugopalacharyalu and Mr. L. N. S. Prakash Goteti.

I thank Dr. K. S. Subramaniam Moosath and Dr. T. V. Madhu for their help in

difficult times.

I would like to thank Mr. Arun kumar for his valuable suggestions and kind help regarding computer related problems.

I thank Mr. Koshy and Mrs. Saramma for their role in bringing me to this esteemed institution.

I am indebted to my uncle Commdt. K. S. R. Nair, aunty Mrs. Prasanna Nair and cousins Mr. Mahesh and Mr. Maneesh for their hospitality and affection shown towards me.

I thank my sister Mrs. Rema Jayaprakash, brother-in-law Mr. Jayaprakash, father-in-law Mr. K. Narayana Moorthy, mother-in-law Mrs. Sushama Moorthy, sister-in-law Mrs. Indu Ajith and brother-in-law Mr. Ajith Prasad for their moral support and encouragement.

To reach this stage of life I have been fortunate in getting affection from my parents, whose sacrifices throughout my upbringing and in particular, during the course of the present work are commendable.

It is the time to record my gratitude and thanks to my grandfathers and grandmothers whose kind blessing made me to complete this work.

Finally, an invaluable debt to be recorded here is that of my wife Mrs. Bindu for her support, understanding, patience and affection which enabledme to carry out my work smoothly.

S Y N O P S I S

Introduction

When charged particles are incident on crystals along one of the major crystallographic direction, they penetrate larger distances in these crystals than when the particles are incident along random direction*. This effect is known as channeling [1-3]. This term visualises atomic rows and planes as guides that steer charged particles along the channels between rows and planes by means of correlated series of gentle small angle collisions [4]. The main result of these small angle collisions are to avoid all small impact parameter process like RBS, inner shell excitations etc. Basically the projectile interacts with free electron gas and some of the outer most shells of target atoms.

Channeling techniques find their applications in many frontier areas of physics, Ion beam analysis, semiconductor superlattices studies [5] crystal defect studies, backscattering analysis and ion implantation are very few among them. Using this technique one can improve the depth resolution of the ion scattering method and improve its sensitivity to light impurities [4]. Both Rutherford backscattering and channeling are simultaneously used for studying various phenomenon occuring in strained layer superlattices [5]. The channeling effect can be and has been used to locate foreign atoms in a crystal and the energy dependence of dechanneling gives information of the nature of the defects and magnitude of the dechanneling cross section is used to find the amount of damage

A thorough knowledge of Charge density and Interatomic potential is basis for a better understanding of any phenomena in physics in general and in the field of channeling and its applications in particular [2,6]. Most of the interatomic potentials (Thomas-Fermi type) and corresponding continuum potentials [2,6] used in the channeling studies are of statistical nature. We have tried to relax the statistical nature inherent in all the Thomas-Fermi type potentials and obtain a suitable potential which takes into account

of the atomic shell structure of th© atom. We have developed a shell charged density [7], and using the Poisson equation, corresponding shell interatomic potential was calculated. The planar and axial cases of the potential are also derived and tested in its compatibility in various fields of Channeling like Electronic Stopping power in various energy regions [7], Z_1 oscillations in Electronic Stopping power [8], Channeling Radiation studies [9], and Strained Layer Superlattices [10]. A comparison of the results with experimental results and earlier theoretical calculations shows good agreement. Naturally this potential gives a better physical picture of the interactions, because of the shell structure inherent in the calculations which carry the signature of the particular atom and its structure involved in the interaction.

CONCEPTS USED IN THE THESIS

i. Channeling

The influence of the crystal lattice on the trajectories of ions penetrating into the crystal is known as channeling [4], as explained in the introduction.

When a charged particle moves along certain major crystallographic directions under specific conditions it may not be able to feel the interaction due to individual atoms sitting at various lattice sites but rather experiences a collective effect of all the atoms sitting along a particular axial or planar directions. The basic conditions for channeling to occur as proposed by Lindhard [1,2] are stated and discussed below. The particle velocity component parallel to the axial or planar direction is such that the time of flight to cross one lattice spacing is less than the collision time with any individual target atom [2]. This implies that before the particle can experience the field of one atom, it is already in the field of the next atom along the string or plane and it will see only continuum potentials instead of individual atom field. Mathematically this

condition Cor continuum approximation can be written as

$$\frac{r_{min}}{v \sin \psi} \rangle \frac{d}{v \cos \psi} \quad (1)$$

for small incident angle ψ, equation (1) gives $r_{min}) d\psi$, where ψ is the angle of incidence of a moving particle with velocity v, r_{min} is the minimum distance of approach to the string and d is the interatomic spacing along the axis. The continuum axial potential is derived by finding the average of the interatomic potential along the string (axial) and is given by

$$U(r) = \int_{-\infty}^{\infty} \frac{dz}{d} V(\sqrt{z^2 + r^2}) \quad (2)$$

where z is the longitudinal direction, r is the distance from the string and $V(R)$ is the interatomic potential. The continuum planar potential is obtained by finding the average of the interatomic potential over the particular plane and is given by

$$V(y) = 2\pi N d_p \int r V(\sqrt{r^2 + y^2}) dr \quad (3)$$

where N is the bulk density of atoms in the crystal, d_p is the interplanar spacing and y is the distance measured from the plane [2].

ii. Z_1 Oscillations in Electronic Stopping Power

The electronic stopping powers of solids for low-velocity channeled heavy ions exhibit an oscillatory dependence on the charge Z_1 of the incident channeled ions. This is called Z_1 oscillations [11,12]. This occurs in random case also. But the magnitude of oscillations is diminished and the maximum to minimum ratio of electronic stopping power is lower in random case. The maxima of the electronic stopping power occurs around $Z_1 = 6, 20, 38$ and minima around $Z_1 = 10, 29$ and 47 [2,8]. In this low velocity region ($v < v_o Z_1^{2/3}$, where v_o is Bohr velocity), the nuclear stopping power is small compared with electronic

•topping power and it further suppressed because close collisions of incident ions with target atoms are completely avoided in the channeling.

According to Briggs and Pathak [12], the energy low is attributed to the scattering of target electrons in the potential field of the moving projectile and most of the stopping power contribution comes from a transfer of momentum between the electrons of the ion and those of the target atom because of overlap of electronic clouds as the ion passes. This transfer of momentum can be considered to be affected by the elastic scattering of the target electrons through the charge cloud of the moving ion.

The mean energy lost per unit path length by an ion with velocity v has been shown to be

$$-\frac{dE}{dx} = nmv^2 Q_d \tag{4}$$

where n is the density of electrons m is the electron mass and Q_d is the momentum transfer cross section and is given by [13]

$$Q_d = \frac{4\pi}{k^2}\sum_l (l+1)\sin^2(\eta_l - \eta_{l+1})$$

where $\hbar k$ is the electron momentum in the centre of mass frame. The phase shift η_l of the the /-th partial wave of the electron wave function can be calculated by numerically solving the radial part of Schrodinger equation

$$\frac{d^2G_l}{dr^2} + [k^2 + U(r) - \frac{l(l+1)}{r^2}G_l] = 0 \tag{6}$$

where G_l is the radial wavefunction corresponding to the l-th partial wave and k is the electron wavenumber corresponding to the projectile velocity given by $k = \sqrt{2mE/\hbar^2}$ for an energy E and $U(r) = (2m/\hbar^2)V(r)$ where $V(r)$ represents interaction between target electron and projectile.

Since the potential between the electron and projectile $V(r)$ varies more rapidly than $1/r$, the asymptotic form of the radial wave function can be written as

$$G_l(r) \sim \sin(kr - \frac{l\pi}{2} + \eta_l) \tag{7}$$

In the absence of an atomic field, eq.(6) gives the solution whose asymptotic form is

$$G_l(r) \sim (kr - \frac{1}{2}l\pi) \ . \tag{8}$$

The magnitude of the phase shift η_l is determined by the competition between the attractive potential $V(r)$ and the repulsive centrifugal potential $l(l+1)/r^2$ and is computed by finding the shift in the nodes of solution (7) with respect to the corresponding node of the solution (8) for large r.

iti. Channeling Radiation

When a relativistically fast charged particle is channeled in a crystal, it undergoes periodic motion due to steering by major crystallographic axes or planes, this back and forth accelerated transverse motion of charged particles yields observable electromagnetic radiation. This is called channeling radiation [9].

The longitudinal relativistic motion results in Lorentz contraction along the axes or planes and hence the strength of the continuum potential is enhanced by & factor γ (= $1/\sqrt{1-(v^2/c^2)}$). This happens in the rest frame of particle. For the observation of electromagnetic radiation in the laboratory frame, the emitted radiation frequency is Doppler-shifted in the forward direction by a factor 2γ, so overall enhancement in the frequency, of the order of $2\gamma^2$ results for forward emission. The observed frequency is given *by* $\omega - 2r^2\omega_o$, where ω_o is the original frequency due to spontaneous transition among the discrete eigenstates for transverse motion supported by the continuum planar or axial potential of the crystal.

iv. Strained *Layer* **Superlattices** [SLS]

Strained layer superlattices (SLS) consist of alternating layer structures with a **slight** lattice mismatch, so that for sufficiently thin layers, no misfit defects or dislocations are generated [5]. The resonance phenomena like Catastrophic Dechanneling Resonance (CDR) and Resonance Channeling have proved to be very **useful** for probing important properties of SLS. CDR occurs when the path length per layer (s) of a SLS matches with **halfwavelength** (A/2) of planar channeled ion beam, i.e., A/2 = s. The complimentary phenomena of resonance channeling occurs when A = a. Dechanneling is maximum in CDR case because a large fraction of planar channeled particles are simultaneously focussed on to channel wall under resonance conditions.

The equation of motion for a particle in a SLS is given by

$$\frac{d^2x}{dz^2} + \frac{1}{2E_z}\frac{d}{dx}U(x) = \sum_{j=1}^{n}(-1)^j \Delta\psi\delta(z - js)$$

where x and z are the transverse and longitudinal displacement of channeled particle respectively and x is measured **from** the midpoint between the planes, E_z is the longitudinal energy, $\Delta\psi$ is the angular shift at each interface, δ denotes Dirac delta function, n is the total number of layers and $U(x)$ is the averaged continuum planar potential given by

$$U(x) = Y(l - x) + Y(l + x) - 2Y(l) \qquad (10)$$

where $Y(x)$ is the planar potential and $l = d_p/2$. The tilt is represented by Dirac delta function on the **R.H.S.** of the equation (9). This tilt is a result of elastic accommodation of strain and is a direct measurement of strain in SLS [5].

v. The Potentials used in the thesis

[a)] Moliere potential.

Moliere interatomic potential is given as [2]

$$V_M(R) = \frac{Z_1 Z_2 e^2}{R} \sum_{i=1}^{3} a_i \exp(-b_i R) \tag{11}$$

with a_1=0.35, a_2=0.55, a_3=0.1, b_1=0.3/a, b_2=1.2/a, b_3=6/a.

where Z_1 and Z_2 are the atomic numbers of projectile and target atoms respectively, a is the Thomas Fermi screening radius and is given by

$$a = \frac{0.8853 a_o}{(Z_1^{2/3} + Z_2^{2/3})^{1/2}} = 0.8853 a_B \tag{12}$$

where $a_B = a_o/(Z_1^{2/3} + Z_2^{2/3})^{1/2}$ is the Bohr screening parameter, and a_o is the Bohr radius.

The Moliere axial potential is derived using continuum approximation and is given by

$$U_M(r) = \frac{2 Z_1 Z_2 e^2}{d} \sum_{i=1}^{3} a_i K_o(b_i r) \tag{13}$$

where K_o is the modified Bessel function of order zero. The Moliere planar potential is derived using the equation (3) and is given by

$$Y_M(y) = 2\pi N d_p Z_1 Z_2 e^2 \sum_{i=1}^{3} a_i \frac{e^{-b_i y}}{b_i} \tag{14}$$

[b)] Lindhard potential.

Lindhard interatomic potential is given as [2]

$$V_L(R) = \frac{Z_1 Z_2 e^2}{R} \left(1 - \frac{R}{\sqrt{R^2 + c^2 a^2}}\right) \tag{15}$$

with $c = \sqrt{3}$, where c is the Lindhard constant. Lindhard axial potential is given as

$$U_L(r) = \frac{2 Z_1 Z_2 e^2}{d} \; ln \; \left(1 + \frac{c^2 a^2}{r^2}\right)^{1/2} \tag{16}$$

and Lindhard planar potential is given by

$$Y_L(y) = 2\pi N d_p Z_1 Z_2 e^2 [\sqrt{y^2 + c^2 a^2} - y] \tag{17}$$

[c)] Biersack's universal potential.

Biersack's universal interatomic potential is given by [14]

$$V_U(R) = \frac{Z_1 Z_2 e^2}{R} \sum_{i=1}^{4} p_i \exp(-q_i R) \tag{18}$$

with $p_1 = 0.1818, p_2 = 0.5099, p_3 = 0.2802, p_4 = 0.02817$, $q_1 = 3.2/a, q_2 = 0.9423/a, q_3 = 0.4029/a, q_4 = 0.2016/a$.

Biersack's universal axial potential is given by [7]

$$V_U(r) = \frac{2Z_1 Z_2 e^2}{d} \sum_{i=1}^{4} p_i K_o(q_i r) \tag{19}$$

Biersack's universal planar potential is given by [7]

$$Y_U(y) = 2\pi N d_p Z_1 Z_2 e^2 \sum_{i=1}^{4} p_i \frac{e^{-q_i y}}{q_i} \tag{20}$$

[d)] Bohr Potential.

Bohr interatomic potential is given by [2]

$$V_B(R) = \frac{Z_1 Z_2 e^2}{R} e^{-R/a_B} \tag{21}$$

Bohr axial potential is given as

$$U_B(r) = \frac{2Z_1 Z_2 e^2}{d} K_o(r/a_B) \tag{22}$$

Bohr planar potential is given by

$$Y_B(y) = 2\pi N d_p Z_1 Z_2 e^2 e^{-(y/a_B)}/a_B \tag{23}$$

All the above mentioned potentials are based on the Thomas Fermi statistical model where screening due to electrons is included statistically.

vi. Shell Charge Density

Using one-term slater orbitals with optimized exponent given by Clementi and Raimondi [15], the spherically symmetric electron density due to one atom at a distance R from the centre is given by [7]

$$\rho(R) = \frac{1}{4\pi}\sum_j \frac{\omega_j}{(2n_j)\,!}(2\xi_j)^{2n_j+1}R^{2n_j-2}e^{-2\xi_j R} \tag{24}$$

where ξ_j is the optimised orbital exponent, ω_j is the occupation number of the j-th shell, and n_j is the principal quantum number.

The axial electron charge density at a distance r from the string is calculated using continuum approximation and given by [7]

$$\rho_A(r) = \frac{1}{\pi d}\sum_j \frac{\omega}{(2nj)!}\sum_{m=o}^{n_j-1} \frac{2^{2m}(2(n_j-m))!(n_j-1)!(\xi_j)^{n_j+m+2}r^{n_j+m}K_{n_j-m}(2\xi_j r)}{(n_j-m-\frac{1}{2})(n_j-m)(m)!((n_j-m-1)!\,)^2} \tag{25}$$

The planar electron charge density at a distance y from a single plane is calculated using continuum approximation and is given by [7]

$$\rho_P(y) = \frac{N dp}{2}\frac{(2\xi_j)^{2n_j}}{2n_j}\omega_j \exp(-2\xi_j y)\sum_{k=0}^{2n_j-1}\frac{y^{2n_j-k-1}}{(2\xi_j)^k(2n_j-k-1)!} \tag{26}$$

vii. Shell Interatomic Potential and Continuum Potentials.

The shell interatomic potential is calculated from shell charge density. Using Poisson equation [7]

$$\nabla^2 V = -\,4\pi\rho \tag{27}$$

and we get after some detailed calculations involving integration of the above Poisson equation using $\rho(r)$ from equation (24)

$$V_S(R) = \frac{Z_1 e^2}{R}\sum_j \frac{\omega_j}{2n_j}e^{-2\xi_j R}\sum_{k=1}^{2n_j}\frac{k}{(2n_j-k)!}(2\xi_j R)^{2n_j-k} \tag{28}$$

The corresponding axial and planar potentials are derived using continuum approximation and is given below.

The shell axial potential is given by [7]

$$U_S(r) = \frac{2Z_1 e^2}{d}\sum_j \frac{\omega_j}{2n_j}\sum_{k=1}^{2n_j}\frac{k}{(2n_j-k)!}(2\xi_j r)^{2n_j-k}\left(\frac{d^{2n_j-k}}{d(2\xi_j r)^{2n_j-k}}K_o(2\xi_j r)\right) \tag{29}$$

The shell planar potential is given by [7,9].

$$Y_S(y) = 2\pi N dp Z_1 e^2 \sum_j \frac{\omega_j}{2n_j} \sum_{k=1}^{2n_j} k(2\xi_j)^{2n_j-k} \sum_{m=o}^{2n_j-k} e^{-2\xi_j y} \frac{y^m}{m!(2\xi_j)^{2n_j-k-m+1}} \qquad (30)$$

The thesis includes eight chapters. The chapters are as follows.

1. Introduction
2. Electronic Stopping Power (Random Case)
3. The Shell Model Charge Densities and Potentials
4. Electronic Stopping Power (Channeling Case)
5. Z_1 oscillations
6. Strained Layer Superlattices
7. Channeling Radiation
8. Concluding Remarks

A brief description of above mentioned chapters are given below.

Chapter I: Introduction

Channeling phenomenon is analysed on the basis of Lindhard continuum approximation. Some of its important applications in the field of material science are outlined. The statistical type potentials which are frequently used in the thesis are also discussed.

Chapter II: Electronic Stopping Power (Random Case).

A brief outline of the experimental setup of the electronic stopping power measurement carried out at the 15 MV pelletron facility at the Nuclear Science Centre, New Delhi, India are given here. Then the experimental results are compared and discussed with the results obtained using existing theoretical models like LSS, Bethe theory etc.

Chapter III: The Shell Model Charge Densities and Potentials

Motivation to study channeling theory using shell model charge densities and potentials are given in the first section of the chapter.

Then shell model charge density and corresponding axial and planar charge densities were compared with other statistical type potentials. The shell interatomic potential is then derived from shell charge density using Poisson equation. Corresponding axial and planar potentials are also derived using continuum approximation and compared with Moliere, Lindhard, Biersack's Universal and Bohr potentials.

Chapter IV: Electronic Stopping Power (Channeling Case)

Theory of stopping power for both high energy and low energy regions are outlined. The electronic stopping power of Silicon for He ions (MeV regions) and protons (keV region) are calculated using shell model charge density. The position dependence of the stopping power of 160 MeV alpha particles channeled along the < 110 > axis in silicon is also calculated. The results are compared with other theoretical and experimental results.

Chapter V: Z_1 oscillations.

Z_1 oscillations in the electronic stopping powers of elements are discussed on the basis of Briggs-Pathak theory. The shell model charge density is used to calculate the stopping powers of silicon and tungsten for ions ranging from $Z_1 = 6$ to $Z_1 — 35$. The results are compared with experimental results also.

Chapter VI: Strained Layer Superlattices (SLS)

Study of strained layer superlattices using shell model potentials are made. The results are compared with experimental results and the results obtained using Moliere and

Biersack's universal potentials.

Chapter VII: Channeling Radiation

The characteristics of the radiation emitted from relativistic positrons and electrons channeled along the < 110 > plane of silicon crystal is calculated using shell model planar potential and compared with experimental results. The effects of dislocations and defects on channeling radiations are also calculated using shell model potentials.

Chapter VIII Concluding Remarks

This chapter contains a summary of work, concluding remarks and comments on possible future work.

Thesis Summary

The shell model charge densities and corresponding shell model potentials axe developed. Based on these models, calculations are made in various fields of channeling like electronic stopping power, channeling radiation, strained layer superlattices etc. The results are compared with other theoretical models and experimental results (if any).

REFERENCES

1. J. Lindhard, K. Dan Vidensk Selsk, Mat. Fys. Medd. 54, No.14 (1965)

2. A.P. Pathak, Radiat. Eff. 61, 1 (1982).

3. D.V. Morgan(ed), Channeling,Theory,Observations and Applications, John Wiley, New York, (1972).

4. Leonard C. Feldman, James W. Mayer, Fundamentals of Surface and Thin Film Analysis North Holland, Elsevier Science Publishing Co., Inc., New York, (1986).

5. J.A. Ellison, S.T. Picraux, W.R. Allen and W.K. Chu, Phys. Rev. B37, 7290 (1988).

6. I.M. Torrens, Interatomic Potentials, Academic Press, New York (1972).

7. V. Hari Kumar and A.P. Pathak, Phys. Stat. Sol(b), 177, 269 (1993).

8. V. Hari Kumar and A.P. Pathak, J. Phys. C. 5, 3163 (1993).

9. V. Hari Kumar and A.P. Pathak, Phys. Stat. Sol(b), 182, 51 (1994).

10. V. Hari Kumar and A.P. Pathak, Proc. DAE Solid State Phys. Symp. Jaipur (India) , Vol. 37C, p. 185, (1994).

11. A.P. Pathak, Phys. Rev. B22, 96 (1980).

12. J.S. Briggs and A.P. Pathak, J. Phys. C 6, L153 (1973).

13. H.S.W. Massey and E.M.S. Burhop, Electronic and Ionic Impact Phenomena, Vol. 1, Oxford, Clarendon (1969).

14. D.J. O'Conner and J.P. Biersack, Nuclear, Instrum and Methods, B15, 14 (1986).

15. E. Clementi and D.L. Raimondi, J. Chem. Phys. 38, 2686 (1963).

Table of Contents

Chapter 1

INTRODUCTION

1.1 HISTORICAL EVOLUTION OF CHANNELING CONCEPT

During the first decades of this century, *x - ray diffraction experiments* clearly established the existence of crystal lattices and the *wave nature* of *x - rays.* Prior to the postulation of *Bragg law, W. H.* and *W. L. Bragg* tried to explain the *Laue pattern* as the scattered photons passing out of the crystals through open channels existing in crystals [1]. They carried out experiments in which the crystal was rotated through an angle and expected the *Laue pattern* also to rotate through the same angle. Contrary to the expectation the *Laue pattern* rotated twice the angle and the rest is history .... If a particle should pass through these crystals, two essential conditions should be satisfied by the them. [2] (i) It should find an open space between the rows of atoms (this was realised by *Braggs).* (ii) There must be a force acting which steers the particle towards the middle of the channel. These two ideas were realised by *Stark* in 1912 and he proposed an experiment with protons which bore a striking resemblance to a series of experiments performed much later in *sixties* which eventually lead to the discovery of *Channeling.* These experiments were mainly *Range measurements* [5,6] and *Sputtering* experiments [7,8]. *Sputtering experiments* showed that *Sputtering ratio* for ions bombarding a single crystal depends on the crystal orientation [7], directional dependence of the saturation value of collected ions and the *Sputtering yield* for *Copper* crystal bombarded with *Krypton* ions. *Range*

experiments **reported** [5,6] anomalously long ranges for heavy ion stopping in polycrystalline *Aluminium* and *Tungsten.* In 1963 *Robinson* and *Oen* prompted by the definitive indications of directional effects, performed computer simulation of slowing down of 1 - 10 keV *Cu* atoms in various crystals and found that the ions with initial velocities lying close to principal axial directions penetrate to abnormally large distances in the crystal [9]. This phenomenon was named as *Channeling* and was further confirmed by the experimental work with monocrystalline targets [10,11]. A considerable amount of work have been done in this field during last three decades and the areas of its applications are also widening, keeping its pace with scientific progress. The advances in the research field of Channeling theories, experiments and applications have been compiled frequently and periodically and published in several review articles and books [2,12-19].

The Channeling phenomenon is understood on the basis of *Lindhard's Continuum approximation* theory and discussed in section 1.2. The various applications of Channeling phenomena is described in section 1.3 and in the last section the outline of the chapter is framed out.

1.2 CONTINUUM MODEL

As mentioned in the previous section, when charged particles are incident on crystals along one of the major crystallographic directions,or planes they penetrate larger distances in these crystals than when they are incident along random directions. This effect is known as *Channeling* [14-16] and in short it is the influence of the crystal lattice on the trajectories of ions penetrating into the crystal. This term visualizes atomic rows and planes as guides that steer charged particles along the channels between rows and planes by means of correlated series of gentle small angle collisions [20] (Fig. 1.1). The main result of these small angle collisions are to avoid all small impact parameter processes like

RBS, inner shell excitations etc. Basically the projectile interacts with free electron gas and some of the outer most shells of target atoms. These charged particles moving along major crystallographic directions under channeling conditions are not able to feel the interaction due to individual atoms sitting at various lattice sites hut rather experience a. collective effect of all the atoms sitting along that particular axial or planar directions. The basic conditions for channeling to occur as proposed by Lindhard [21] are stated and discussed below. The particle velocity component parallel to the axial or planar direction is such that the time of flight to cross one lattice spacing is less than the collision time with any individual target atom [16,21]. This implies that before the particle can experience the potential field of one atom, it is already in the potential field of the next, atom along the string or plane and it will see only continuum potentials instead of individual atom field. Mathematically this condition for continuum approximation can be written as

$$\frac{r_{min}}{v \sin \psi} > \frac{d}{v \cos \psi}$$

which for very small ψ reduces to

$$r_{min} > d\,\psi \qquad (1.1)$$

where ψ is the angle of incidence of the moving particle with velocity v, r_{min} is the minimum distance of approach to the string and d is the interatomic spacing along the axis (Fig. 1.2). Since the steering of the channeled particle involves collisions with many atoms , one may consider in a continuum model that the nuclear charge of the atoms in a *row (plant)* is uniformly averaged along the *row (plane)* [20]. The continuum axial potential is given by [16]

$$U(r) = \int_{-\infty}^{\infty} \frac{dz}{d}\, V(\sqrt{z^2 + r^2}) \qquad (1.2)$$

where z is the longitudinal direction, r is the distance from the string and $V(R)$ is the interatomic potential. The continuum planar potential is derived using the equation given by [16]

$$Y(y) = N\, d_p \int_0^\infty V(\sqrt{r^2 + y^2})\; 2\,\pi\, r\, dr \tag{1.3}$$

where N is the bulk density of atoms in the crystal, d_p is the interplanar spacing and y is the distance measured from the plane . Inorder to elucidate the basic properties of channeling phenomenon, We introduce an interatomic potential proposed by *Lindhard.* (various other interatomic potentials and corresponding continuum potentials are dealt in detail in *chapter 3).* The Lindhard interatomic potential is given by

$$V(R) = Z_1 Z_2\, e^2 \left(\frac{1}{R} - \frac{1}{\sqrt{R^2 + C^2 a_T^2}} \right) \tag{1.4}$$

Where $C = \sqrt{3}$ is the Lindhard constant, Z_1 and Z_2 are the charge numbers of projectile and target atoms respectively, e is the electronic charge and a_T is the *Thomas-Fermi screening distance* given by

$$a_T = \frac{0.8853\; a_o}{\sqrt{Z_1^{2/3} + Z_2^{2/3}}} \tag{1.5}$$

where a_o is the *Bohr radius.* Using *continuum approximation* (equation (1.2)), the axial potential can be written as

$$U_L(r) = \frac{Z_1\, Z_2\, e^2}{d} \ln \left[\left(\frac{C\, a_T}{r} \right)^2 + 1 \right] \tag{1.6}$$

where d is the average distance between two atoms in the rows. The critical angle ψ_c above this angle of incidence, the *continuum approximation* (equation (1.1)) becomes invalid and is calculated using conservation of energy equation. The total energy E of a particle inside the crystal is [16,20]

$$E = \frac{p_{\|}^2}{2\,M} + \frac{p_{\perp}^2}{2\,M} + U(r) \tag{1.7}$$

where M is the mass of the particle, $p\backslash\backslash$ ($= p \cos\psi$) and $p\pm$ ($= p \sin\psi$) are the parallel and perpendicular components of the momentum with respect to the axial direction. The first term and last two terms of the equation (1.7) are equal to the Longitudinal and Transverse energies respectively. For very small incident angles the transverse energy $E\pm$ can be written as

$$\begin{aligned} E_{\perp} &= \frac{p^2\,\psi^2}{2\,M} + U(r) \\ &= E\,\psi^2 + U(r) \end{aligned} \tag{1.8}$$

The first and second terms of the equation (1.8) correspond to kinetic energy and potential energy of the projectile (particle) respectively. The total and transverse energies are conserved.

The critical angle is determined by equating the transverse energy at the turning point $U(r_{min})$ to the transverse energy at the midpoint $E\psi_c^2$. For high energy particles r_{min} is considerably small and can be neglected in the equation (1.6) and the particle incident with an angle $\psi < \psi_1$ will be channeled and is given by

$$\psi < \psi_1 = \sqrt{\frac{2\,Z_1\,Z_2\,e^2}{d\,E}} \tag{1.9}$$

For low energy incident particles, one should use the full expression of the equation (1.6) and the particles will be channeled with an incident angle less than ψ_2 and is given by

$$\psi < \psi_2 = \sqrt{\frac{C\,a_T\,\psi_1}{d\,\sqrt{2}}} \tag{1.10}$$

Based on the concept of closest approach r_{min} (Fig. 1.2) one can calculate the *Minimum yield* χ_{min}, ie, fraction of channeled particles for incidence parallel to the crystal axis ($\psi = 0$) [15]. Around each axis there is an area πr_{min}^2 in which particle cannot channel and particles incident at $r > r_{min}$ can channel. If R_o is the radius of the channel, the minimum yield χ_{min} is defined as

$$\chi_{min} = \frac{\pi\, r_{min}^2}{\pi\, R_o^2} \tag{1.11}$$

The corresponding Lindhard continuum planar potential is calculated using equation (1.3) and is given by [16]

$$Y_L(y) = 2\,\pi\, Z_1\, Z_2\, e^2\, N\, d_p \left[\sqrt{(y^2 + C^2\, a_T^2)} - y \right] \tag{1.12}$$

The critical angle for planar channeling ψ_p is given by [16]

$$\psi_p = \sqrt{\frac{2\,\pi\, Z_1\, Z_2\, e^2\, N\, d_p\, a_T}{E}} \tag{1.13}$$

If y_{min} is distance of closest approach to the plane, the corresponding minimum yield χ_p for planar channeling is given by [20],

$$\chi_p = \frac{2\, y_{min}}{d_p} \tag{1.14}$$

which is substantially larger than corresponding value r_{min} for axial channeling.

The concept of distance of closest approach to the string or plane implies that channeled ions oscillate between the strings or planes of atoms and it never penetrates closer to the string than r_{min} or y_{min}. The minimum distance of approach can be approximated to the *Thomas Fermi Screening distance* a_T for many practical cases. All the close encounter processes like' *nuclear reaction* etc are least likely to happen in channeling situations.

A similar orientation effect called *Blocking* occurs for positively charged particles coming out of lattice sites inside a crystal. This implies that the particle is either emitted from the nucleus at one of the lattice sites (through processes like radioactivity) or results due to the large angle *Rutherford Scattering* of incident beam [15]. Since the impact parameters involved in large angle scattering are several orders of magnitude smaller than the zero-point thermal vibration amplitudes for atoms in crystals, the two types of particle emission are indistinguishable. The role of the incident beam is to create particles that emerge from the lattice sites. *Blocking* and *Channeling* phenomenon are identical and reciprocal to each other in certain conditions where the incident particles,energies, crystals and crystal directions are same in both experiments and the energy loss of the particle to crystal is negligible. In the absence of energy loss processes the *Channeling* and *Blocking* processes are related to one another by *time reversal* [15,21]. In measuring a channeling dip one determines the probability of a well collimated incident beam having a head-on collision with the nucleus of the target atom. This probability is measured for various relative orientations of the incident beam and the target. The same procedure is repeated for *Blocking* experiment, where it determines the probability that particle emerging from an atomic nucleus will hit a well collimated detector. This *time reversal rule* has been verified experimentally [22]

Although *Lindhard's Continnum model* which is based on a classical theory, successfully predicts important features like *critical angle and minimum yields* and their dependence on fundamental parameters (Z_1, Z_2, E etc), for lighter particles like positrons and electrons one needs quantum mechanical treatment. A criterion has been derived for validity of quantum mechanical versus classical description. This requires that *the product of mass of the particle and strength of the interaction between the particle and the crystal should remain small for validity of quantum mechanical treatment* [16,23-25].

1.3 APPLICATIONS

Channeling techniques find their applications in many frontier areas of physics. Ion implantation, defects and radiation damages studies, backscattering analysis, semiconductor superlattices studies are very few among them. Using this technique one can improve the depth resolution of the ion scattering method and improve its sensitivity to light impurities . Both Rutherford backscattering and channeling are simultaneously used for studying various phenomenon occuring in *Strained layer superlattices* (discussed thoroughly in *chapter 6).* The channeling effect can be and has been used to locate foreign atoms in a crystal and the energy dependence of dechanneling gives information of the nature of the defects. The magnitude of the dechanneling cross section is used to find the amount of damage present in the crystal.

Channeling techniques are extensively used for preparation and characterization of new materials through ion implantation [17,26,27] Since the channeled ions penetrate deep in to the material *(Range* is very large compared to random case), the final depth reached by the ions can be increased for a given incident energy. In channeling situations the head-on collision of atom with the ion is very rare and consequently the *radiation damage* caused by the beam is very low in this case. The range distribution of the ions are very sensitive to the dechanneling effects due to *temperature, defects* etc. This factor partly limits the reliability of channeling technique in Ion implantation studies

The channeling techniques can be and has been used to determine the lattice site of an impurity in a single crystal. When the impurity is situated on a regular lattice site (ie substitutional) it will have no effects on the channeling. However, when it is located at an interstitial position, it may obstruct the path of channeled particles along certain directions and may be shadowed by the atomic strings along certain other directions (Fig. 1.3). Hence by performing channeling experiments along some of these directions

one can determine precise location of the impurity. The other important factor to realize is that the dechanneling cross sections clue to certain type of defects or dislocations are energy dependent [16,28-30]. So by probing the ion beams through different orientations by observing the nature of energy dependence on the dechanneling cross section one will be able to pinpoint the type of defects or dislocations present in the crystal.

Steering of high energy (GeV region) charged particle passing through *bent crystals* using channeling technique have immense practical applications [31]. This is because the crystal field with its $\sim 10^{13}$ Vm^{-1} exceeds by many orders of magnitude any external field produced in the laboratory [18] and can replace large and expensive magnets used in the laboratory for bending of beams.

Channeling radiation emitted from relativistic channeled particles [32] have the prospects of constructing intense tunable X *-ray* and γ - ray source. Theory and properties of this channeling radiation are extensively discussed in *chapter 7.*

1.4 OUT LINE OF THE THESIS

The Electronic stopping power studies in the random case are discussed in the next chapter with the support of the experiment which we performed at *Nuclear Science Centre New Delhi, India* using a relatively new technique *(ERDA, Elastic Recoil Detection Analysis)* to get the ion beam.

A thorough knowledge of Charge density and Interatomic potential is basis for a better understanding of any phenomena in physics in general and in the field of channeling and its applications in particular. Most of the interatomic potentials (Thomas-Fermi type) and corresponding continuum potentials used in the channeling studies are of statistical nature. We have tried to relax the statistical nature inherent in all the Thomas-Fermi type potentials and obtain a suitable potential which takes into account of the atomic

shell structure of the atom. We have developed a shell charged density and using the Poisson equation, corresponding shell interatomic potential was calculated. The planar and axial cases of the potential are also derived. This is the main feature of *chapter 3.* In *chapter 4,* the electronic stopping power for channeling case is discussed. The Shell model charge densities are used to calculate the position dependence of stopping power in planar and axial cases. The theoretical results are compared with the experimental data and the results obtained from other theoretical models.

Z\ oscillations in the Electronic Stopping powers of elements are discussed on the basis of *Briggs- Pathak theory and* the actual stopping powers have been calculated using shell model charge density in *chapter 5.* The results are compared with the experimental results also.

The effectiveness of using shell model continuum potenials are tested in the frontier fields of channeling like *Strained Layer Superlattices* and Channeling Radiation. The results are discussed in *chapter (i* and *chapter* 7 respectively with the support of experimental data and the results from other theoretical models.

Chapter 8 contains a summary of work presented in the thesis with some concluding remarks and comments on possible future work.

References

[1] M. von Lau *Historical Introduction to International Tables for X-ray Crystallography*, Vol. 1, Eds. N. F. M. Henry and K. Lonsdale, (Kynoch Press, 1952)

[2] M. W. Thompson *Contemp. Phys*, 9, 375, (1968).

[3] J. Stark *Z. Phys.*, 13, 973, (1912).

[4] J. Stark and G. Wendt *Ann. Phys.*, 38, 921, (1912).

[5] J. A. Davies, J. D. McIntyre, R. L. Gushing and M. Lounsbury *Can. J. Chem.* 38, 1535, (1960).

[6] J. A. Davies, J. Friesen and J. D. Mclntyre *Can. J. Chem.*, 38, 1526, (1960).

[7] P. K. Rol, J M. Fluit, F. P. Vichbock and M. DeJong *Proc. Fourth. Int. Conf. on Ionization Phenomena in Cases,* (Ed.) N. R. Nilsson, (North Holland, Amsterdam) ,page 257, (1960).

[8] 0. Almen and G. Bruce *Nucl Instrum. Methods,* 11, 279, (1961).

[9] M . T. Robinson and 0. S. Oen *Appl. Phys. Lett.,* 2, 30, (1963).

[10] G. R. Piercey, F. Brown, J. A. Davies and J. A. McCargo *Phys. Rev. Lett*, 10, 399, (1963).

[11] H. O. Lutz and R. Sizmann *Phys. lett*, 5 ,113, (1963).

[12] A. F. Tulinov *Sov. Phys. Uspekhi*, 8, 864, 1966).

[13] S. Datz, C. Erginsoy, C. Leibfried and H. O. Lutz *Ann. Nucl. Sci.*, 17, 129, (1967).

[14] *Channeling, Theory, Observations and Applications,* (Ed.) D. V. Morgan, (John Wiley & Sons, New York), (1973).

[15] D. S. Gemmel *Rev. Mod. Phys,* 46, 129, (1974).

[16] A. P. Pathak *Radial Eff.* ,61, 1, (1982).

[17] L. C. Feldman, J. W. Mayer and S. T. Picraux *Material Analysis by Ion Channeling,* (Academic Press, New York), (1982).

[18] A. H. S0rensen and E. Uggerhøj *Nature*, 325, No.22, 311, (1987).

[19] A. P. Pathak *Atomic and Molecular Physics,* (Ed.) A. P. Pathak, (Narosa, New Delhi), page 165, (1992).

[20] L. C. Feldman and J. W. Mayer *Fundamentals of Surface and Thin Film Analysis,* (North Holland, New York) (1986).

[21] J. Lindhard *K. Dan. Videnskab. Selskab. Mat. Fys. Mc.dd.*, 34, No. 14, (1965).

[22] E. B0gh and J. L. Whitton *Phys. Rev. Lett.*, 19, 553, (1967).

[23] R. E. DeWames, W. F. Hall and G. W. Lehman *Phys. Rev.*, 148, 181, (1966).

[24] A. P. Pathak and M. Yussouf *Phys. Rev.*, B 2, 4723, (1970) .

[25] A. P. Pathak *Phys. Rev.,* B 9, 2406, (1974).

[26] G. Dernaley *Rep. Prog. Phys.*, 32, 405, (1969).

[27] W. K. Chu, J. W. Mayer and M. A. Nicolet *Backscattering Spectrometry,* (Academic Press, New York), (1978).

[28] J.J. Quillico and J. C. Jousset *Phys. Rev.*, B 11, 1791, (1975).

[29] J. Mory and Y. Quere *Rad. Eff.,* 13, 57, (1972).

[30] Y. Quere *Phys. Rev.,* B 11, 1818, (1975).

[31] A. W. Saenz and II. Uberall (Eds.) *Coherent Radiation Sources,* (Springer - Verlag, Berlin), (1985).

[32] R. A. Carrigan Jr. and J . A. Ellison (Eds.) *Relativistic Channeling, {* NATO AS] Series Vol. B 165), (Plenum, Now York), (1987).

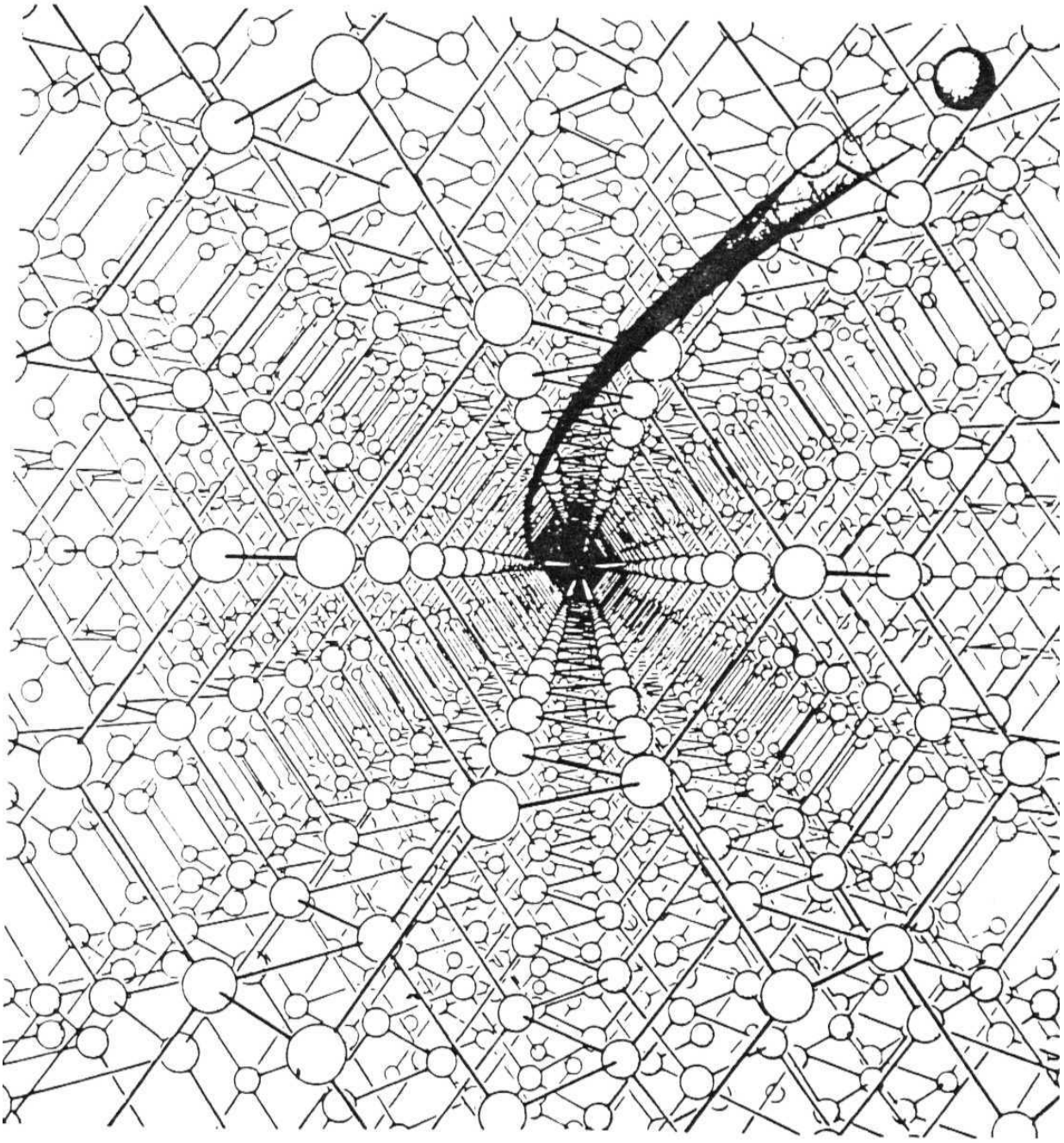

Kg 1.1: **View down the < 110 > axial channel in a diamond structure crystal showing the spiral path followed by a typical channeling particle. (After *W. Brandt, Scientific American*, 218, 90, (1968).)**

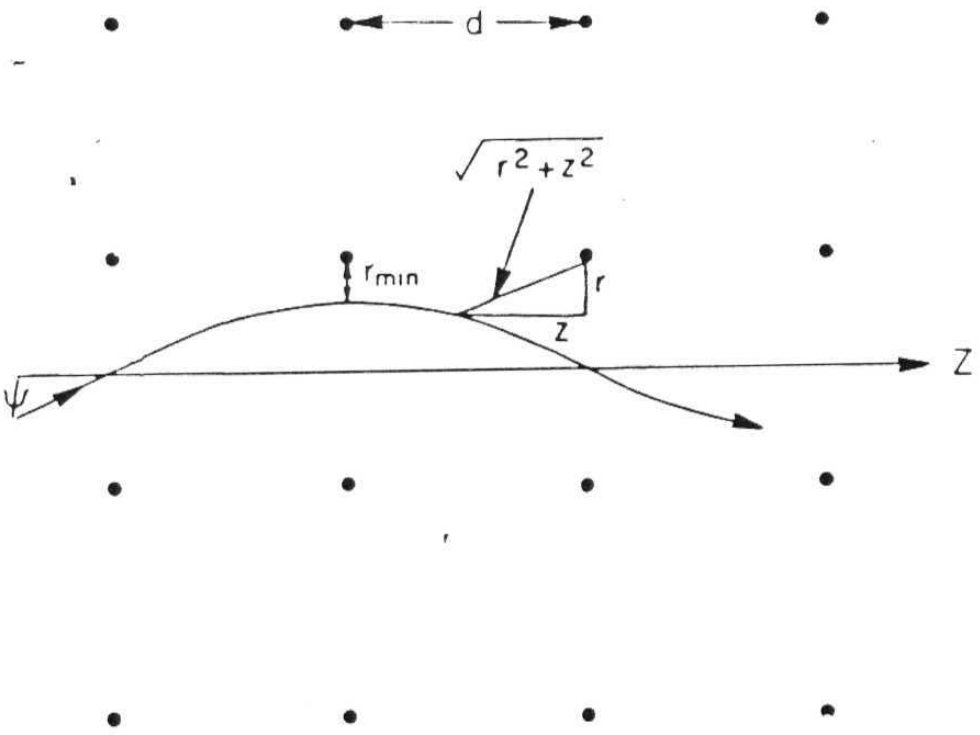

Fig 1.2: **A channeled trajectory allowing various quantities such as *incident angle* ψ , *minimum distance of approach* r_{min} and *interatomic distance d***

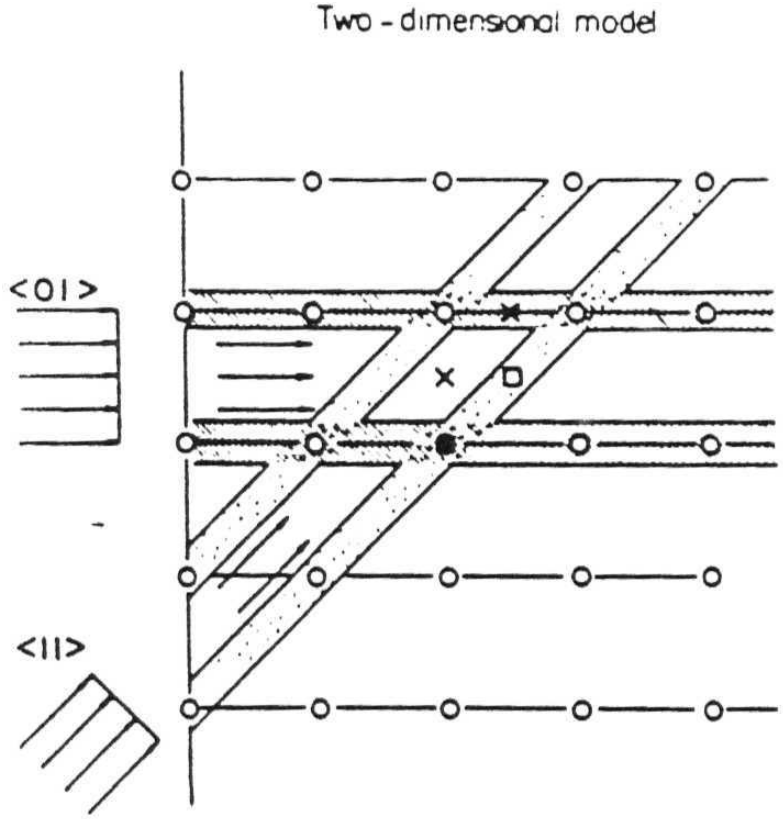

	Directional effect ?		
	●	x	□
<01>	Yes	50%	No
<11>	Yes	No	Yes

Fig 1.3: A two **dimensional** model illustrating how the **channeling** effect may be used to locate foreign atoms in a crystal AB shown by the table three possible sites for a foreign atom (•, □ and x) can be readily distinguished by **comparing** the **channeling** behaviour along the < 01 > and along the < 11 > direction

Chapter 2

ELECTRONIC STOPPING POWER (Random Case)

2.1 INTRODUCTION

Even after many decades of its experimental observation and theoretical interpretation, the study of energy loss of charged particle propagating through solids is still attracting attention of researchers and is used extensively for probing and analysing various phenomenon occuring in the field of atomic, nuclear physics and condensed matter physics [1,2]. Charged particle loses its energy through two processes. (i). *electronic energy loss*, where the particle loses energy through inelastic collision (excitation,ionization) with target electrons. (ii).*nuclear energy loss*, where the energy of the particle is transferred to the target nucleus resulting in atomic vibrations and possible displacement / dislodging of these atoms / ions. Nuclear stopping is predominant only at very low velocities ($\sim$ 10 keV/amu)and at higher velocities it can be neglected. Any correlation between nuclear and electronic stopping can be completely ignored except for single scattering studies [3] and for very thin targets. The total stopping cross sections of ions in the solids is the sum of contribution from the electronic and nuclear stopping cross sections. The velocity dependence of stopping power, as an ion passes through solid is elucidated below.

When an energetic ion moves in a solid (target) with a velocity higher than the velocity of innermost orbital of the solid, most of its electrons are stripped off and essentially a bare nucleus moves through the solid (Region I in Fig. 2.1.) [4]. As this energetic ion

loses energy to the target through various processes such as excitation and ionization of the target, its velocity decreases. When the velocity approaches a velocity equal to that of electrons in the innermost orbit, the probability of capturing an electron in that particular orbit increases, where as the probability of losing an electron from that shell decreases, so that electrons are captured in that inner shell. When the ion velocity further decreases and becomes comparable to the velocities of successive orbital electrons , then the electrons are captured successively in those shells (Region II in Fig. 2.1.), and consequently at velocities of the order of *critical velocity* ($v_c = v_o Z_1^{2/3}$), a neutral atom moves in solid (where v_o is the Bohr velocity and Z_1 is the atomic number of projectile ion). The region of velocities below these velocities is called *low velocity region* (Region III in Fig. 2.1.), where the rate of electronic energy loss decreases with decreasing velocity. At low energies, nuclear stopping beomes significant. The main effect is dislodgement of atoms from their bonding states and creation of *radiation damage* in the target material [4]. When the energy of the primary displaced atom is large enough to dislodge more atoms, a *damage cascade* is induced giving rise to secondary and other higher order damage cascades. For still lower energies of incident ions the chemical binding among the atoms of the target material is more important and energy is given to the target crystal as a whole; in this case the ion is said to be stopped in the target.

Only a few energy loss data for heavy ions are available in the low velocity region [5] A knowledge of accurate heavy ion stopping powers in various elements and compounds are essential from both fundamental and practical points of view. Heavy ion beams are routinely used in Ion Beam Analysis techniques for depth profiling and elemental analysis of materials [6]. In addition to their utility in Ion Beam Analysis techniques, energy loss values are essential input parameters for most nuclear physics experiments, such as life time measurements by the Doppler shift attenuation technique, analysis of data recorded by particle track detectors,etc. Therefore, applications of the basic energy

loss or stopping power data are significant.

We have performed a series of energy loss measurements of various target-ion combinations in the energy range of 1.0 to 5.0 atomic units of velocity at Nuclear Science Centre (*N.S.C.*),New Delhi, India [7,8]. We have been systematically carrying out the stopping power experiments in the low velocity region using heavy ions (Z_1 — 8 — 29) with a broader perspective to supplement the insufficient stopping power data available in this region. It was theoretically predicted that the Z_1 oscillations in the channeling electronic stopping power [4] will damp out, when one increases the projectile velocity above $2-3v_o$ [9]. So far this prediction eludes experimental verification due to inadequate stopping power values in this region as mentioned earlier. We hope we can verify this theory in near future specially when channeling experiments are possible al, *N.S.C.* New Delhi. As of now, in the absence of Goniometer at this Palletron, we have been able to do only random stopping power measurements. To ensure optimum usage of the beam time, we have developed an ingenious method for doing energy loss measurement using *Elastic Recoil Detection Analysis* (ERDA) experiment. As a new approach, recoil ions produced in heavy ion scattering (ERDA) were utilised for energy loss measurements. Secondary recoils of the required Z_1 value generated by the bombardment of high energy heavy ion on a particular target is utilized here. So the various secondary ion beam can be produced by merely changing the targets. The energy loss of the recoil ions was measured by keeping two surface barrier detectors, with and without target foil, at the same recoil angle, with their gain matched with pulsers before the experiment. Different energies of the secondary beam could be selected by changing the detection angle. A similar technique has also been used for stopping power measurements by anotlier group [10-12]. The details of the experiment are outlined in the section 2.2, the theoretical models used to compare the experimental results are discussed in section 2.3 and results and future programme of ongoing experiment is discussed in the section 2.4

2.2 EXPERIMENTAL DETAILS

The electronic energy loss measurements were carried out at the 15 MV Palletron facility at the Nuclear Science Centre, New Delhi, India [7]. A Schematic diagram for experimental setup is shown in Fig.2.2. A well collimated primary beam of ^{127}I and ^{192}Au ions (80 -130 MeV) were used to generate secondary recoil ions of various species of targets. Targets with different Z's were mounted on the target ladder of a scattering chamber facility of the Palletron.The recoiled ions were then detected by surface barrier detectors before and after their passage through the mylar (carbon) foils. Rectangular Ta slits of 4mm X 8mm area defined the solid angle for the detection geometry. As the incident energy is below the Coulomb barrier, only Rutherford scattering is possible.

The experiment was carried out in a scattering chamber of 1.5m diameter [13]. The rotatable detector arm mounted inside could be moved from outside the vacuum. The angle of detection could be changed with a precision of 0.05°. The vacuum in the scattering chamber was 1×10^{-6} Torr. The target ladder could also be rotated and there was a provision for *in vacuo* transfer of the target. This facility therefore gave the advantage that the energy of the recoiled ion beams could be varied by changing the forward angle of detection. Since the elastic primary beam will not be scattered beyond $\theta_{max} = \sin^{-1}(M_t/M_p)$,the detection angles larger than θ_{max} could be chosen for different recoil ion beams, thereby avoiding large count rates from the elastic events. The targets were tilted with respect to the primary ion beam direction so that the recoils were obtained in the reflection geometry. The stopping cross sections were determined by measuring the energy of the recoil ions with and without the mylar (carbon) foils using surface barrier detectors with depletion depths of $60\mu m$. The thickness of the mylar (carbon) film was measured by alpha - energy loss method. The surface barrier detectors were energy calibrated using an ^{241}Am alpha source. Care was taken to monitor the energy calibrations

of the detectors at regular intervals by using the standard pulsers duly adjusted before the start of the experiments.

Two detectors, one with the mylar (Carbon) foil and another without the foil, were mounted in slots provided in the scattering chamber angular arms. These slots were 6° apart from each other. The detectors were swung into the path of the recoil beams one after the other and the energy spectrum of the secondary recoils were recorded. The difference in the measured energies of the particles in the two detectors gave us the energy loss in the foil.

The incident primary beam will produce secondary recoil beams of a range of energies, depending on the depth from which the recoils are emerging. For the recoils generated from the surface, the energy is given by

$$E_{rec} = \frac{4M_pM_t}{(M_p + M_t)^2} E_o \cos^2 \phi_R \tag{2.1}$$

where M_p and M_t are the masses of the primary ion beam and target atom (in atomic-mass units) respectively, ϕ_R is the recoil angle in degrees, which was varied to carry out the measurements at different energies.

The experimental values deduced have errors of about 3.5% which includes errors arising from the foil thickness measurements and errors in the calculations of recoil energies from spectra. To minimize the energy uncertainty resulting from kinematic broadening, the detector solid angles were taken to be about 0.2 msr. The surface barrier detectors generally had pulse height defects [14] for detection of heavy ions. This defect would lead to an incorrect energy determination of the particles. Since the pulse height defect increases with the mass of the ion and its energy, it was estimated [14] for Ti ions of energy 27 MeV and was found to be 0.05 MeV. Therefore, the error resulting from this effect is 0.05%.

2.3 THEORETICAL CALCULATIONS

An exhaustive collection of stopping power data and various theoretical models were reported elsewhere [15-18]. Most of our ion velocities belong to low velocity region and some are just above this region. LSS theory [19] which is based on the assumption that the electron density in the target varies slowly with position, can be used to get. a theoretical estimation of electronic stopping power in this low velocity region. Varelas - Biersack approximation [20] holds good in intermediate energy region, and Bethe formula [18,21] can be used to calculate electronic stopping power in high velocity region. It is to be noted that, we have used Bethe formula only to apply Varelas - Biersack approximation to electronic stopping power in the intermediate velocity region.

At low velocities ($v < v_o Z_1^{\cdot} = v_c$), the stopping power can be written as $N.S_e$, where N is the number of atoms per unit volume and S_e is the electronic stopping cross section per atom. According to LSS theory [19], which is based on Thomas Fermi model, the electronic stopping cross section can be written as

$$S_{E,L} = \xi\ 8\pi\ e^2 a_o \frac{Z_1 Z_2}{Z} \frac{v}{v_o} \qquad \textbf{(2.2)}$$

Where e is the electronic charge and Z_1 and Z_2 are the atomic numbers of projectile ion and target atom respectively, a_o is the Bohr radius, the constant ξ is of the order of $Z_1^{1/6}$ and $Z^{2/3} = Z_1^{2/3} + Z_2^{2/3}$.

The electronic stopping power $(dE/dx)_e$ is given by [19]

$$\left(\frac{dE}{dx}\right)_e = N S_{E,L} \qquad \textbf{(2.3)}$$

where N is the atomic density. The electronic stopping power can be evaluated in $MeV/mg/cm^2$ units and is given as

$$\left(\frac{dE}{dx}\right)_e = 11.532790 \ \xi \ \frac{Z_1 Z_2}{A_2 \ Z} \ \frac{v}{v_o} \tag{2.4}$$

where A_2 is the mass number of target atom. Another related quantity of interest is *Reduced stopping power* $(dE/dx)_R$ defined as

$$\left(\frac{dE}{dx}\right)_R = \left(\frac{dE}{dx}\right)_e \times \left(\frac{Z}{\xi \ Z_1 \ Z_2}\right) \tag{2.5}$$

Both the energy loss and velocity of the ions are reduced in such a way that the LSS values fall on a straight line intersecting the origin [22] (shown in Fig.2.3). For Mylar, we have used *Bragg's Rule* for calculating stopping power. According to *Bragg's Rule,* energy loss of a compound target is the sum of the energy losses of the constituent elements weighted by the abundance of the elements [2]. We have also calculated the stopping power of Mylar by substituting the effective atomic number of Mylar ($Z_{eff} = 6.46$) in the equation 2.2. At high velocities ($v > v_c$), Bethe formula can be used to calculate stopping power. Bethe formula is given by

$$S_{E,H} = \frac{4\pi Z_1^2 Z_2 e^4}{mv^2} \ N \ \ln \frac{2mv^2}{I} \tag{2.6}$$

Where / is the mean excitation energy of a target atom. The logarithmic term *L{X)* can be replaced by an universal function of a parameter X — $v^2/\ v_o^2 Z_2$. For low velocities [23] $X < 10$.

$$L(X) = 1.36X^{1/2} - 0.016X^{3/2} \tag{2.7}$$

Fano [24] found that above equation overestimate $L(X)$ for stopping media of low atomic number, since the statistical treatment was not expected to be valid for atoms containing only a few electrons [25].

For intermediate energy region, there is no concrete theory that can satisfactorily explain the stopping power maximum. Varelas - Biersack [20] suggested an approximation for stopping power in the intermediate energy region. This is given in terms of values obtained using low velocity formula $S_{E,L}$ and high velocity formula $S_{E,H}$ as

$$S_{E,IM}^{-1} = S_{E,L}^{-1} + S_{E,H}^{-1} \tag{2.8}$$

we have used this approximation to estimate stopping powers in the intermediate region.

2.4 RESULTS AND DISCUSSION

2.4.1 MYLAR

To best of our knowledge a very few energy loss measurements have been carried out for ^{48}Ti and ^{16}O ions in Mylar $(C_{10}H_8O_4)$ foil [25-30] . The choice of the mylar was due to its wide application in ERDA experiments with thin windows for gaseous detectors. The energy loss of ^{16}O and ^{48}Ti ions in Mylar foil were theoretically calculated using LSS formula, Bethe formula and Varelas Biersacks approximation using these formulae with and without *Bragg's rule* and results are tabulated in Table 2.1. *Bragg's rule* calculations gave slightly lesser values of stopping power. Calculations based on LSS formulation (using effective Z_2 (Mylar)= 6.46) gave almost same values as experimental result except for 0.11 Mev/amu ^{48}Ti ions. It is already a well known fact that the LSS Theory under estimates the stopping power values at low velocities. For 0.62 (MeV/amu) ^{16}O ions, Varelas - Biersack approximation gave better value compared to the other methods. This is expected because the 0.62 (MeV/amu) ^{16}O ions belong to the intermediate energy region. We also calculated the stopping power of Mylar for both ions using Ziegler scaling laws [31]. For calculating proton stopping power of mylar for equal velocities of ^{16}O and

^{48}Ti ions we used the scaling formula given in the appendix of Reference [32]. Both TRIM-92 and Ziegler scaling calculations gave slightly higher values than experimental values in all cases. Jin Chang wen *et al* [30] reported that at lower energies there is a remarkable disparity between TRIM-92 and experimental values. We didn't observe such difference in the case of ^{48}Ti ions.

2.4.2 CARBON

Electronic stopping powers of Carbon [thickness = 72μ gm/cm] were experimentally measured using ERDA technique for ^{16}O, ^{27}Al, ^{48}Ti, ^{56}Fe and ^{64}Cu ions. Our experimental results were compared with experimental data obtained from *M. Abdesselam et. al.* in the same energy range [10 12] and theoretical as well as semi empirical models. These results are shown in Table 2.2 - 2.4 respectively. Typical spectra obtained in these experiments and the method of analysis has already been indicated in our earlier study [7]. We notice from the table that LSS theory is valid upto the *crtical velocity limit* v_c and the corresponding *critical energy* E_c is calculated for each projectile ion. For ^{16}O, ^{27}Al, ^{48}Ti, ^{56}Fe and ^{64}Cu the E_c values are 6.35, 20.47, 73.37, 106.96 and 141.40 MeV respectively. The LSS values agree better for the ion energies above 0.7 MeV/amu. Follower ion energies these values tend to lie increasingly lower than the experimental values as one goes towards the low ion energies. For lower energy values, (For ^{48}Ti, E/A < 0.945 Mev/amu, ^{56}Fe and ^{64}Cu, all data in Table 2.4) LSS theory underestimates electronic stopping power and for higher energy values (For ^{27}Al, E/A > 0.45 Mev/amu) it overestimates the stopping power. This behaviour is one of the shortcomings of LSS theory and is explicitly shown in Fig.2.3. For ^{16}O case, Varelas Biersack approximation [20] gives a good estimation of electronic stopping power. LSS theory is not valid in this region ($v > v_c$) because all the energies of oxygen ions fall in the intermediate energy region

(For this reason, we did not plot oxygen data in fig.2.3). There is a. reasonable agreement between experimental data and values based on TRIM-92 code. However, there is a tendency of these values remaining some what higher than experimental values. The experimental data obtained from *M. Abdesselam et. al.* [10-12] in the same energy range are in good agreement with our results.

2.4.3 FUTURE PLANS

Our technique of performing the energy loss measurements is simple and convenient, specially when it is desired to cover a wide range of ion energies for various ion species. However, experimental data may require higher precision in order to discern oscillations in stopping power as a function of Z_1 (for constant velocity values) in a given absorber. Also, it has been felt that the absorber thickness needs to be varied as the ion energies are changed over a wide range. It is planned to overcome these limitations by modifying the experimental set up to (i) permit a tilt in the absorber holder position, (ii) use of dE-E gas detector telescope or even a focal plane detector placed in a Recoil Mass Spectrometer (RMS). The dE (gas) - E (Semiconductor) detector can help in the present set up to provide Z_1 - discrimination, whenever required. The RMS helps in covering, forward recoil angles between $0°$ and $30°$, not available presently. We have measured the electronic stopping power of mylar and carbon specifically in the projectile velocity region greater than $2 — 3\ v_o$ (shown in Table 2.1 - 2.4). As mentioned earlier, it has been theoretically predicted [9] that above $2 — 3\ v_o$ units of projectile velocities, Z_1 oscillations in the electronic stopping power washout. With the existing data, we can't deduce any such effect and we will be shortly measuring the stopping power of carbon and other target materials for various species of ions which were not covered so far in our experiments [7,8]. More importantly, the channeling stopping power measurements are planned for medium velocity region near maxima as soon as goniometer is acquired at

N.S.C palletron facility. The channeling stopping power data is available either in high velocity region [33,34] or low velocity region where the oscillations exist and have been adequately explained.

References

[1] W. K. Chu, J. W. Mayer and M. A. Nicolet *Backscattering Spectrometry,* (Academic Press, New York 1978).

[2] L. C. Feldman and J. W. Mayer *Fundamentals of Surface and Thin Film Analysis,* (North Holland, New York 1986).

[3] P. Loftager F. Besenbacher 0. S. Jensen and V. S. Sørensen *Phys. Rev* A **20**,1443, (1979).

[4] A. P. Pathak *Radiat. Eff.* 61, 1, (1982).

[5] J. F. Ziegler *Ion Implantation Science and Technology,* (Academic Press, New York 1988).

[6] J. R. Bird and J. S. Williams, *Ion Beams and Material Analysis* (Academic Press, New York 1989).

[7] N. Nath, 0. P. Dahinwal, A. Bhagwat, D. K. Avasthi, V. Hari kumar and A. P. Pathak *Surface and Coatings Technology* 66, 231, (1994).

[8] V. Hari kumar, A. P. Pathak, N. Nath, S. K. Sharma, A. Bhagwat and D. K. Avasthi *Radiation Effects and Defects in Solids,* **132,** 211, (1994).

[9] A. P. Pathak *Phys. Rev.* B. 22, 96, (1980).

[10] M. Abdesselam, J. P. Stoquert, G. Guillaume, M. Hage-Ali, J. J. Grob and P. Siffert *Nucl. Instrum. Methods.,* B 72, 7, (1992).

[11] M. Abdesselam, J. P. Stoquert, G. Guillaume, M. Hage-Ali, J. J. Grob and P. Siffert *Nucl. Instrum. Methods.,* B 72, 293, (1992).

[12] M. Abdesselam, J. P. Stoquert, M. Hage-Ali, J. J. Grob and P. Siffert *Nucl. Instrum. Methods.,* B 73, 115, (1993).

[13] D. K. Avasthi, A. Tripathi, S. Venkatraman and S. K. Datta *NSC internal Rep NSC/TR/DKA/92/16,*NSC, New Delhi 1992).

[14] M. Ogihara, Y. Nagashima, W. Galster and T. Mikumo *Nucl. Instrum. Methods,* A **251,** 313, (1986).

[15] L. C. Northcliffe and R. F. Schilling *Nucl. Data. Tables*, A 7 233, (1970).

[16] S. P. Alhen *Rev. Mod. Phys.* 52, 121, (1980).

[17] J. F. Ziegler, J. P. Biersack and U. Littmark *The Stopping and Range of Ions in Solids* Vol. 1 (Pergamon Press, New York 1984).

[18] P. Sigmund *Nuclear. Instrum. Methods.* B 85, 541, (1994).

[19] J. Lindhard, M. Scharff and II. E. Schiott *Kgl. Danske. Vidcnskab. Srlskab. Mat. Fys. Medd.* 33, No. 14, (1963).

[20] C. Varelas and J. P. Biersack *Nuclear. Instrum. Methods.* 79, 213, (1979).

[21] H. Bethe Ann. Physik 5(5), 325, (1930).

[22] H. Pape, II.- G. Clerc and K. - H. Schmidt *Z Physik* A 286, 159, (1978).

[23] J. Lindhard and M. Scharff *Kgi Danske. Videnskab. Selskab. Mat. Fys. Medd.* 27, No. 15, (1953).

[24] U. Fano *Ann. Rev. Nucl. Sci* 13 1, (1963).

[25] J. B. Cumming and V. P. Crespo *Phys. Rev* **161,** 287, (1967).

[26] T. E. Pierce, W. W. Bowman and M . Blann *Phys. Rev.* **172,** 287, (1968). •

[27] J. Raisanen and E. Rauhala *Phys. Rev.* B. 36, 9776, (1987).

[28] E. Rauhala and J. Raisanen *Phys. Rev.* B. 37, 9249, (1988).

[29] J. Raisanen and E. Rauhala *Phys. Rev.* B. 41, 3951, (1989).

[30] Jin Changwen, Lu Xiting, Huang Xiaojing, Ye Yanlin, Xin Zanghuang, Liu Hong tao and Jiang Dong xing *Phys. Rev.* B. 48,6858, (1993).

[31] J. F. Ziegler *Appl. Phys. Lett.* 31, 544, (1977).

[32] J. F. Ziegler and J. M. Manoyan *Nucl. Instrum. Methods* B 35, 215, (1988).

[33] 0. N. Jarvis, A. C. Sherwood, C. Whitehead and M. W. Lucas *Phys. Rev.* , B 16, 3880, (1977).

[34] O. N. Jarvis, A. C. Sherwood and C. Whitehead *Radiat. Eff.*, 36, 215, (1978).

Experimental and Theoretical Values of Stopping Power of *Mylar* for *Ti* and *0* ions.

Table - 2.1

Ion	Energy (MeV/amu)	*STOPPING POWER* *KeV / A°* Expt	Trim-92	LSS	Bethe	Ziegler scaling	Varelas Biersack
Ti	0.11	0.27	0.27	0.19 (0.17)		0.25	
	0.29	0.32	0.36	0.31 (0.28)		0.40	
	0.42	0.37	0.40	0.37 (0.34)		0.43	
	0.55	0.41	0.42	0.42 (0.39)		0.44	
O	0.62	0.13	0.14	0.27 (0.24)	0.32 0.29)	0.15	0.15 (0.13)

Values shown in brackets are calculated using Bragg's rule.

Experimental and Theoretical **Values of Stopping Power of** *Carbon* **for** *O* **and** *Al* ions.

Table - 2.2

Ion	V x 10^8 (cm/sec)	E (Mev/amu)	*STOPPING POWER* (*Mev-cm²/mg*)				
			EXPT	TRIM-92	LSS	BETHE	V-B
O	10.03	0.52	9.3	9.9	15.1	21.5	8.9
	11.55	0.69	8.3	9.6	17.4	18.3	8.9
	13.05	0.88	8.3	9.2	19.7	16.3	8.9
	14.39	1.07	8.3	8.7	21.7	14.3	8.6
Al	7.87	0.32	16.2	16.5	15.7		
	9.33	0.45	16.7	17.5	18.7		
	10.77	0.60	16.4	18.1	21.6		
	12.04	0.75	16.9	18.1	24.1	52.3	16.5
	13.34	0.92	16.0	17.7	26.7	41.2	16.2
	14.52	1.09	15.0	17.3	29.0	37.3	16.3

The experimental stopping powers **meausered** (for **energies** close to the **energies** of our **experiments**) for *O* in *carbon* by *M. Abdesselam et. al.* [11] are given below (Incident energy value (*MeV/amu*) and corresponding stopping power value (*MeV-cm?/mg*) is given in brackets).

0.50 (9.69), 0.73(9.32), 1.04(8.46).

Experimental and Theoretical Values of Stopping Power of *Carbon* for *Ti* ion.

Table - 2.3

Ion	V x 10^8 (cm/sec)	E (Mev/amu)	*STOPPING POWER* (*Mev-cm²/mg*)		
			EXPT	TRIM-92	LSS
Ti	5.73	0.17	18.9	23.4	14.9
	6.67	0.23	22.3	25.3	17.4
	8.23	0.35	28.0	27.2	21.4
	8.90	0.41	28.9	29.0	23.2
	9.74	0.49	31.2	29.9	25.3
	10.41	0.56	31.7	30.6	27.1
	11.13	0.64	32.9	31.1	29.0
	11.72	0.71	34.4	31.5	30.5
	12.36	0.79	35.5	31.8	32.2
	12.97	0.87	34.4	32.0	33.8
	13.48	0.94	33.9	32.1	35.1

The experimental stopping powers measured (for energies close to the energies of our experiments) for *Ti* in *carbon* by *M. Abdesselam et. al.* [11] are given below

(Incident energy value (*MeV/amu*) and corresponding stopping power value (*MeV - cm²/mg*) is given in brackets).

0.45 (31.09), 0.69 (31.71), 0.78 (32.06), 0.89 (32.36), 0.98 (32.37)

Experimental and Theoretical Values of Stopping Power of *Carbon* for *Fe* and *Cu* ions.

Table - 2.4

Ion	V x 10^8 (cm/sec)	E (Mev/amu)	*STOPPING POWER* (*Mev-cm²/mg*)		
			EXPT	TRIM-92	LSS
Fe	6.52	0.22	25.1	27.2	18.3
	7.87	0.32	29.9	29.9	22.1
	9.01	0.42	32.5	32.7	25.3
	10.12	0.53	33.8	34.7	28.4
	11.47	0.68	35.4	36.3	32.2
	12.36	0.79	35.6	37.1	34.7
Cu	6.37	0.21	26.0	28.4	18.8
	7.49	0.29	28.7	31.7	22.0
	8.69	0.39	33.3	34.2	25.5
	9.74	0.49	37.0	36.8	28.7
	10.77	0.60	37.9	38.7	31.7

The experimental stopping powers meausered (for energies close to the energies of our experiments) for *Cu* in *carbon* by *M. Abdesselam et. al.* [10] are given below (Incident energy value (MeV/amu) and corresponding stopping power value (MeV-cm^2/mg) is given in brackets).

0.55 (37.63), 0.72 (40.94).

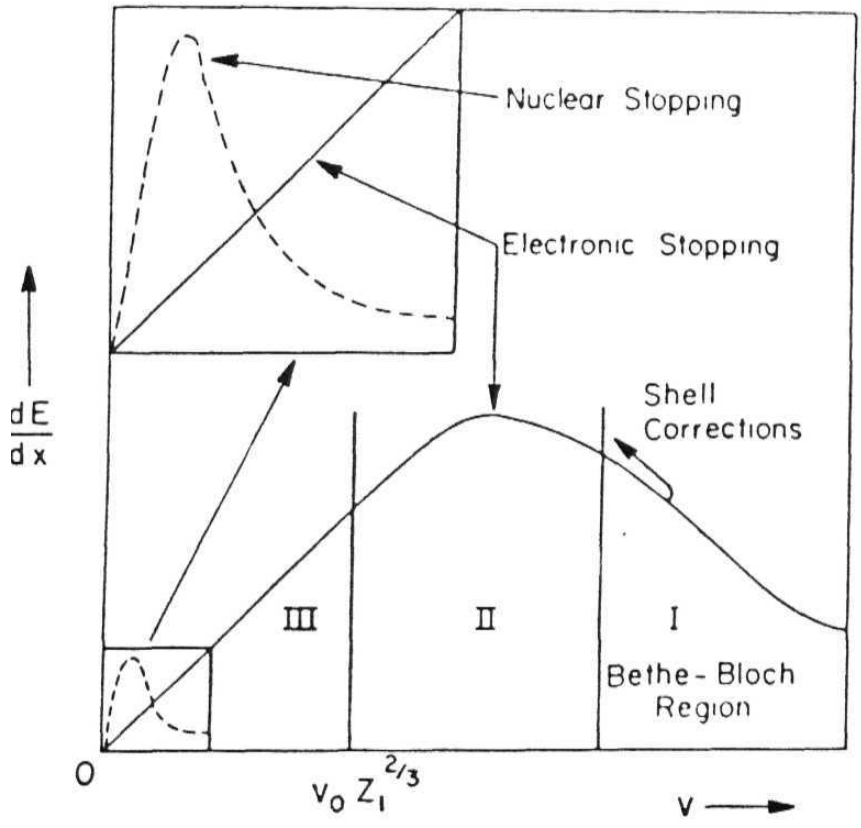

Fig 2.1: Schematic classification of different energy loot region*. The curves are qualitative and coordinates are not to scale. The *solid curve* represents *electronic energy loss* and dotted *curve* represents *nuclear energy* /OM.

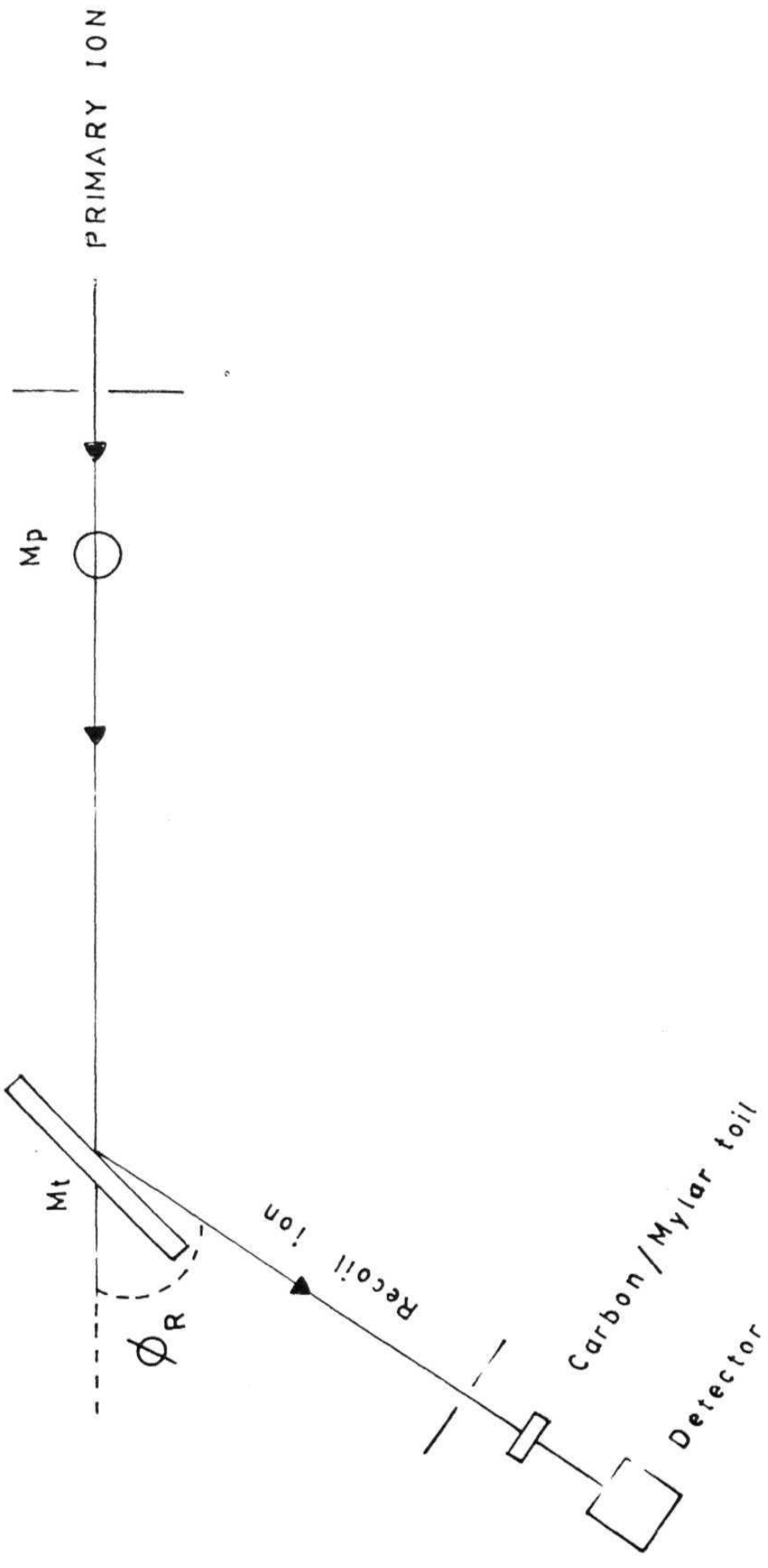

Fig 2.2: **Schematic** diagram of *ERDA* **exper imental** letup,

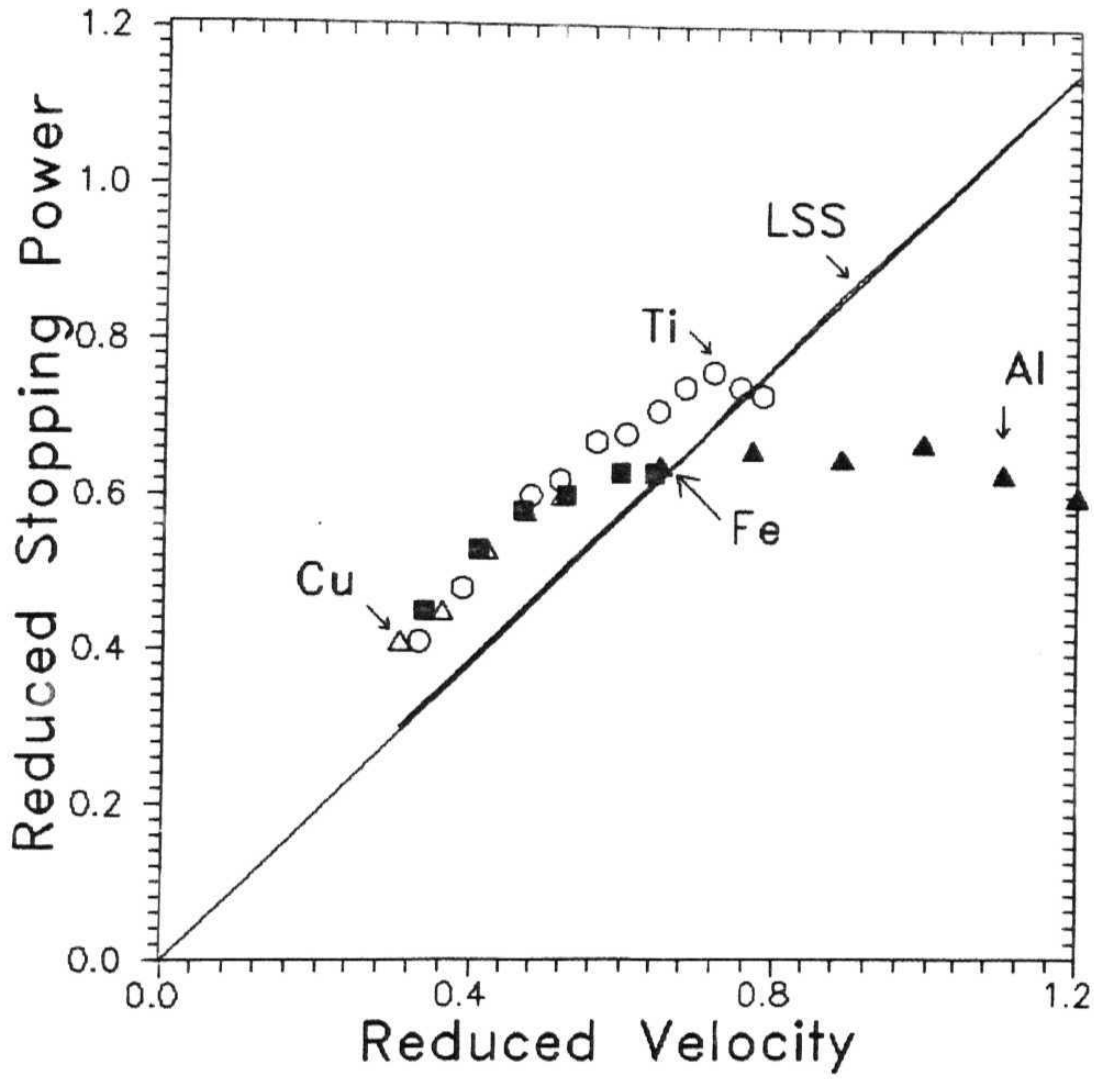

Fig 2.3: The *Reduced Stopping Power* $(dE/dx)_R$ in *MeV cm*^{2} / my) as a function of *Reduced ion velocity* (V_{red}). *Solid line* represents *LSS* values, filled triangles represent energy loss of *"Al* ions, open circles show energy loss of ^{48}Ti ions, filled squares represent energy loss of ^{56}Fe ions and open triangles show the energy loss of ^{64}Cu ion*.

Chapter 3

THE SHELL MODEL CHARGE DENSITIES AND POTENTIALS

3.1 INTRODUCTION

A detailed knowledge of interatomic potential is needed for better perception understanding and interpretation of various observation in the field of atomic collisions. Comprehensive work has been done to study this basic quantity from different points of view and has been reviewed in the literature [1-7]. Interatomic potential can be deduced using various methods. Each method has its own applications and limitations. The Interatomic potential can be obtained from crystal data such as phonon dispersion curve, elastic constants, compressibility and x - ray lattice constants [8]. But this procedure cannot be used for obtaining potentials for small nuclear separations [3]. Specific application of these interatomic potentials have been discussed in connection with channeling problem also [9–11] . Since the rate of energy loss is a function of transverse oscillation frequency of the projectile ion in the channel, Continuum potentials [9,10] can be and have been deduced from the channeling energy loss data. [12,13].

A closely related quantity is charge density sampled by the channeled particles. The interatomic potential can be derived from charge density using Poisson equation. The position dependence of stopping power in planar [14-16] and axial channels [17] has been studied by using Shell model for target atomic charge densities with reasonable success.

Earlier these Shell densities were found to reproduce the Z_1 oscillations [10,18-21] in channeling stopping powers very accurately (Z_1 is the atomic number of projectile ion). This provided us the motivation to probe deep into the fundamental quantity like inter-atomic potential which is derived from the Shell charge density using Poisson equation [22]. We derived an expression for both the charge density and interatomic potential in an analytical form. Corresponding axial and planar cases are also derived in the same analytical framework [23]. This Shell potential relaxes the statistical nature of Thomas Fermi Potentials [4,10] by including Shell structure thus providing a realistic picture of the situation. At the same time we still have analytical expressions for all quantities in axial and planar cases.

Shell charge densities and corresponding potentials are discussed in next section. Various types of Thomas - Fermi type potentials which are used to compare the Shell potentials are given in section 3.3. Results are discussed in the last section.

3.2 SHELL CHARGE DENSITIES AND POTENTIALS

Using one-term slater orbitals with optimized exponent given by dementi and Raimondi, the spherically symmetric electron density due to one atom at a distance *R* from the centre is given by [24,25]

$$\rho_S^{at}(R) = \frac{1}{4\pi} \sum_j \frac{\omega_j}{(2n_j)\,!} (2\xi_j)^{2n_j+1} R^{2n_j-2} e^{-2\xi_j R} \tag{3.1}$$

where ω_j, n_j and ξ_j are the occupation number, principal quantum number and the optimized orbital exponent of j th shell respectively. The orbital exponent ξ is given by

$$\xi = \frac{(Z-\sigma)}{n^*} \tag{3.2}$$

where $Z - \sigma$ is the effective Z seen by a given electron, ie., the nuclear charge seen by the electron, after screening by other electrons. σ is the screening constant and n^* is effective quantum number [24].

The axial electron charge density at a distance r from the string is calculated using continuum approximation (*chapter 1* equation 1.2) [9,10] and given by [17],

$$\rho_S^{ax}(r) = \frac{1}{\pi d}\sum_j \frac{\omega}{(2nj)!}\sum_{m=o}^{n_j-1}\frac{2^{2m}(2(n_j-m))!(n_j-1)!(\xi_j)^{n_j+m+2}r^{n_j+m}K_{n_j-m}(2\xi_j r)}{(n_j-m-\frac{1}{2})(n_j-m)(m)!((n_j-m-1)!\,)^2} \quad (3.3)$$

Where d is the interatomic spacing along the string. The planar electron charge density at a distance y from a single plane is calculated by making planar average using continuum approximation and is given by [14,16]

$$\rho_S^{pl}(y) = \frac{Nd_p}{2}\sum_j \frac{(2\xi_j)^{2n_j}}{2n_j}\omega_j \exp(-2\xi_j y)\sum_{k=0}^{2n_j-1}\frac{y^{2n_j-k-1}}{(2\xi_j)^k(2n_j-k-1)!} \quad \textbf{(3.4)}$$

Where N is the bulk density and d_p is the interplanar spacing. The shell interatomic potential is calculated from shell charge density. Using Poisson equation

$$\nabla^2 V = -4\pi\rho \quad (3.5)$$

and we get after some detailed calculations involving integration of the above Poisson equation using *p(r)* from equation 3.1

$$V_S(R) = \frac{Z_1 e^2}{R}\sum_j \frac{\omega_j}{2n_j}e^{-2\xi_j R}\sum_{k=1}^{2n_j}\frac{k}{(2n_j-k)!}(2\xi_j R)^{2n_j-k} \quad \textbf{(3.6)}$$

where e is the electronic charge and R is the interatomic distance. The corresponding axial and planar potentials are derived using continuum approximation [9,10] and is given below.

The shell axial potential is given by [23]

$$U_S(r) = \frac{2Z_1 e^2}{d}\sum_j \frac{\omega_j}{2n_j}\sum_{k=1}^{2n_j}\frac{k}{(2n_j-k)!}(2\xi_j r)^{2n_j-k}\left(\frac{d^{2n_j-k}}{d(2\xi_j r)^{2n_j-k}}K_o(2\xi_j r)\right) \quad \textbf{(3.7)}$$

For getting the above equation we used the relation [26]

$$\int_u^\infty (x^2 - u^2)^{(\nu-1)} \; e^{-(\mu x)} \; dx \;=\; \frac{1}{\sqrt{\pi}} \left(\frac{2u}{\mu}\right)^{(\nu-1/2)} \; \Gamma(\nu) \; K_{\nu-1/2}(u,\mu); \qquad (3.8)$$

$u > 0$, real $\mu > 0$, real $\nu > 0$.

The shell planar potential is given by [23]

$$Y_S(y) = 2\pi N d_p Z_1 e^2 \sum_j \frac{\omega_j}{2n_j} \sum_{k=1}^{2n_j} k(2\xi_j)^{2n_j-k} \sum_{m=o}^{2n_j-k} e^{-2\xi_j.y} \frac{y^m}{m!(2\xi_j)^{2n_j-k-m+1}} \qquad (3.9)$$

3.3 SCREENED COULOMB POTENTIALS

Although interatomic potential can be accurately deduced using Self-consistent methods, this procedure requires enormous computational time. At small nuclear separations, it is appropriate to use screened coulomb potential with a screening function derived from Thomas Fermi theory [13]. Thomas Fermi type potentials, which are based on the Fermi - Dirac theory of free electron gas are extensively used in various fields of nuclear, atomic and molecular physics. The general form of Thomas - Fermi type interatomic potential can be written as

$$V(R) \;=\; \frac{Z_1 \; Z_2 \; e^2}{R} \;\; \phi \; (\frac{R}{a_T}) \qquad (3.10)$$

where Z_2 is the atomic number of target atom, $\phi(x)$ is called Thomas - Fermi screening function and should satisfy the condition that $\phi(x) \;\rightarrow\; 1$ as $x \rightarrow 0$. Thomas - Fermi screening radius a_T is given by

$$a_T \;\approx\; \frac{0.8853 \; a_o}{(Z_1^{2/3} + Z_2^{2/3})^{1/2}} = 0.8853 \; a_B \qquad (3.11)$$

where $a_B = a_o/(Z_1^{2/3} + Z_2^{2/3})^{1/2}$ is the Bohr screening parameter, and a_o is the Bohr radius. Screened coulomb potentials based on Moliere [27] and Lindhard [9] analytical approximation to Thomas - Fermi screening function are mainly used in channeling studies and Lindhard interatomic and corresponding continuum potentials have already been described in *chapter 1.* Moliere version of interatomic , axial and planar continuum potentials are given below.

[a)] Moliere Potential.

Moliere interatomic potential is given as [10,27]

$$V_M(R) = \frac{Z_1 Z_2 e^2}{R} \sum_{i=1}^{3} a_i \exp(-b_i R) \tag{3.12}$$

with $a_1 = 0.35$, $a_2 = 0.55$, $a_3 = 0.1$, $b_1 = 0.3/\ a_T$, $b_2 = 1.2/\ a_T$, $b_3 = 6.0/\ a_T$.

The Moliere axial potential is derived using continuum approximation and is given by [10,23]

$$U_M(r) = \frac{2Z_1 Z_2 e^2}{d} \sum_{i=1}^{3} a_i K_o(b_i r) \tag{3.13}$$

where K_o is the modified Bessel function of order zero and the corresponding planar potential is derived and is given by [10,23]

$$Y_M(y) = 2\pi N d_p Z_1 Z_2 e^2 \sum_{i=1}^{3} a_i \frac{e^{-b_i y}}{b_i} \tag{3.14}$$

[b)] Biersack's Universal Potential.

Biersack's universal interatomic potential [4] is derived by taking into account the exchange and correlation energies unlike Moliere or Lindhard interatomic potentials. This potential is frequently used in low energy stopping studies [28]. Biersack's universal interatomic potential is given by [3,4]

$$V_U(R) = \frac{Z_1 Z_2 e^2}{R} \sum_{i=1}^{4} p_i \exp(-q_i R) \tag{3.15}$$

with $p_1 = 0.1818, p_2 = 0.5099, p_3 = 0.2802, p_4 = 0.02817$, $q_1 = 3.2/a_T$, $q_2 = 0.9423/a_T$, $q_3 = 0.4029/a_T$, $q_4 = 0.2016/a_T$.

Biersack's universal axial potential is given by [23]

$$U_U(r) = \frac{2Z_1 Z_2 e^2}{d} \sum_{i=1}^{4} p_i K_o(q_i r) \tag{3.16}$$

Biersack's universal planar potential is given by [23]

$$Y_U(y) = 2\pi N d_p Z_1 Z_2 e^2 \sum_{i=1}^{4} p_i \frac{e^{-q_i y}}{q_i} \tag{3.17}$$

[c)] Bohr Potential.

Bohr screened coulomb potential [29] has a simple analytical form but it provides excessive screening at larger distance. This limits its applications to short range interaction studies. Bohr interatomic potential is given by [10,29]

$$V_B(R) = \frac{Z_1 Z_2 e^2}{R} e^{-R/a_B} \tag{3.18}$$

Bohr axial potential is given as [23]

$$U_B(r) = \frac{2Z_1 Z_2 e^2}{d} K_o(r/a_B) \tag{3.19}$$

Bohr planar potential is given by [23]

$$Y_B(y) = 2\pi N d_p Z_1 Z_2 e^2 e^{-(y/a_B)}/a_B \tag{3.20}$$

All the above mentioned screened coulomb potentials are compared with corresponding Shell potentials and shown in fig 3.1 - 3.3.

3.4 RESULTS AND DISCUSSION

Both Shell charge density and Shell potential were derived in a phenomenological form which can be used as potential alternative for numerical computer simulation methods. The shell potential and shell charge density are free from statistical nature and shell structure inherent in the calculations carries the signature of particular target atoms involved in the problem. Naturally this potential gives a better physical picture of interaction compared to the other statistical type potentials. The comparison graphs (Fig.3.1 - 3.3) show that at short and medium distances (1—2 A^o), shell potential matches well with other potentials and yields slightly smaller values compared to Lindhard, Moliere and Biersack Universal potential but larger than those for Bohr potential at larger distances. This means screening of shell potential at larger distances is small compared to Bohr potential. However these larger distances (> 3 A^0) are not of much interest in channeling situation. The reasonable agreement at short and medium distances is encouraging enough for utility of shell potential. As mentioned earlier due to its close analytical forms (though it looks complicated) , Shell charge densities can be used effectively for channeling energy loss studies [23]. Shell potentials are successively used for problems involving effects of defects on channeling and channeling radiation [30] and computer simulation studies of Strained Layer Superlattices [31]. These applications are elucidated in the following chapters.

References

[1] I. M. Torrens, *Interatomic Potential* (Academic Press, New York) (1972).

[2] C. Foster, I. H. Wilson and M. W. Thompson *J. Phys. B* 15, 1332, (1972).

[3] W. D. Wilson, L. G. Haggmark and J. P. Biersack *Phys. Rev.*, B 15, 2458, (1977).

[4] D. J. O'Connor and J. P. Biersack ,*Nuclear. Instrum. Methods*, B 15, 14, (1986).

[5] J. Lindhard *Kgl. Danske. Videnskab. Selskab. Mat. Fys. Medd.*, 36, No.10, (1968).

[6] P. T. Wedepohl *Solid. Stat. Comm.*, 4, 479, (1966).

[7] P. T. Wedepohl *J. Phys. B,* 1, 307, (1968).

[8] R. A. Johnson *J. Phys. F: Met. Phys,* 3, 295, (1973).

[9] J. Lindhard *Kgl. Danske. Videnskab. Selskab. Mat. Fys. Medd.*, 34, No.14, (1965).

[10] A. P. Pathak *Radiat.Eff.*, 61,1 (1982).

[11] A. P. Pathak *phys. stat. sol. (b).* 93, K 181, (1979).

[12] S. Datz, B. R. Appleton and C. D. Moak *Channeling, Theory, Observation and Applications,* ed. D. V. Morgan, (John Wiley & Sons, London) (1973).

[13] M. T. Robinson *Phys. Rev.* **179,** 327, (1969).

[14] A. P. Pathak *phys. stat. sol. (b).* 86, 751 (1978).

[15] A. P. Pathak *J. Phys. C: Solid State Phys.* 8, L341, (1975).

[16] A. P. Pathak *phys. stat. sol. (b).* 71, K35, (1975).

[17] R. Agnihotri and A. P. Pathak *Nuclear. Instrum. Methods.* B **67,** 39, (1992).

[18] J. S. Briggs and A. P. Pathak *J. Phys. C: Solid State Phys.* , 6, L153, (1973).

[19] J. S. Briggs and A. P. Pathak *J. Phys. C: Solid State Phys.* , 7, 1929, (1974).

[20] A. P. Pathak *J. Phys. F: Met. Phys,* 4, 1883, (1974).

[21] A. P. Pathak *Phys. Rev.* B 22, 96, (1980).

[22] V. Harikumar, A. P. Pathak and R. Agnihotri *Proceedings of DAE Solid State Physics Symposium (Varanasi,India)* 34 C, 157, 1991.

[23] V. Hari kumar and A. P. Pathak *phys. stat. sol (b),* 177, 269, (1993).

[24] E. Clementi and D. L. Raimondi *J. Chem. Phys.* 38, 2686, (1963).

[25] E. Clementi, D. L. Raimondi and W. P. Reinhardt *J. Chem Phys.* 47, 1300, (1967).

[26] I. S. Gradshteyn and I. M. Ryzhik *Tables of Integrals, Series and Products* (Academic Press, Orlando (Florida)),(1980), (page.322) .

[27] G. Moliere *Z. Naturforschung,* A 2,133, (1947).

[28] J. F. Ziegler, J. P. Biersack and U. Littmark *Stopping and Ranges of Ions in Matter,* Vol. 1 Eds., J. F. Ziegler, (Pergamon, New York) (1984).

[29] N. Bohr *Kgl. Danske. Videnskab. Selskab. Mat. Fys. Medd,* 18, 8, (1948).

[30] V. Hari kumar and A. P. Pathak *phys. stat. sol.* 6, 182, 51, (1994).

[31] A. P. Pathak and V. Hari kumar *Nucl. Instrum. and Methods,* B, (1995) (in press).

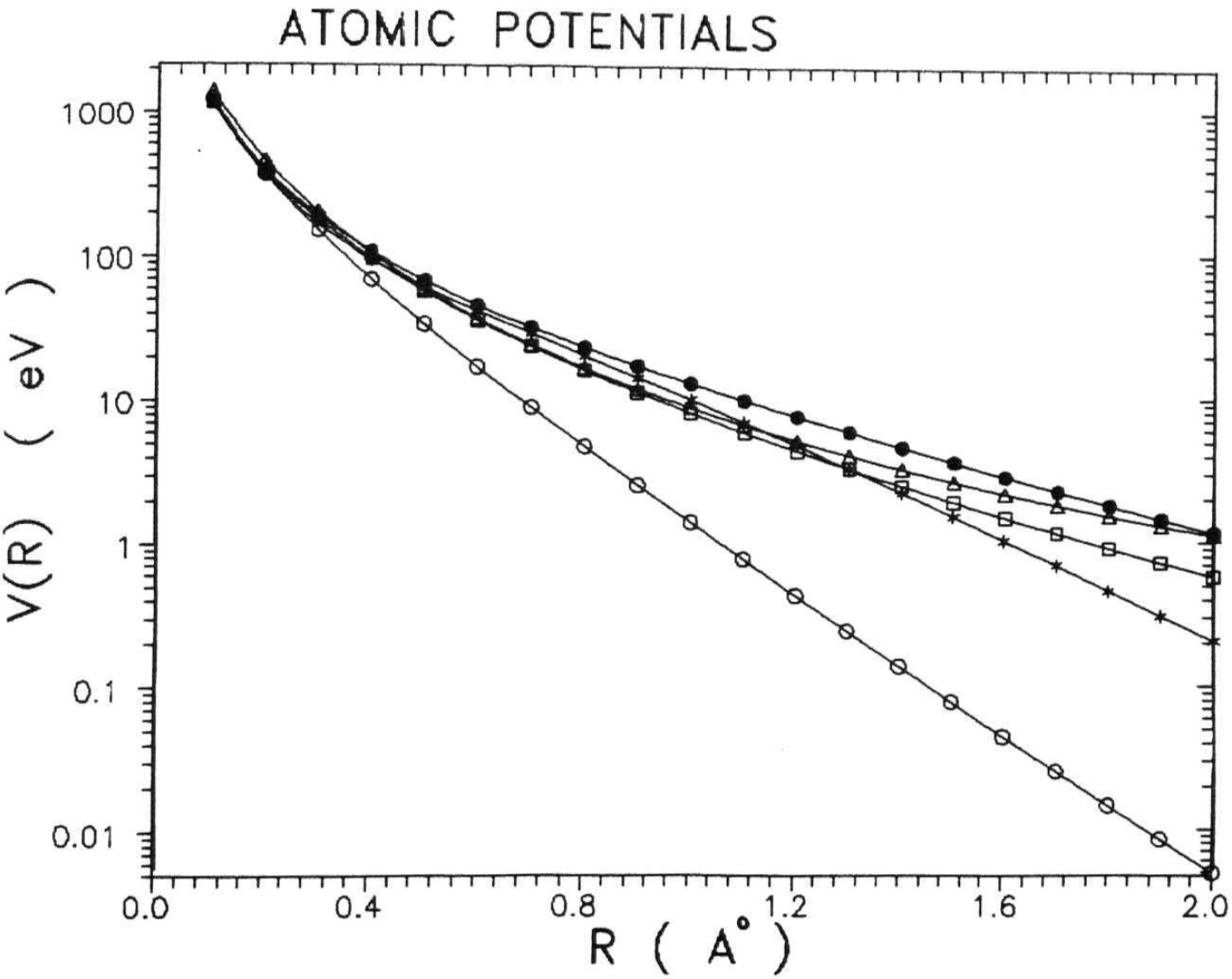

Fig **3.1:** **Moliere(** •), Lindhard (Δ), **Biersack's** Universal (D), **Bohr** (o) and Shell (*) *interatomic potentials* as a function of the interatomic distance (A) for *protons* in ***Silicon.***

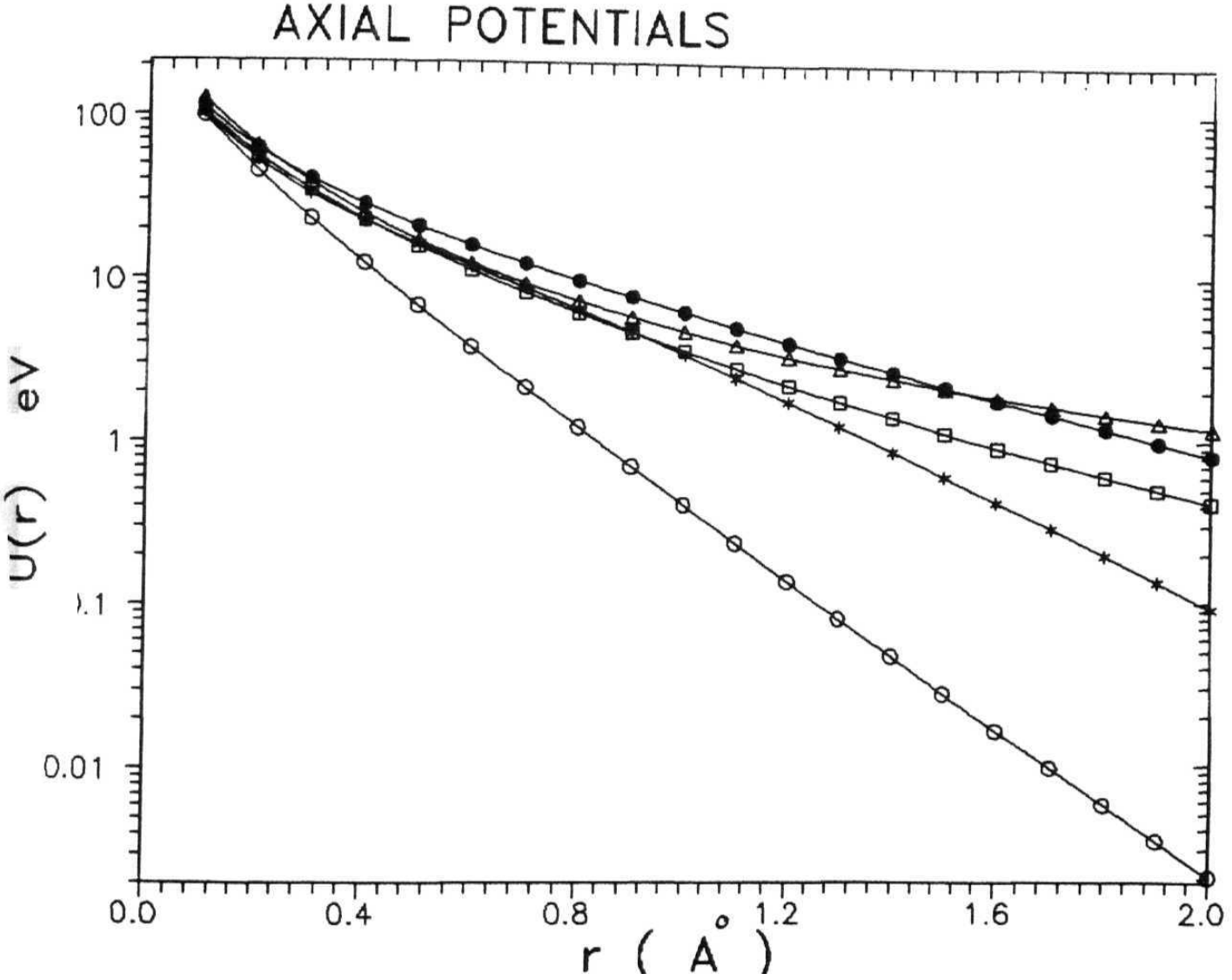

Fig 3.2: Moliere(•), Lindhard (Δ), Biersack's Universal (□), Bohr (o) and Shell (*) *axial potentials* as a function of distance (r) from the string along the < 110 > axial channel for *protons* in *Silicon*

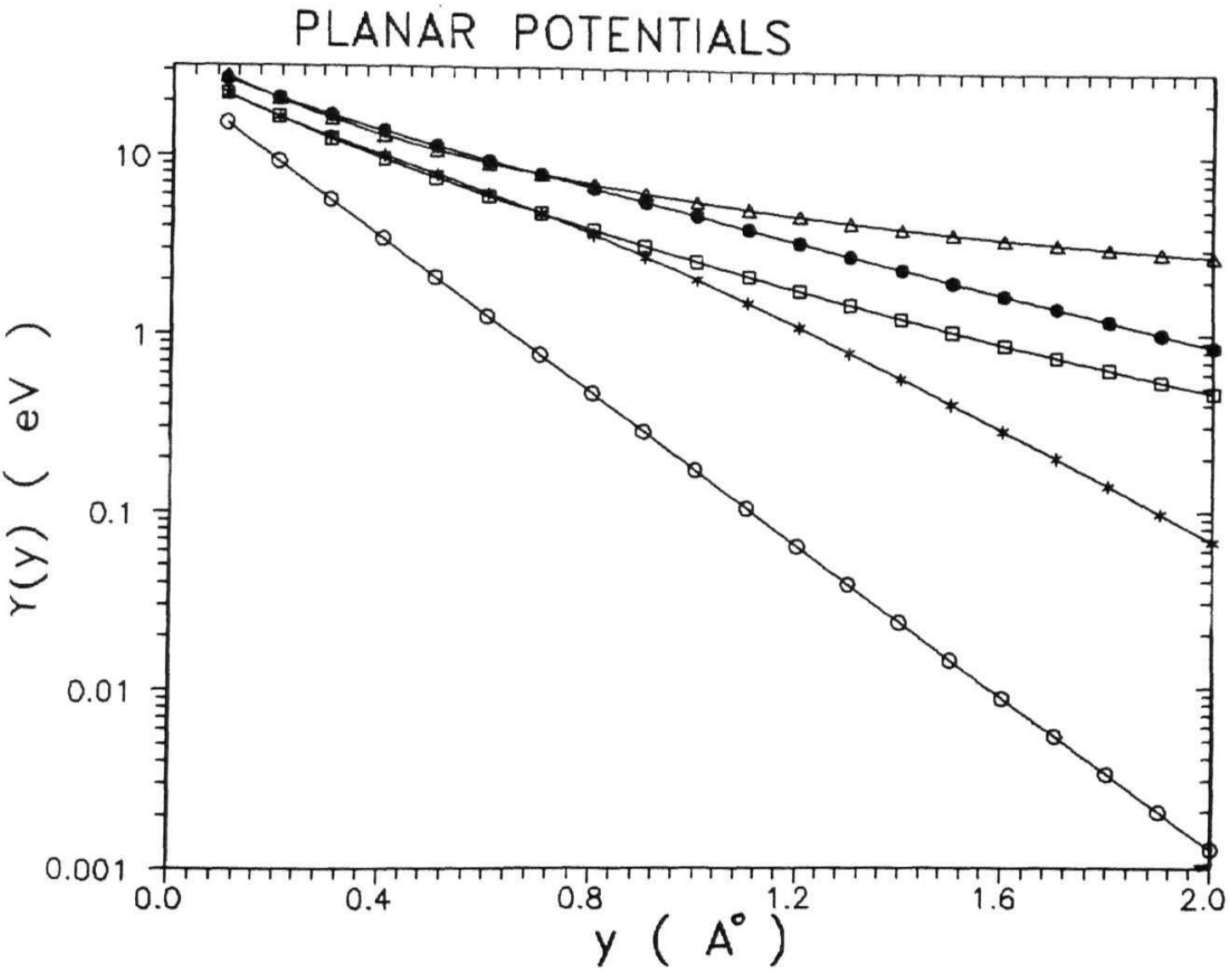

Fig 3.3: Moliere(•), Lindhard (Δ), Biersack's Universal (□), Bohr (o) and Shell (*) *planar potentials* along the (110) plane as a function of the distance from the plane (*y*) for *protons* in *Silicon*.

Chapter 4

ELECTRONIC STOPPING POWER (Channeling Case)

4.1 INTRODUCTION

In the previous chapter, we have introduced shell model charge density based on the wave functions of Clementi *et al.* [1,2]. Corresponding shell model interatomic potential and continuum potentials were derived [3] and these potentials were shown to be in good agreement with other screened coulomb type potentials. Even though Clementi wave functions form a more physically acceptable basis for determining the potential between a charged particle and a free atom, one should verify its usefulness in applications in different areas of channeling studies. Since channeling phenomenon arises basically because all collisions with target atoms are avoided and projectile ion interacts only with the electron in the solid, a fundamental quantity like charge density derived from Clementi wave functions [1,2] should yield good results for physical quantities of interest. Shell model charge density can be successfully used in position dependent stopping power calculations for both planar [4-6] and axial [7] cases. Stopping power calculations using shell charge densities give better results compared to *Lindhard's local density approximation* [8], where one calculates local electronic stopping power using local electron density obtained from Lindhard's statistical charge densities. In our theory independent contribution of each electron is taken into account for calculating local electronic stopping power.

An introduction to position dependence of stopping power is given in section 4.2 and the problems concerning the position dependence of stopping power in planar and axial cases are discussed rigorously in section 4.2.1 and 4.2.2 respectively. Results are summarized in the last section.

4.2 POSITION DEPENDENCE OF STOPPING POWER

It has been already established from various experimental and theoretical studies [8–14] that the rate of electronic energy loss during the channeling of charged particles is approximately half of the random energy loss. This is infact not surprising, because channeling particle avoids the large angle scattering by atoms on the normal lattice sites of the crystal [8] and it feels only a collective continuum potential due to lattice atoms which steers the particle deep in to the crystal planes or axis. Extensive experimental studies [15-17] of the channeling of lighter and heavier ions were made for both planar and axial cases and the position dependence of stopping power for planar case was deduced. An accurate knowledge of position dependence of stopping power of ions is very essential when one is concerned with the effects of defects on the energy loss of channeled particle. Hence the position dependence of stopping power is calculated using both shell planar and shell axial charge densities and compared with experimental and other theoretical formalisms in the following sections.

4.2.1 PLANAR CASE

Robinson has proposed an anharmonic oscillator model [10,11] for explaining the energy loss - spectra produced in beams of energetic ^4He and ^{127}I ions transmitted through planar channels in thin *Au* single crystal [18–21]. Position dependence of stopping power of planar channeled ions has been deduced by the comparison of his anharmonic oscillator

model with planar channeling experiments based on the observation that the stopping power of these ions were proportional to the transverse oscillation frequency of the ions. According to this anharmonic oscillator model, the planar electronic stopping power $S_E^{pl}(x)$ as a function of the distance from the midpoint of two channel can be written as

$$S_E^{pl}(x) = s_o + s_1(\sigma(x) - 1) \tag{4.1}$$

where s_o and s_1 are energy dependent quantities (but they are independent of x) and should be determined experimentally. The position dependent function $\sigma(x)$ is given by

$$\sigma(x) = \frac{d}{dx} \left[\frac{2}{Y_2''(0)}(Y_2(x) - Y_2(0))^{1/2}\right] \quad 0 \leq x \leq l \tag{4.2}$$

vvhere $Y_2(x)$ is the planar potential due to both the planes separated by a distance d_p — 2/ and primes denote differentiation with respect to x. To reduce the complexities of function *cr(x)* for most of the conventional interatomic potentials, *Robinson* used the long range term of the three term Moliere potential (chapter 3, equation 3.15 &3.17) and $\sigma(x)$ reduced to [11]

$$\sigma(x) = \cosh\left(\frac{b_1\, x}{2}\right) \tag{4.3}$$

This expression is valid only near the middle of the channel, because for large x one should include other two terms of Moliere potential.

A more detailed quantum mechanical treatment accounting for transition probabilities of bound electron in crystal incorporating the transitional probability of ionizations was found to give a still faster variation of $S_E^{pl}(x)$ with *x* [22]. Although *Detmann et. al.* [12] and *Esbensen et al.* [13] formulated an impact parameter method which is derived from first priniciples, do not take into account of the independent electron contribution. Even after the inclusion of independent electron contribution [23], this modification was aimed only at calculating stopping power of hyperchanneled particles, so the results can be

compared only with that type of experiments. More recently *Namiki et al* [24] introduced a quantum treatment incorporating shell corrections and independent contribution of bound electrons to the energy loss. A short description of electronic stopping power calculations using shell planar and axial charge densities are given below.The results are compared with results obtained using above mentioned different formalisms in both planar and axial cases respectively.

To calculate the electronic stopping power S_E from theoretical consideration, one should add the stopping power contribution from conduction, valence and core (bound) electrons. The conduction electrons can be assumed to form uniform electron gas and their contribution to stopping power is thus position - independent and is given by [12,25]

$$S_{E,cond} = \frac{4\ \pi\ Z_1^2\ e^4}{m\ v^2}\ \ \rho_{cond}\ \ \ln\ \frac{2mv^2}{\hbar\omega_p} \tag{4.4}$$

where Z_1 is the atomic number of incident ion, e is the electron charge, m is the electron mass, v is the ion velocity, $\hbar\omega_p$ is the plasmon energy due to the conduction electron of uniform density ρ_{cond} and the plasmon frequency ω_p is given by

$$\omega_p = \sqrt{\frac{4\ \pi\ \rho_{cond}\ e^2}{m}} \tag{4.5}$$

Based on the theory of *Bohm* and *Pines* [26], *Appleton et. al* [9] divided the total contribution to stopping power due to valence electrons (considered as Fermi gas) in to two parts, one due to collective plasma oscillations (which uses the total density of valence electron ρ_{val}) and second due to single particle excitation (which uses local electron density ρ_{loc}) • The valence electrons contribution to the total electronic stopping power can be written as

$$S_{E,val} = \frac{4\ \pi\ Z_1^2\ e^4}{m\ v^2}\ \ [\rho_{val} \ln \frac{v}{v_F} + \rho_{loc}(x)\frac{2mvv_F}{I}] \tag{4.6}$$

where v_F is the Fermi velocity, / is the average binding energy of the valence shell. Fermi

velocity v_F is given by

$$v_F = \frac{\hbar}{m}(3\pi^2 \rho_{val})^{1/3} \tag{4.7}$$

The contribution from core (bound) electrons can be formulated based on the kinetics of scattering of bound electrons. According to the procedure adopted by *Briggs* and *Pathak* [27] one should first calculate the local electron density due to each shell at the position of moving charged particle and then one considers the direct scattering of this electron density from the propagating particle. The minimum energy that these electrons could take away from the moving particle will be their binding energies in the shell and maximum is ofcourse $2mv^2$ [4]. We have used one term slater orbital with optimized exponents given by *Clementi et al* [1,2] to calculate effective electron density as function of position in the channel. Using continuum approximation (ie by averaging the charge density equation (3.1) for whole plane), we can calculate the electron density at a distance *y* from the plane. The planar shell charge density at a distance *y* from single plane is given by (*chapter 3* equation 3.4)

$$\rho_S^{pl}(y) = \frac{N\ d_p}{2} \sum_j \frac{(2\ \xi_j)^{2n_j}}{2\ n_j}\ \omega_j\ e^{-2\xi_j y} \sum_{k=o}^{2n_j-1} \frac{y^{2n_j-1-k}}{(2\ \xi_j)^k (2n_j-1-k)!} \tag{4.8}$$

We have used Lindhard planar charge density [34] for comparing the stopping power results calculated using shell planar density (eq. 4.8). Lindhard planar charge density is given by

$$\rho_L^{pl}(y) = \frac{Z_2\ N\ d_p}{2} \frac{C^2 a_T^2}{(y^2\ +\ C^2 a_T^2)^{3/2}} \tag{4.9}$$

where a_T is the *Thomas- Fermi* screening radius and $C\ \{= \sqrt{3}\}$ is the *Lindhard* constant. Using these equations (eq. 4.8 & 4.9) we can calculate the electron density due to both planes surrounding the channel at a distance *x* from the half way point between the plane and is given by

$$\rho_2^{pl}(x) = \rho_1\left(\frac{d_p}{2} - x\right) + \rho_1\left(\frac{d_p}{2} + x\right) \tag{4.10}$$

where $\rho_1(x)$ is the planar charge density due to one plane by equation (4.8 & 4.9). The planar charge density ρ_2 *(x)* due to two *Si* (111) planes calculated using Shell and Lindhard planar charge densities are shown in Fig. 4.1. Thus the contribution from core electrons becomes

$$S_{E,core} = \frac{4\ \pi\ Z_1^2\ e^4}{m\ v^2} \sum_j \rho_2^{pl}(x) \ln \frac{2mv^2}{I_j} \tag{4.11}$$

Total electronic stopping power due to conduction, valence and core electrons can be written as

$$S_E^{pl} = \frac{4\ \pi\ Z_1^2\ e^4}{m\ v^2} \left[\rho_{cond} \ln \frac{2mv^2}{\hbar\omega_p} + \rho_{val} \ln \frac{v}{v_F} + \rho_{loc}(x) \frac{2mvv_F}{I} + \sum_j \rho_{2,j}^{pl}(x) \ln \frac{2mv^2}{I_j}\right] \tag{4.12}$$

We have used equation 4.12 to calculate the variation of planar stopping power of GO MeV ^{127}I ions in the $Au(100)$ channel as a function of *x*. The results are also compared with *Robinson's* [10,11] calculations based on experimental observations [18,20] and also the results based on quantum mechanical treatment of *Ohtsuki* and *Kitagawa* [29]. This is shown in Fig. 4.2. *Robinson* has not used the short range terms of Moliere interatomic potential [28,30] to calculate the position - dependent function $\sigma(x)$ (eq. 4.3) because of the complication involved with formalism and there is a need for improvement in this model for large values of *x* [5]. Other factor of disagreement arises from the fact that we didn't incorporate any exchange effects in inner electron excitations as has been suggested by *Ohtsuki et al* [31].

We have calculated the stopping power of 4.8 MeV α particles channeled along *Au* (111) planes and found that the stopping power of well channeled particles was 15.28 *ev/A* which compare well with the experimental value of 16.50 $ev/\AA$ obtained in the experiments of *Mory* [32]. The binding energies of different shells were taken from reference [33]. Then we calculated the position dependence of the stopping power of 3 MeV a particles channeled along *Au* (100) planes as a function of *x*. This is shown in Fig. 4.3. It is found that inner shells start contributing for $x > 0.6\ d_p/2$ where d_p is the

interplanar spacing $(d_p/2 = 1.0197\AA)$. We have compared our results with results of *Robinson* **[10,11]** and those of *Namiki et. al.* [24]. Near the planes the results based on quantum perturbation theory [22] overestimate the *Robinson*'s curve and our results are in good agreement with the calculations of *Namiki et. al.* We have also calculated the stopping power of a particles channeled along (111) planes of *Si* . Results are compared with experimental [35] and theoretical calculation using Lindhard charge density. This is shown in Fig.4.4.

4.2.2 AXIAL CASE

We have calculated the position dependence of stopping power for axially channeled particles incorporating detailed atomic shell structure electron densities and averaging along the axis to obtain the axial electron density at the position of moving particle. The axial shell charge density at a distance *r* from the string is given by *(chapter 3* ,equation 3.3),

$$\rho_S^{ax}(r) = \frac{1}{\pi d}\sum_j \frac{\omega}{(2nj)!}\sum_{m=o}^{n_j-1}\frac{2^{2m}(2(n_j-m))!(n_j-1)!(\xi_j)^{n_j+m+2}r^{n_j+m}K_{n_j-m}(2\xi_j r)}{(n_j-m-\frac{1}{2})(n_j-m)(m)!((n_j-m-1)!\ )^2} \tag{4.13}$$

We have also used Lindhard axial charge density for position dependent axial stopping power calculations. The Lindhard axial charge density is given by [34]

$$\rho_L^{ax}(y) = \frac{Z_2}{\pi\ d}\ \frac{C^2a_T^2}{(r^2\ +\ C^2a_T^2)^2} \tag{4.14}$$

When a charge particle is channeled along a major crystallographic direction of the target material it will see only the geometry of the channel axis and not the whole structure of the target material. The physical effects realized by the charged particle will therefore depend on the geometry of the channel, so that under the channeling conditions

the number density of target atoms seen by the projectile will differ from that of the bulk density of atoms. For elucidating this point we have taken a specific example of *Si* < 110 > case. When the incident charged particle (α particle or proton) is moving along a < 110 > axial direction of silicon single crystal, it will see only the six strings of silicon atoms around it (shown in Fig.4.5) and will not see the whole crystal structure. Therefore the number density seen by projectile will differ from that of bulk density of target atoms. Hence the contribution of the valence electrons to the stopping power due to collective plasma oscillations is not the same for channeled and random impact [3].

In silicon crystals the < 110 > axial channel is very nearly symmetric and we can approximate that six rows form a regular hexagon (Fig.4.5). If r' is measured from the centre of channel 0, the electron density due to all strings with respect to *0* will be

$$\begin{aligned}\rho_S^{ax}(r') &= \frac{1}{\pi d}\sum_{p=1}^{6}\sum_{j}\frac{\omega}{(2nj)!}\sum_{m=o}^{n_j-1}\frac{2^{2m}(2(n_j-m))!(n_j-1)!(\xi_j)^{n_j+m+2}}{(n_j-m-\frac{1}{2})(n_j-m)(m)!((n_j-m-1)!\ )^2} \\ &\times\sqrt{r'^2+R_o^2-2R_o r'\cos(\frac{p\pi}{3})^{n_j+m}} \\ &\times K_{n_j-m}(2\xi_j\sqrt{r'^2+R_o^2-2R_o r'\cos(\frac{p\pi}{3})}) \qquad (4.15)\end{aligned}$$

The number density of target atoms seen by the projectile inside < 110 > axial channel of silicon is taken to be given by the phenomenological expression for the number density

$$n_e(r') = \frac{1}{\pi d}\sum_{p=1}^{6}\frac{1}{\left(r'^2+R_o^2-2r'R_0\cos(\frac{p\pi}{3})\right)} \qquad (4.16)$$

where r' is the distance measured from the channel axis and R_o is the radius of hexagon (shown in Fig 4.5). Therefore the effective valence electron density at any point inside the *Si* < 110 > channel is

$$\rho_{val}^{ax}(r') = 4n_e(r') \qquad (4.17)$$

It is evident from the above equation that the valence electrons contribution to stopping power due to plasma oscillations is position dependent. The Shell and Lindhard charge

densities for *Si* < 110 > axis are plotted in Fig 4.6. To calculate axial electronic stopping power of *Si* < 110 >, the $\rho_2^{pl}(x)$ (eq. 4.10) should be replaced by $\rho_s^{ax}(r')$ (eq. 4.15).

We have estimated the variation of normalized stopping power for 160 MeV α particles using Lindhard and Shell charge densities as a function of the distance r' from the centre of the < 110 > axial channel in silicon. This is plotted in Fig. 4.7. The agreement with earlier more detailed numerical calculation [13] which do not yield usable analytical expressions, was found to be good as shown in Fig. 4.7. The statistical charge densities obtained from Lindhard's formulations are much too fast as shown in the same figure.

We have calculated the position dependence of the stopping power of 160 MeV α particles along *Si* < 110 > direction and tabulated the stopping power contribution from Plasmons, Valence and Core electron contribution to the total stopping power in the *Table 4.1.* The results are compared with experimental data [16] and earlier theoretical results [13,23]. We have also calculated the electronic stopping power for the same case using a position independent number density. The table shows good agreement with experimental results for calculations incorporating position dependent number density. This justifies our argument that under channeling conditions the number density of target atoms seen by the projectile will differ from that of the bulk density of atoms. Similar calculations were done for stopping power of 4 MeV protons channeled along < 110 > axis of silicon single crystal. The results are compared with experimental data [36] and earlier theoretical calculations [12,23]. We do not observe any considerable contribution from core shells as mentioned by *Beloshitsky et. al.* [37] and even half way between channel centre and axis, the contribution from core shells are negligible and most of the contributions come from Plasmon excitations. This case is tabulated in *Table 4.2.*

We also calculated the channeling energy losses of α particles in the energy range from 0.15 to 18 MeV along the < 110 > axis in silicon and compared with experimental [35] results and stopping power calculation using Lindhard charge density. Electronic stopping

power **calculations** using shell charge density compare well with the experimental results than those obtained by using Lindhard charge density. This is shown in Fig.4.8. We have plotted proton channeling energy losses in silicon in the intermediate energy region (40 to **300** keV) in Fig.4.9. Our calculated values lie in between the most probable and best channeled particles. Of course we did not use the thickness as parameter in our calculation, but we adopted an analytical method rather than an iteration method to calculate stopping power. The calculations were done using shell and Lindhard charge densities and the results were compared with experimental data [38]. We also compared our calculation for proton stopping power for < 110 > Si in the energy range of 30 - 1000 keV with experimental results of *Camera et. al.* [39]. Eventhough the maximum stopping-power occurs at same energy range ($\sim$ 70 keV), magnitude of maximum stopping power is underestimated in shell calculations. This is shown in Fig. 4.10.

4.3 CONCLUSION

The effective electron density used for stopping power calculations in both axial and planar case were derived by taking the respective average density due to different shells of target atoms. The position dependence of stopping power thus obtained is in good agreement with experiments [14,16,35,36,38] and earlier theoretical calculations [12,13,22-24]. Inspite of the fact that the impact-parameter dependence of stopping power is more important in channeling case, this method which is based on quantum perturbation theory shows disagreement in comparison with *Robinson* fitting function (equation 4.3) near the atomic string or wall. Although our work is based on phenomenological theory, we have incorporated independent contribution of each electron to the total stopping power. Many of the earlier mentioned quantum mechanical treatment overlooked this fact. Our theory has been firmly and essentially confirmed by the quantum mechanical theory

developed by *Namiki et. al.* [24].

References

[1] E. Clementi and D. L. Raimondi *J. Chem. Phys.* 38, 2686, (1963).

[2] E. dementi, D. L. Raimondi and W. P. Reinhardt *J. ChemPhys.* 47, 1300, (1967).

[3] V. Hari kumar and A. P. Pathak *phys. stat. sol. (b),* **177,** 269, (1993).

[4] A. P. Pathak *phys. stat. sol. (b).* 86, 751 (1978).

[5] A. P. Pathak *J. Phys. C: Solid State Phys.* 8, L341, (1975).

[6] A. P. Pathak *phys. stat. sol. (b).* **71,** K35, (1975).

[7] R. Agnihotri and A. P. Pathak *Nuclear. Instrum.Methods.* B **67,** 39, (1992).

[8] J. Lindhard *Kgl. Danske. Videnskab. Selskab. Mat. Fys. Medd.,* 34, No.14, (1965).

[9] B. R. Appleton, C. Erginsoy and W. M. Gibson *Phys. Rev* **161,** 330, (1967).

[10] M. T. Robinson *Phys. Rev.* **179,** 327, (1969).

[11] M. T. Robinson *Phys. Rev.* B 4, 1461, (1972).

[12] K. Dettmann and M. T. Robinson *Phys. Rev.*, B 10, 1, (1974).

[13] H. Esbensen and J. A. Golovchenko, *Nucl. Phys.*, A **298,** 382, (1978).

[14] O. N. Jarvis, A. C. Sherwood and C. Whitehead *Radiat.Eff.*, 36, 215, (1978).

[15] J. D. Melvin and T. A. Tombrello, *Radial Eff.*, 26, 113, (1975).

[16] O. N. Jarvis, A. C. Sherwood, C. Whitehead and M. W. Lucas *Phys. Rev.*, B 16, 3880, (1977).

[17] C. D. Moak, J. Gomez del Campo, J. A. Biggerstaff, S. Datz, P. F. Dittner, H. F. Krause and P. D. Miller *Phys. Rev.* B 25, 4406, (1982).

[18] H. O. Lutz, S. Datz, C. D. Moak and T. S. Noggle *Phys. Rev. Letters* **17,** 285, (1966).

[19] W. M. Gibson, J. B. Ramussen, P. Ambrosius - Olesen and C. J. Andreen *Can. J. Phys.* 46, 551, (1968).

[20] S. Datz, C. D. Moak, T. S. Noggle, B. R. Appleton and H. 0. Lutz *Phys. Rev.* 179, 315, (1969).

[21] B. R. Appleton, S. Datz, C. D. Moak and M. T. Robinson *Phys. Rev.* B 4, 1452, (1972).

[22] M. Kitagawa and Y. H. Ohtsuki *Phys. Rev.* B 5, 3418, (1972).

[23] K. Dettmann *Z. Phys.* A **272,** 227, (1975).

[24] S. Namiki, H. Nitta and Y. H. Ohtsuki *Phys. Rev.*, B 37, 1448, (1988).

[25] P. Nozieres and D. Pines *Nuovo Cimento*,9, 470, (1958).

[26] D. Pines *Elementary Excitations in Solids* (Benjamin, New York) (1963).

[27] J. S. Briggs and A. P. Pathak *Atomic Collisions in Solids* Ed. S. Datz, B. R. Appleton and C. D. Moak, (Plenum Press, New York) (1975) (page 15).

[28] A. P. Pathak *Radiat.Eff.*, **61,1** (1982).

[29] Y. H. Ohtsuki and M. Kitagawa *Phys. Lett* 40 A, 313, (1972).

[30] G. Moliere *Z. Naturforschung,* A 2,133, (1947).

[31] Y. H. Ohtsuki and M. Kitagawa *phys. stat. sol. (b),* 51, K19, (1972).

[32] J. Mory *Rapport-Commissariat a V Energie Atomique*, (CEA France) Fontenay-aux-Roses, R4745 (1975).

[33] *CRC Handbook of Chemistry and Physics* ed. Robert C. Weast. (CRC Press, Inc.) (Florida) (1987).

[34] A. P. Pathak *phys. stat. sol. (b),* **144,** K177, (1982).

[35] F. H. Eisen, G. J. Clark, J. B0ttiger and J. M. Poate *Radial. Eff.* 13, 93, (1972).

[36] G. J. Clark, D. V. Morgan and J. M. Poate *Atomic Collisions in Solids* eds. D. W. Palmer, M. W. Thompson and P.D. Townsend (Norh Holland Publishing Co., Amsterdam) (1970) (page 388).

[37] V. V. Beloshitsky and M. A. Kumakhov *Radiat. Eff.*, 35,209, (1978).

[38] P. Gehrmann, K. Lenkeit and R. Stolle *phys. stat. sol.(b).,* **131,** 519, (1985).

[39] A. Carnera, G. Delia Mea A. V. Drigo, S. Lo Russo, P. Mazzoldi and G. G. Bentini *Phys. Rev.*, B **17,** 3492 (1978).

Position dependent stopping power of 160 MeV α particles channeled along the < 110 > axis in *Silicon* and comparison with other theoretical and experimental results.

Table - 4.1

	r'	*STOPPING POWER (eV/Å)*			
		Contribution from			
		Plasmons	Valence	Core	Total
Shell	0.0 R_o	0.39	0.05	0.0	0.44
	0.1 R_o	0.40	0.06	0.0	0.46
(S_E^{os})	0.2 R_o	0.41	0.07	0.0	0.48
	0.3 R_o	0.43	0.11	0.0	0.54
	0.4 R_o	0.46	0.16	0.0	0.62
	0.5 R_o	0.52	0.23	0.0	0.75
Shell	0.0 R_o	0.18	0.05	0.0	0.23
	0.1 R_o	0.18	0.06	0.0	0.24
($S_E^{'os}$)	0.2 R_o	0.18	0.07	0.0	0.25
	0.3 R_o	0.18	0.10	0.0	0.28
	0.4 R_o	0.18	0.15	0.0	0.33
	0.5 R_o	0.18	0.21	0.0	0.39

Dettmann [23] = 0.58 $eV/Å$, Esbensen [13] = 0.37 $eV/Å$, Jarvis [16] = 0.54 $eV/Å$.

S_E^{os} → Stopping Power contributions from Plasmon electrons are *position dependent.*

$S_E^{'os}$ → Stopping Power contributions from Plasmon electrons are *position independent.*

Position dependent stopping power of 4 MeV *protons* particles channeled **along the** < 110 > axis in *Silicon* and comparison with other theoretical and experimental results.

Table - 4.2

	r'	*STOPPING POWER (eV/Å)*			
		Contribution from			
		Plasmons	Valence	Core	Total
Beloshitsky		0.31	0.10	0.19	0.60
Shell	0.0 R_o	0.66	0.11	0.0	0.77
	0.1 R_o	0.66	0.12	0.0	0.78
(S_E^{ax})	0.2 R_o	0.68	0.16	0.0	0.84
	0.3 R_o	0.71	0.22	0.0	0.93
	0.4 R_o	0.77	0.32	0.0	1.09
	0.5 R_o	0.86	0.46	0.0	1.32
Shell	0.0 R_o	0.31	0.10	0.0	0.41
	0.1 R_o	0.31	0.11	0.0	0.42
$(S_E'^{ax})$	0.2 R_o	0.31	0.14	0.0	0.45
	0.3 R_o	0.31	0.20	0.0	0.51
	0.4 R_o	0.31	0.30	0.0	0.61
	0.5 R_o	0.31	0.42	0.0	0.73

Dettmann [23] = 0.82 $eV/Å$, Dettmann [12] = 0.74 $eV/Å$, Clark [36] = 0.68 $eV/Å$.

S_E^{ax} → Stopping Power contributions from Plasmon electrons are *position dependent.*

$S_E'^{ax}$ → Stopping Power contributions from Plasmon electrons are *position independent.*

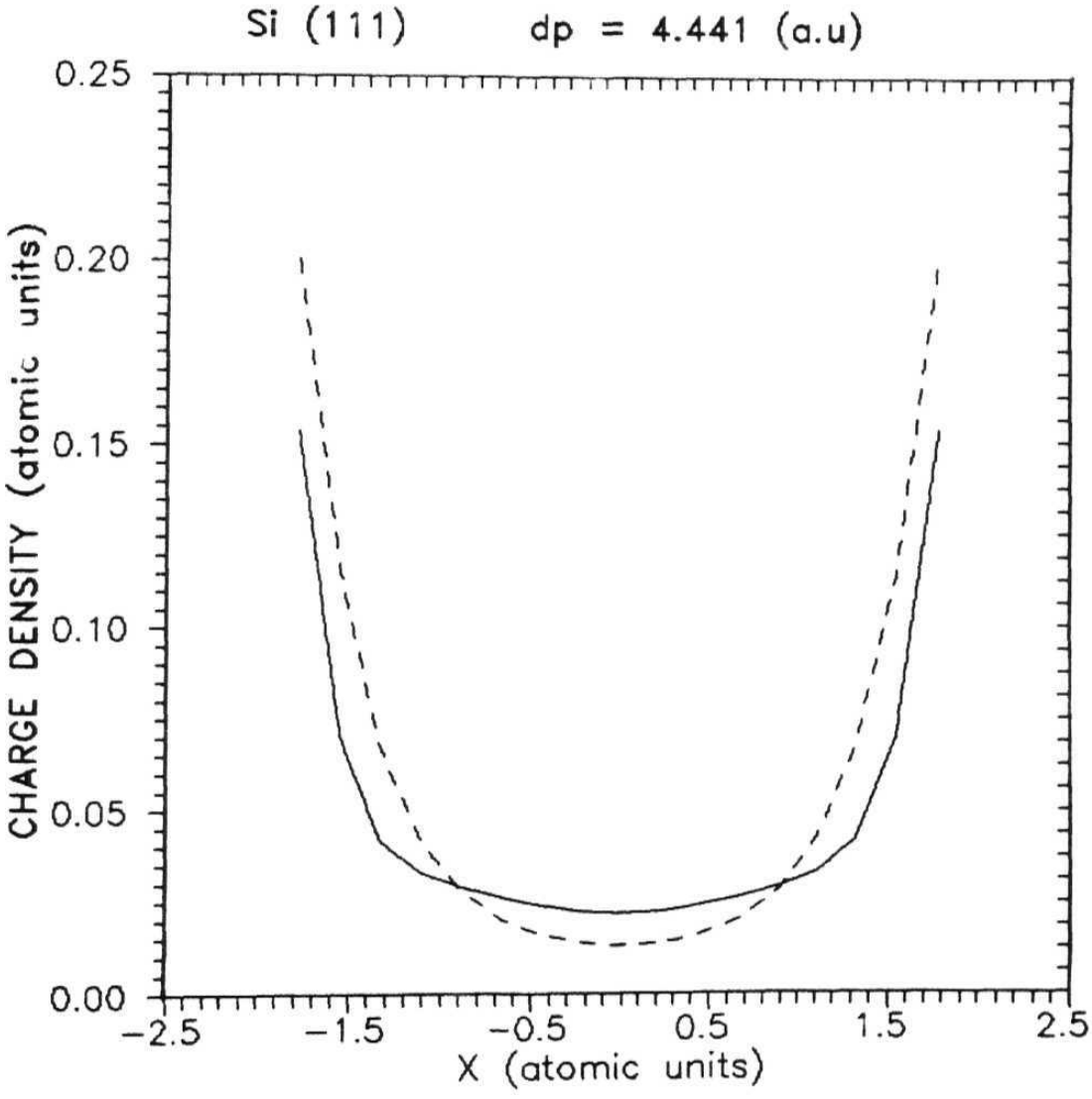

Fig 4.1: ***Charge density*** **due to two planes surrounding the (111) planar channel as a function of z, where z is measured from midpoint of the two planes.** ***Solid curve*** **represents *Shell planar charge density* calculation and *dashed curve* represents *Lindhard planar charge density* calculation.**

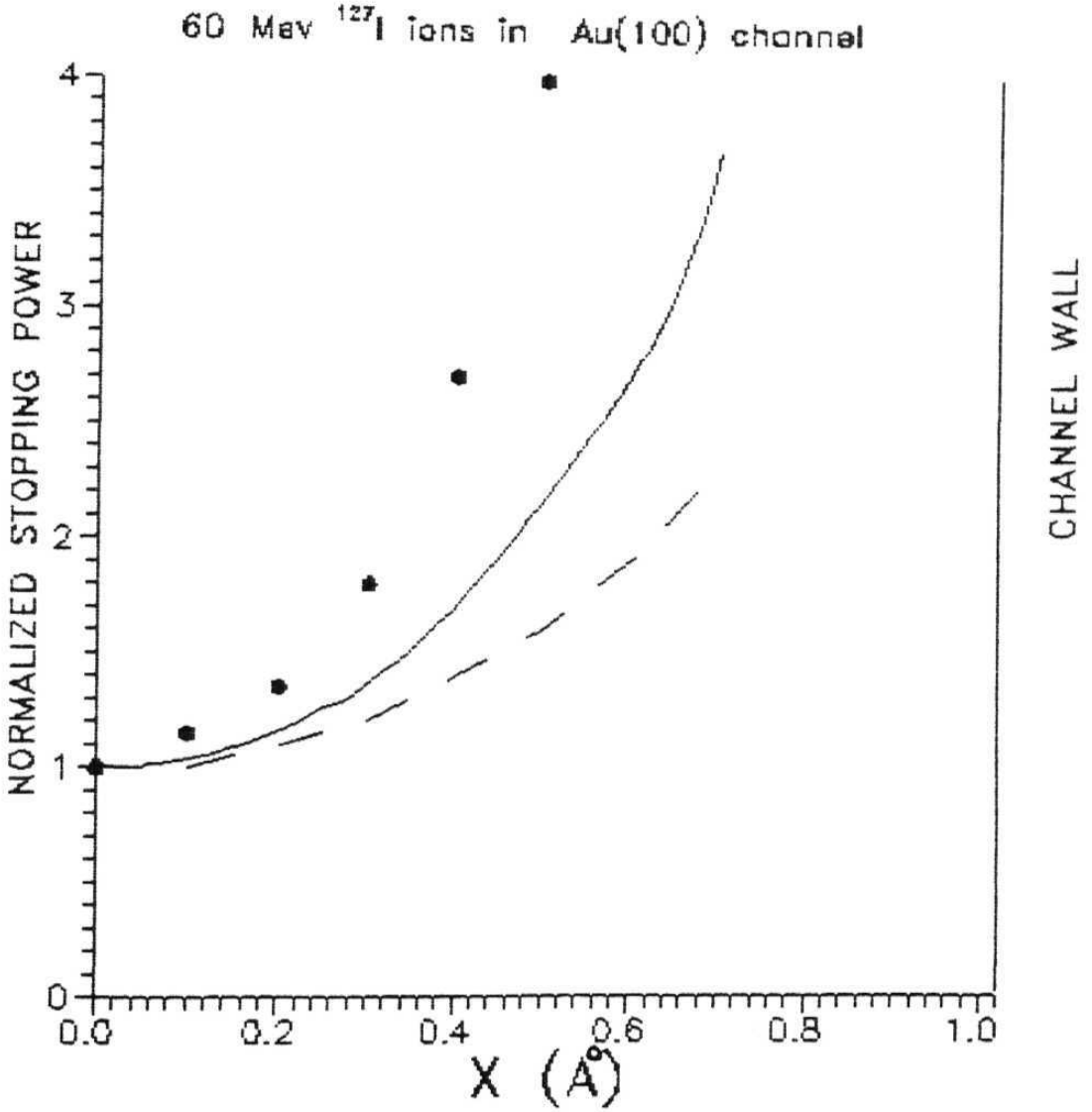

Fig 4.2: Variation of planar stopping power of 60 *MeV* ^{127}I ions in *Au* (100) channel. (•) represents *Ohtsuki and Kitgawa* (local density approximation), dashed curve represents *Robinson's* result and *solid curve* represents results obtained using *shell planar charge density.*

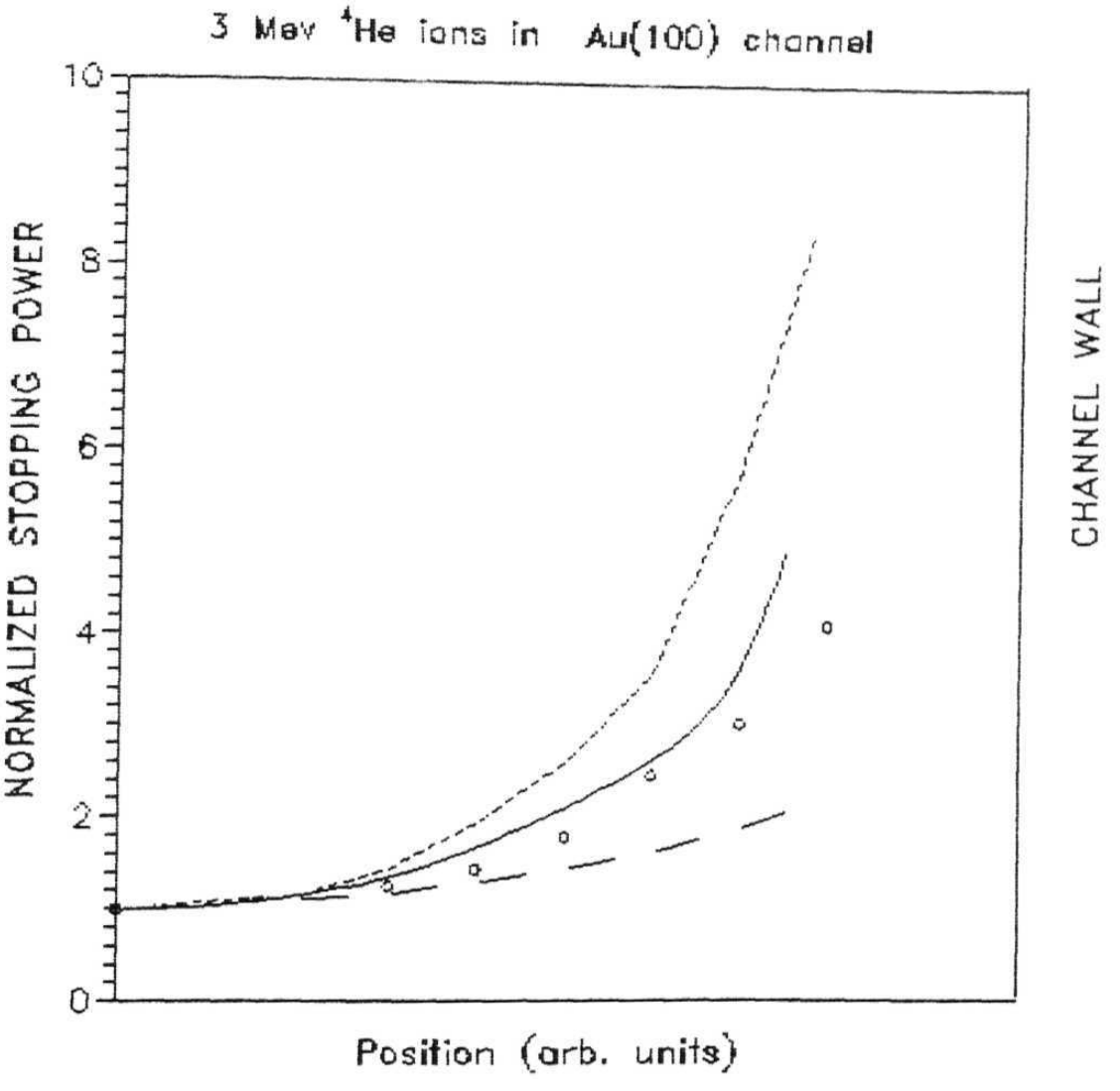

Fig 4.3: Position dependence of normalised stopping power with distance x from the mid-point between the channeling planes for 3 *MeV* α particles incident along *Au* (100) channel. *Dotted line* shows the local density approximation, *dashed line* represents *Robinson's* fitting function, (o) represents results of *Namiki et. al.* and *solid line* represents results obtained using *shell planar charge density.*

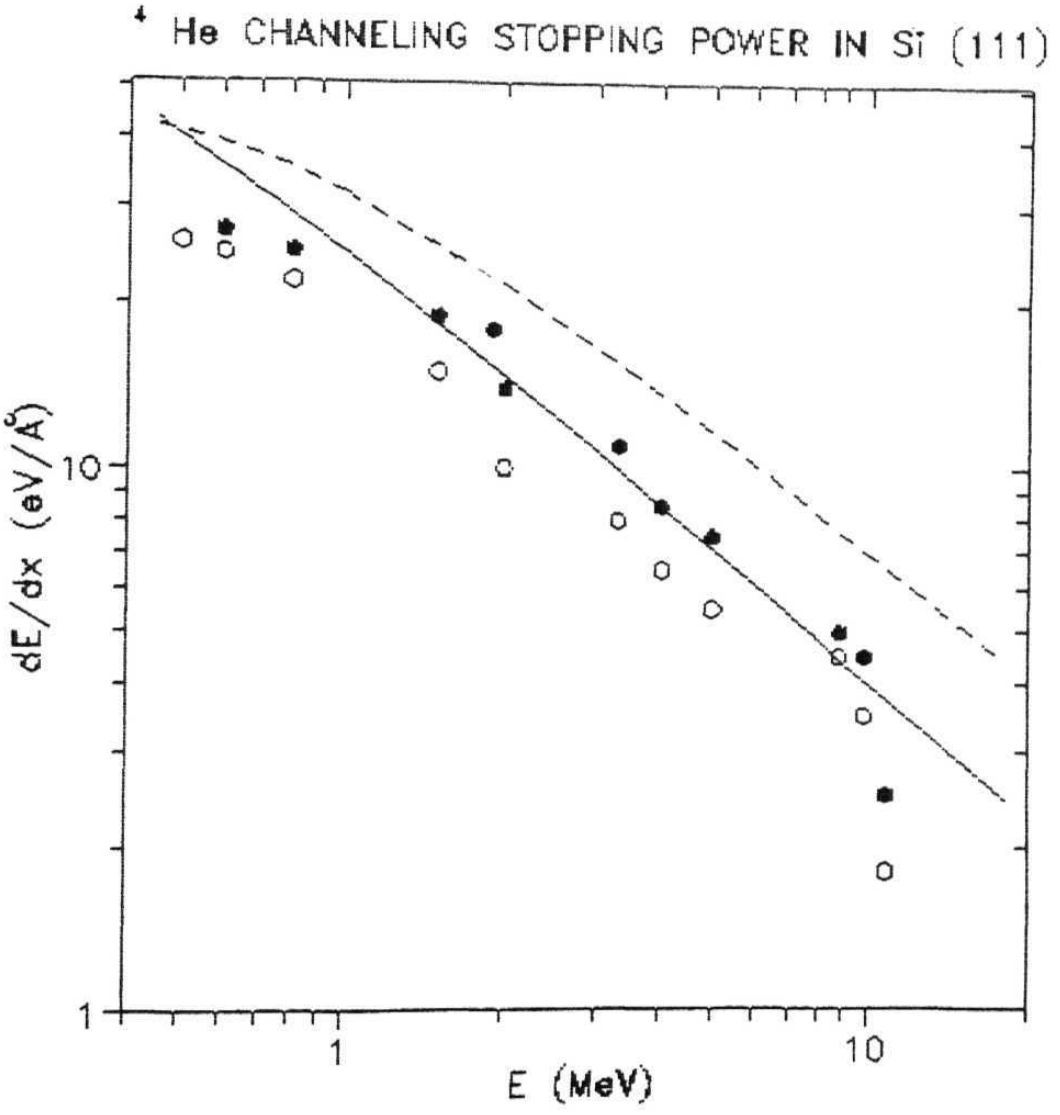

Fig 4.4: The stopping powers for ^4He ions channeled through *Silicon* crystals along (111) plane. *Filled squares* and *open circles* represent *peak edge* and *leading edge* respectively (Ref. 35). The *dashed curve* and *solid curve* represents calculations using *Lindhard* and *Shell planar charge densities* respectively.

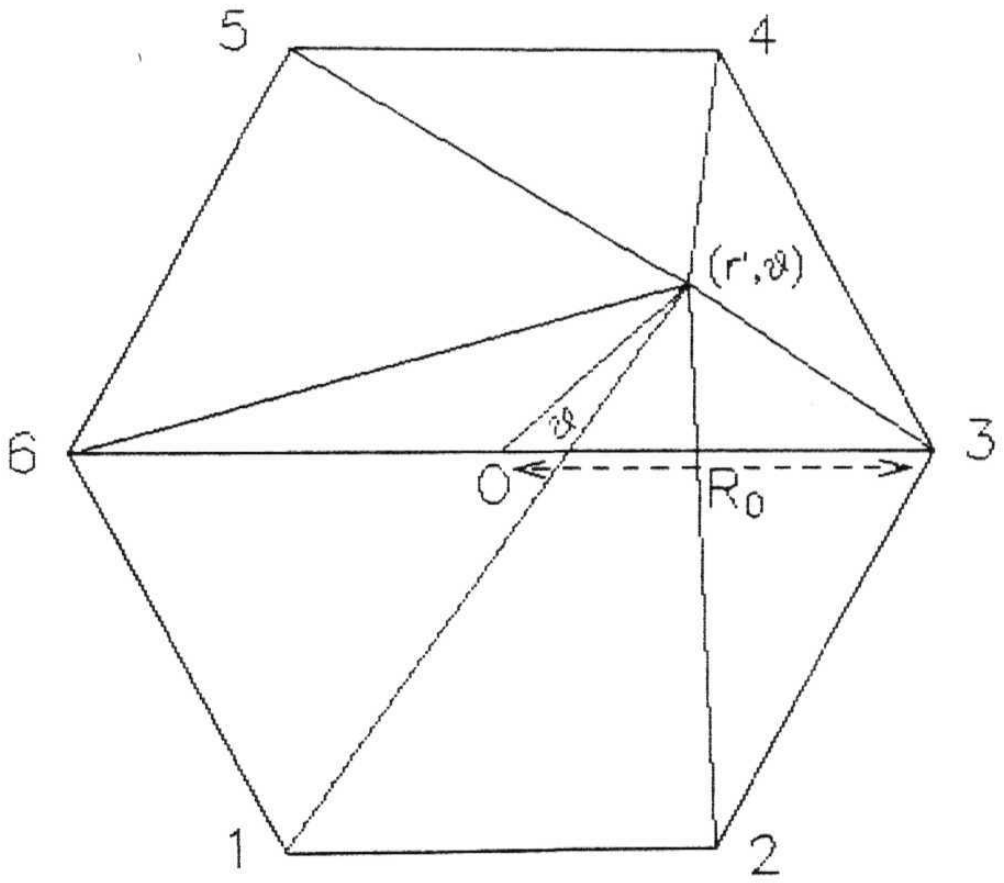

Fig 4.5: **Approximate < 110 > axial channel in diamond structure crystals. Each of the corners represents an axis perpendicular to the plane of drawing.**

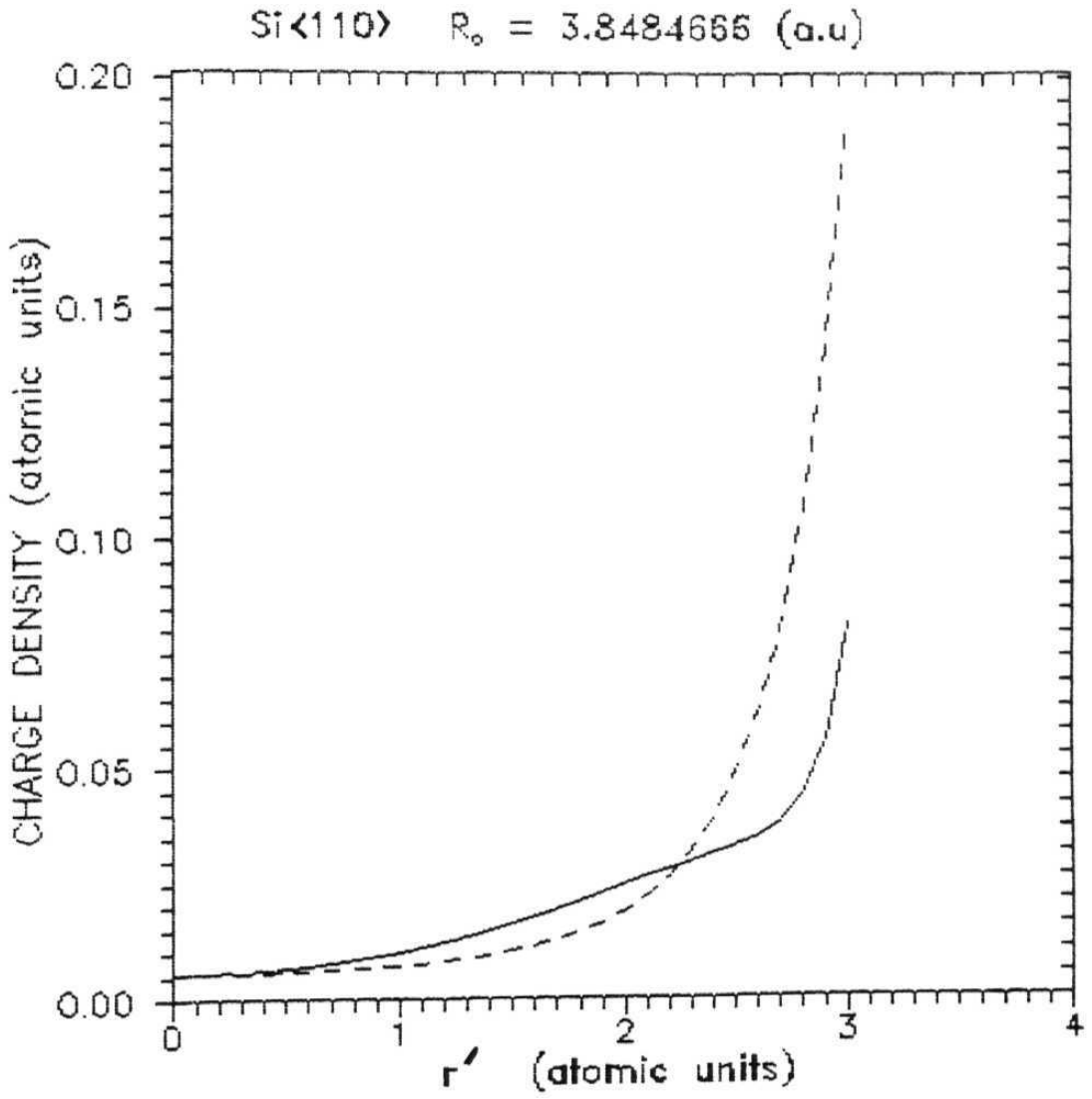

Fig 4.6: **Axial charge densities due to six strings of *Silicon* < 110 > axis as a function r' measured from the centre of channel R_{cr}. *Solid curve* and *dashed curve* represent *Shell* and *Lindhard axial charge densities* calculations.**

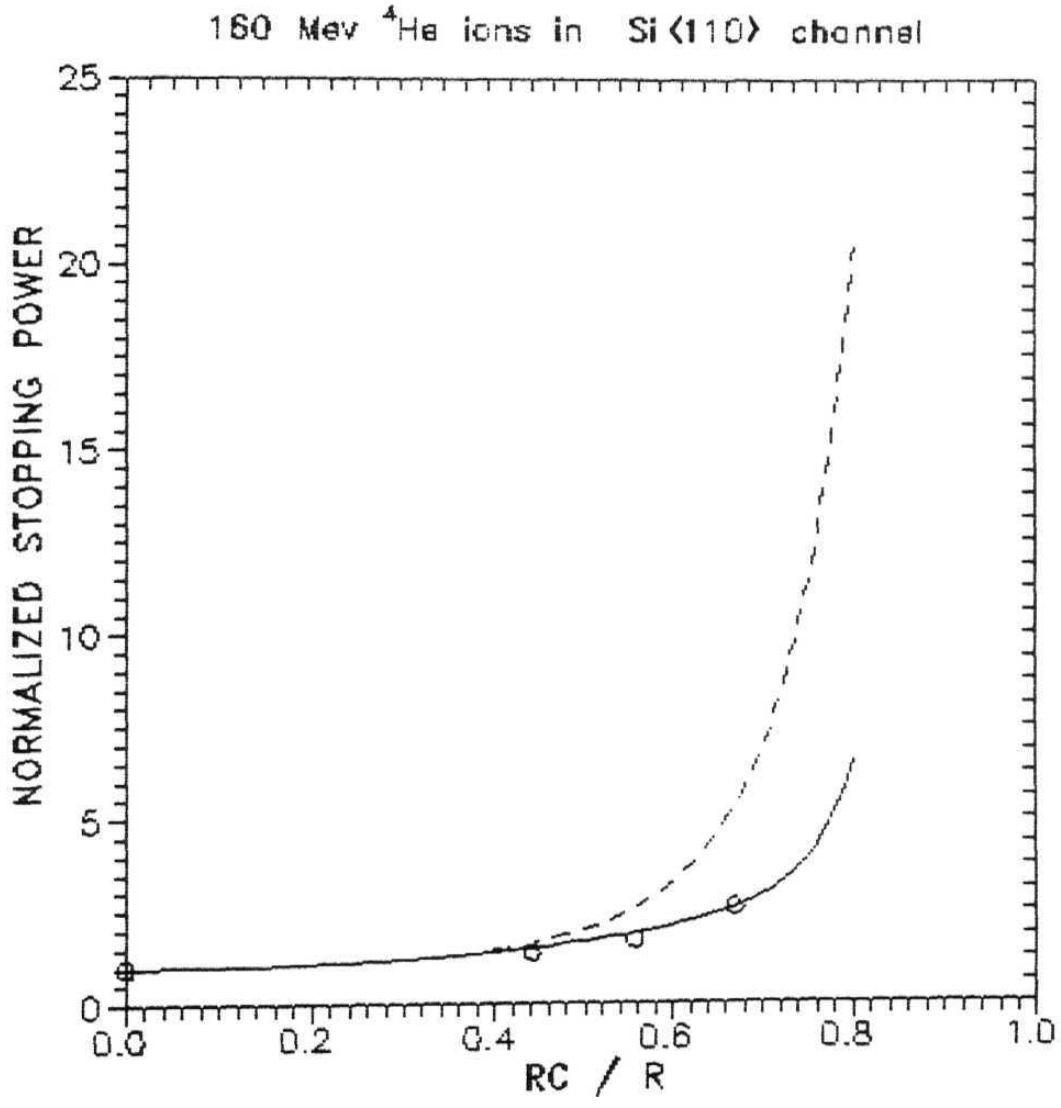

Fig 4.7: **Variation of normalised stopping power for 160 *MeV* α particles as a function of the distance r' from the centre of the < 110 > axial channel in *Silicon* for (i) the present *shell charge density* (*solid curve*) (ii) *Esbensen's result* (o) (Ref. 13) (iii) *Lindhard charge density* (*dashed curve*).**

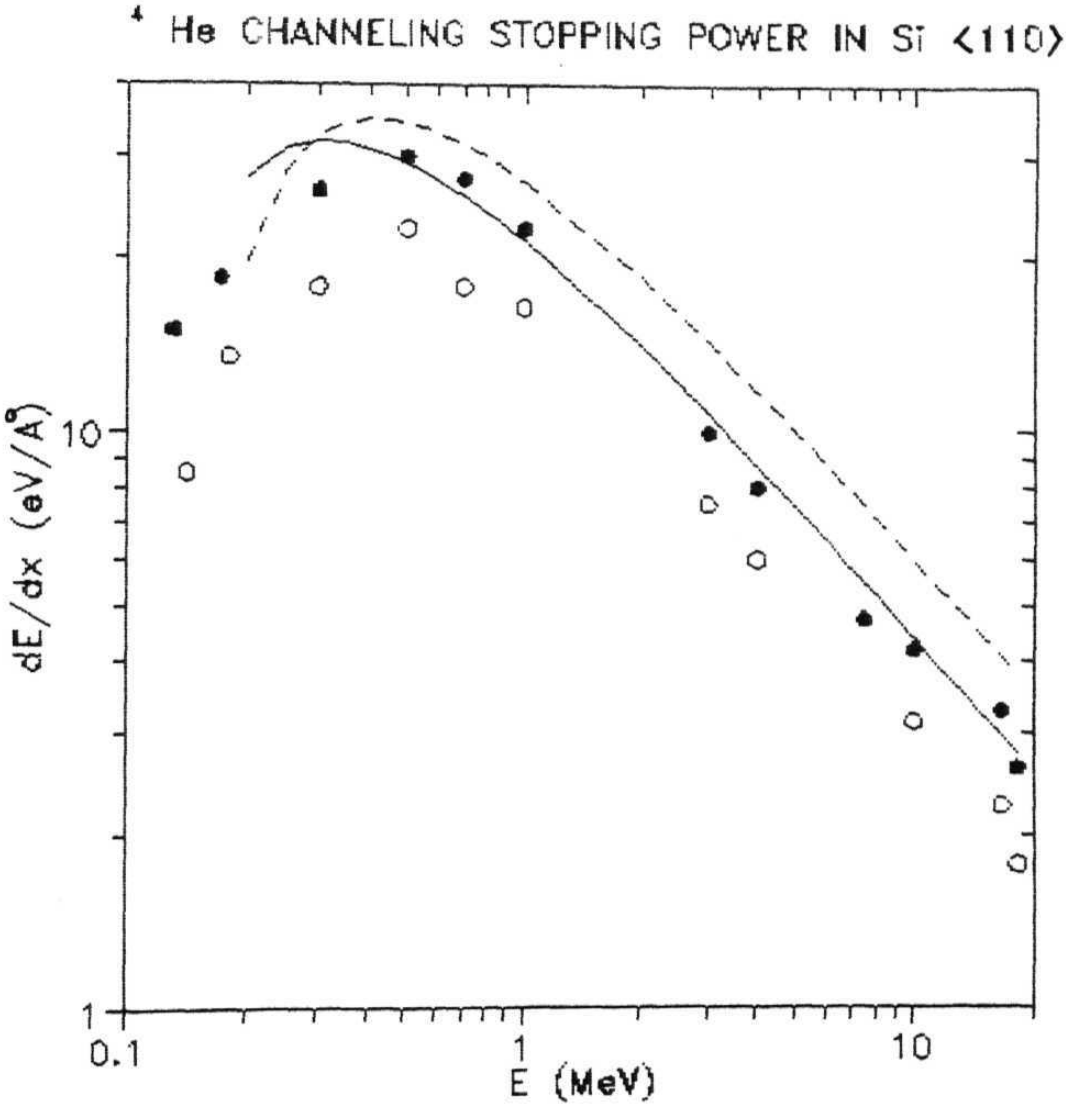

Fig 4.8: Stopping powers of He ions channeled through *Silicon* single crystal along the < 110 > axis. Stopping power values obtained using *shell model axial charge density* (*solid curve*) and *Lindhard axial charge density* (*dashed curve*) are compared with experimental results (Ref 35), where *Filled squares* and *open circles* represent *peak* and *edge* respectively.

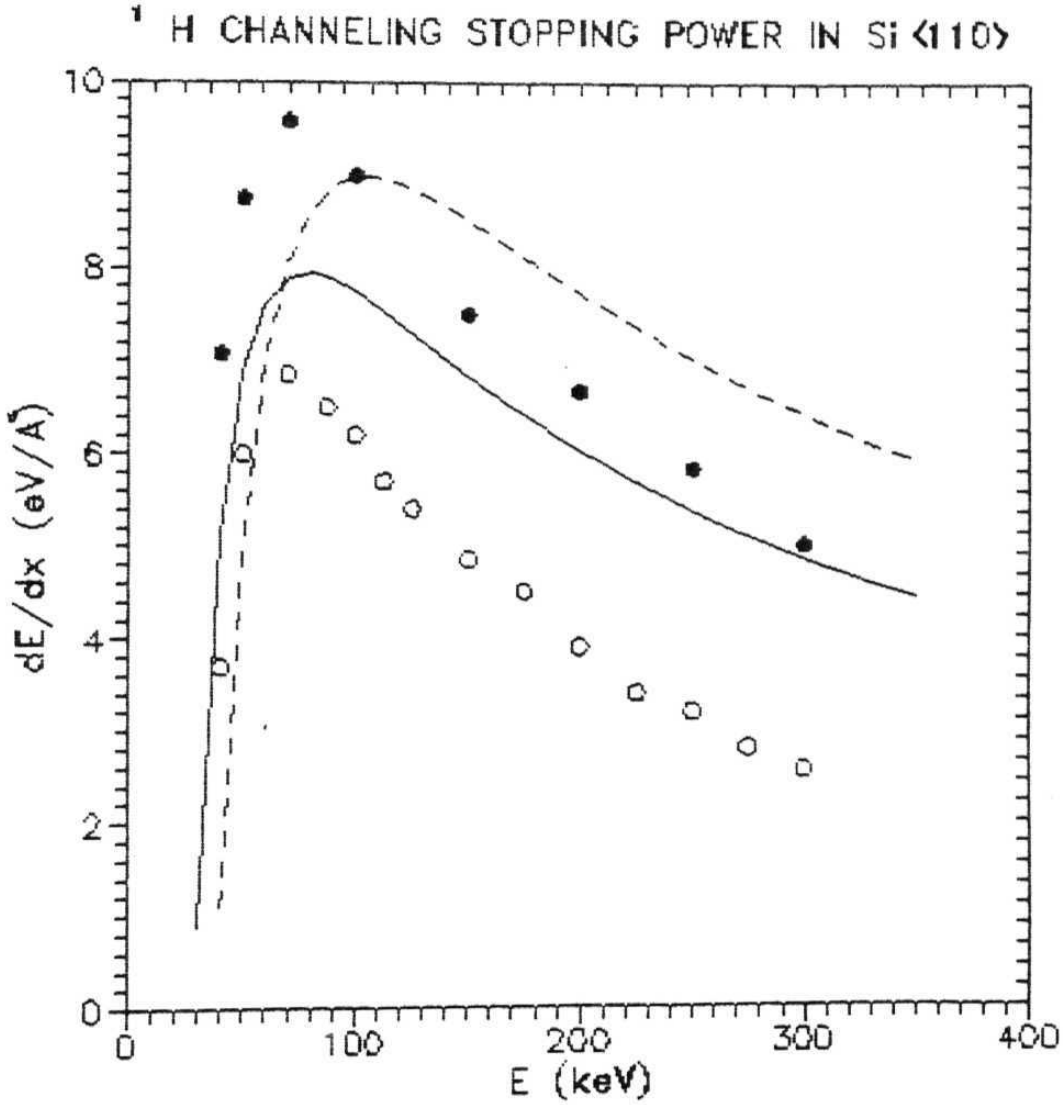

Fig 4.9 *Proton* channeling stopping power in *Silicon* < 110 > axis. Stopping power values obtained using *shell model axial charge density* (*solid curve*) and *Lindhard axial charge density* (*dashed curve*) are compared with experimental results (Ref. 38) where the (•) represents the *most probable energy loss* and (o) represents *energy loss of best channeled particles.*

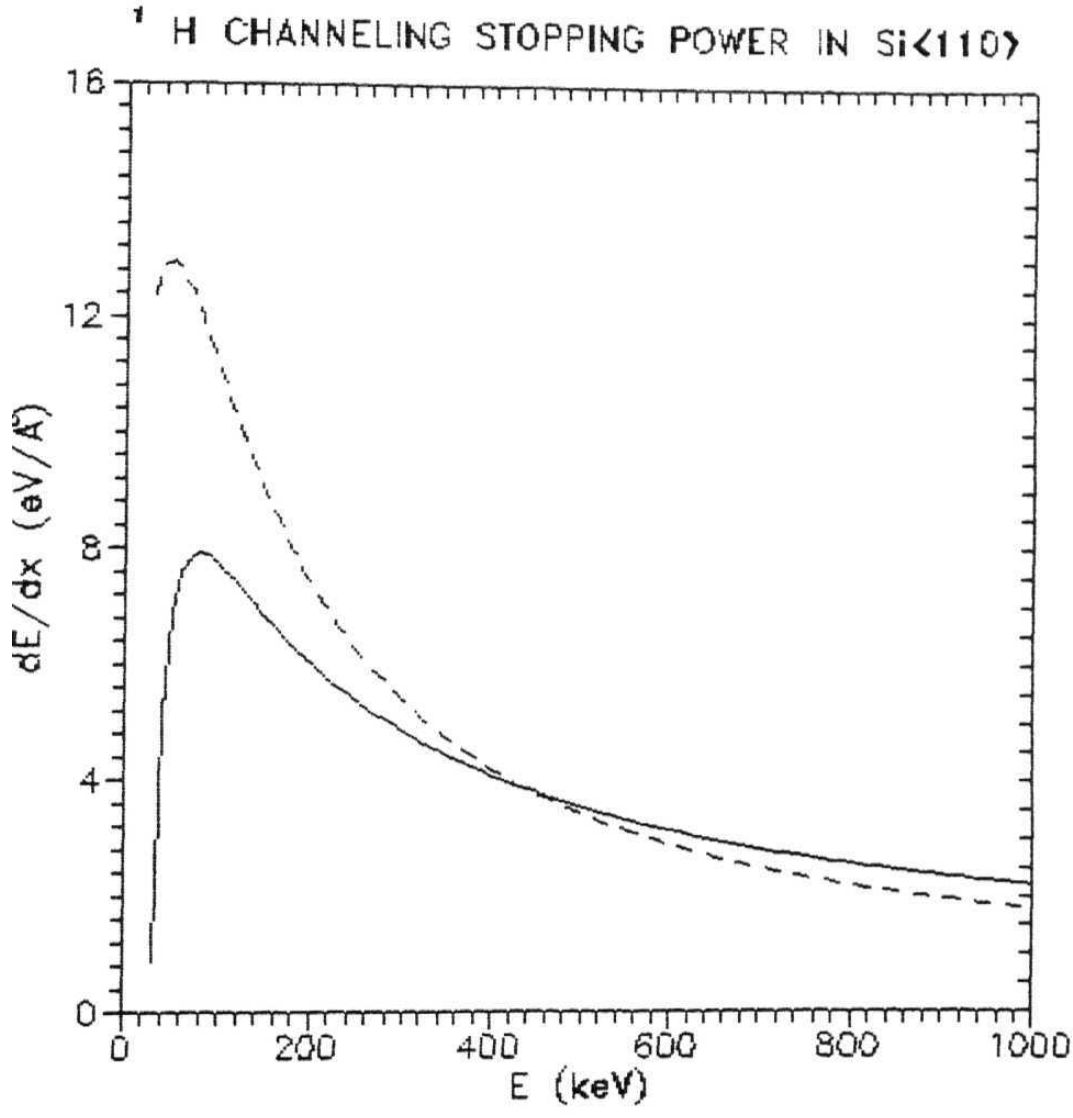

Fig 4.10 ***Proton*** **channeling stopping power in** ***Silicon*** **< 110 > axis. The calculations using** ***shell axial charge density*** **(** ***solid curve*** **) are compared with experimental results (Ref. 39) (** ***dashed curve*** **).**

Chapter 5

Z_1 OSCILLATIONS

5.1 INTRODUCTION

In Chapter 2 and chapter 4 we have dealt with electronic stopping power of atoms for both random and channeling cases respectively. It has been implicitly stated that at a given projectile velocity v, the electronic stopping power of target in low velocity region ($v < v_c = v_o Z_1^{\cdot}$,where v_o is the *Bohr velocity)* increases monotonically with the atomic number Z_1 (equation 2.2). But it has been found that the stopping powers of solids for low velocity channeled and random heavy ions exhibits a periodic (oscillatory) dependence on the charge $Z\backslash e$ of the incident projectile ions [1-6]. This is referred to as Z_1 oscillations. In this velocity region, the nuclear stopping is small compared to electronic stopping and is further suppressed because of the fact that close collisions of incident ions with target atoms are completely avoided in channeling. The maxima of electronic stopping occur (irrespective of channeling or random case and of specific target medium), around $Z\backslash$ — 6,20,38 and minima occur at around $Z\backslash$ — 10,29,47 [7]. In channeling case the ratio of maxima to minima becomes large (as expected) and when the velocity of incoming projectile increases beyond 2 to 3 *atomic units.*, the oscillations gradually damp out and ultimately disappear. In section 5.2 *Briggs - Pathak* [8-10] model for explaining $Z\backslash$ oscillations in electronic stopping power is described in detail with some exposure to earlier theoretical model like *Firsov*'s model [11]. Extension of

Briggs - Pathak model incorporating shell continuum charge density is depicted in section 5.3. Results are discussed in concluding section.

5.2 BRIGGS - PATHAK MODEL

Various theoretical models were formulated for explaining this oscillatory dependence of electronic stopping power on atomic number Z_1 of the projectiles [8-10,12-20]. These were mainly the modifications of *Firsov*'s model [12,13,15,16] and calculations based on Density functional Theory [17,19,21,22]. *Firsov* [11] proposed a model for calculating electronic stopping power at low velocities, where stopping power increases with projectile velocities. The model considers the overlap between the electronic shells of incoming projectile and target atoms as the ion moves inside the target. This results in exchange of electrons between projectile and target atoms. resulting in loss of energy from projectile to target atom [7]. For a mathematical formulation *Firsov* defined a hypothetical plane lying exactly halfway between the atoms for symmetrical case of similar atoms/ions. When an electron crosses this plane, energy transfer takes place through process of momentum transfer of the electron to the atom. In a single collision between two atoms, the energy transfer is given by [7,11]

$$\Delta E = m \int \dot{R} \times dR \int \frac{1}{4} nvds \tag{5.1}$$

where R is the internuclear separation and the surface integral represents the flux with average velocity v across the interaction plane, n being the electron density at this surface [7]. The total energy loss in a collision is given by

$$\Delta E(b) = \frac{4.3 \times 10^{-8}(Z_1 + Z_2)^{5/3} v}{(1 + 0.31(Z_1 + Z_2)^{1/3} b)^5} \tag{5.2}$$

Where $\Delta E(b)$ is evaluated in eV and v and b are given in units of $cm/sec$and A respectively.

Early attempts made to explain theoretically the Z_1 oscillations in electronic stopping power were based on modifying the above mentioned *Firsov*'s theory [12,15]. *Cheshire et. al.* replaced the smooth variation of electronic density assumed in the Firsov theory (equation 5.1) with electronic densities which reflect the shell structure of the projectile atoms. ie, [7]

$$m \int \frac{1}{4} nvds = \frac{1}{4} m \int (\sum_{\alpha} v_{\alpha} \mid \psi_{\alpha} \mid^2 + \sum_{\beta} v_{\beta} \mid \psi_{\beta} \mid^2) ds \tag{5.3}$$

where $\psi_{\alpha,\beta}$ are *Slater orbitals* of the projectile and target atoms and $v_{\alpha,\beta}$ are corresponding velocities in these orbitals. *Cheshire et. al* [16] emulated the procedure of *Clementi* and *Raimondi* [23,24] to obtain the *Slater orbitals* as

$$\psi_{\alpha} = r^{n_{\alpha}-1} \; exp(\xi_{\alpha} r) \; Y_{\ell_{\alpha} m_{\alpha}}(\theta, \phi) \tag{5.4}$$

and used the tables of *Clementi* [25] for various exponents in the wave function of atoms in various charge states. Eventhough these modified theories predict positions of maxima and minima correctly, they fail to explain the large value of maximum to minimum ratio of stopping power shown in experiments. Damping of Z_1 oscillation at higher Z_1 value is another feature which was not explained by these theories. Our calculations are based on semiclassical theory proposed by Briggs and Pathak [8]. In this theory energy loss is attributed to the scattering of target electrons in the potential field of moving projectile. At these low velocities, most of stopping power contribution comes from a transfer of momentum between the electrons of the ion and those of target atom due to overlap of electronic clouds as the ion passes. This transfer of momentum can be considered to be affected by the elastic scattering of the target electrons through the charge cloud of the moving ion. This is similar to the diffusion of electrons through gases. When a heavy atom moving through an uniform electron gas with a velocity v (electrons are considered to have zero velocity,so that the relative velocity of collision is v itself), using simple kinetics of two - body collisions, the energy lost by the atom due to collision with an

electron which is scattered through a centre of mass angle *9* can be written as [8]

$$T_2 = m\, v^2\, (1 - \cos\theta) \tag{5.5}$$

The mean energy lost per unit path length by an ion with velocity v has been shown to be

$$-\frac{dE}{dx} = n\, m\, v^2\, Q_d \tag{5.6}$$

where *n* is the density of electrons, m is the electron mass and Q_d is the *momentum transfer cross section* and is given by

$$Q_d = 2\,\pi \int_o^{\pi} I_o(\theta)\, (1 - \cos\theta)\, \sin\theta\, d\theta \tag{5.7}$$

In terms of the partial wave - phase shifts, the *momentum transfer cross section* can be written as [26]

$$Q_d = \frac{4\pi}{k^2} \sum_{\ell} (\ell + 1) \sin^2(\eta_\ell - \eta_{\ell+1}) \tag{5.8}$$

where $\hbar k$ is the electron momentum in the centre of mass frame. The phase shift η_ℓ of the ℓ-th partial wave of the electron wave function can be calculated by numerically solving the radial part of Schrodinger equation

$$\frac{d^2 G_\ell}{dr^2} + [k^2 + U(r) - \frac{\ell(\ell+1)}{r^2} G_\ell] = 0 \tag{5.9}$$

where G_ℓ is the radial wavefunction corresponding to the ℓ-th partial wave and *k* is the electron wavenumber corresponding to the projectile velocity given by $k = \sqrt{2mE/\hbar^2}$ for an energy *E* and $U(r) = (2m/\hbar^2)V(r)$where *V(r)* represents interaction between target electron and projectile.

Since the potential between the electron and projectile V(r) varies more rapidly than $1/r$, the asymptotic form of the radial wave function can be written as

$$G_\ell(r) \sim \sin(kr - \frac{\ell\,\pi}{2} + \eta_\ell) \tag{5.10}$$

In the absence of an atomic field, equation 5.9 gives the solution whose asymptotic form is

$$G_\ell(r) \sim (kr - \frac{1}{2}\ell\,\pi) \tag{5.11}$$

The magnitude of the phase shift η_ℓ is determined by the competition between attractive potential *U(r)* and repulsive centrifugal potential $\ell(\ell+1)/r^2$ and is computed by finding the shift of nodes of solution (equation 5.10) with respect to the corresponding node of the solution (equation 5.11) for large r. The atomic field *U(r)* in which the target electrons are scattered is taken to be Moliere potential (in Thomas-Fermi statistical model). After the above model was proposed and successfully used to explain not only the Z_1 oscillation and Z_2 variation [27], but also to predict the velocity dependence of these oscillations [28,29], few more alternative models [17-19,30,31] have been proposed in recent years. These are mostly very detailed *Density Functional Theory calculations* [21,22] for *V(r)* which also yield information on the effective change density used in Stopping Power formulae. The agreement with experimental results [5,6] is approximately of the same order as earlier results. Moreover the velocity dependence of Z_1 oscillation in these models have not yet been calculated to show at which projectile velocity, the oscillations should vanish. Calculation of transport cross section at the Fermi velocity as done in these later models is valid only for a degenerate electron gas in metals but certainly not for semiconductors like *Ge* or *Si* or orbital target electrons like $5d$ or *Ad.* Consequently we have made our calculations for *projectile velocities* [8] as earlier because of reasonable agreement with experimental results and analytical applicability to more complicated situations involving defects.

5.3 Z_1 OSCILLATIONS CALCULATIONS USING SHELL CHARGE DENSITY

We have already demonstrated the efficiency in which Shell model charge densities can be incorporated in solving electronic stopping power problems in the last chapter. Shell charge densities are represented by an analytical expression and there is no ambiguity involved in finding the effective charge density *n* using shell charge densities. Moreover it takes the shell structure of atom into account. To demonstrate these points we have taken two specific cases of *Z* oscillations in electronic stopping powers of *Si* and *W* single crystals for ions channeled along < 110 > axis and < 100 > axis of *Si* and *W* respectively.

The axial electron charge density at a distance r from the string is calculated using continuum approximation and given by (*chapter 3*, equation 3.3) [32]

$$\rho_s^{ax}(r) = \frac{1}{\pi d}\sum_j \frac{\omega}{(2nj)!}\sum_{m=o}^{n_j-1} \frac{2^{2m}(2(n_j-m))!(n_j-1)!(\xi_j)^{n_j+m+2} r^{n_j+m} K_{n_j-m}(2\xi_j r)}{(n_j-m-\frac{1}{2})(n_j-m)(m)!((n_j-m-1)!\,)^2} \tag{5.12}$$

In the *Silicon* case, an < 110 > axial channel is nearly symmetric and we approximate that the six rows form a regular hexagon. In the < 100 > channel of *Tungsten*, the four rows form a square. The charge density due to all strings (six for *Si* < 110 > and four for *W* < 100 >) is calculated as a function of distance measured from the channel axis.

The charge density *n* was calculated for individual target atoms along the particular channel [8,9]. Here charge density *n* in equation 5.6 is calculated using equation 5.12. The shell axial charge density is curve fitted to a simple exponential function of the form $\rho_A(r) = ae^{br^2} + c$ where the parameters a, *b* and c are given by *a* = 0.00433592, 6 = 0.4154959, *c* = 0.0122899 for < 100 > *Tungsten* and *a* = 0.000154, 6 = 0.72756310 and c = 0.01221266 for < 110 > *Silicon* . The effective charge density n_{eff} is calculated by

integrating over the space occupied by the projectile ion.

$$n_{eff} = \frac{1}{\pi R_s^2} \int_o^{R_s} 2\pi r \rho_A(r) dr \tag{5.13}$$

where R_s is the relevant space occupied by moving ion and taken as radius of maximum charge density [33] of the outermost shell of projectile ion appropriate to most probable charge state. For example projectiles like rare gases are assumed to be neutral whereas those like alkali metal ions, *Na*, *K* etc., are assumed to be singly charged because their outermost *s* electrons will certainly be stripped off during their motion in solids. In the equation (5.13) r is measured from the centre of the channel. In the case of *Tungsten*, we considered the conduction 6s electrons to contribute a uniform electron gas so that n_{6s} for *Tungsten* is twice the atomic density. The axial charge density is calculated only for shell electrons (i.e., up to $5d$ electrons) i.e.,

$$n(r) = n_{eff}(r) + n_{6s} \tag{5.14}$$

for *Tungsten* case and

$$n(r) = n_{eff}(r) \tag{5.15}$$

for the *Silicon* case.

In atomic units, the equation (5.6) changes tc

$$-\frac{dE}{dx} = 4\pi n \bar{Q}_d \tag{5.16}$$

where $\bar{Q}_d = \sum_\ell (\ell + 1) \sin^2(\eta_\ell - \eta_{\ell+1})$.

The stopping power is calculated using equation (5.16) for various channeling projectile ions for both silicon and tungsten target atoms. This is shown in Fig 5.1 *(Silicon* < 110 >) and Fig.5.2 *(Tungsten* < 100 >) respectively.

5.4 CONCLUSION

We have calculated the stopping power of *Silicon* (along < 110 > axis) and *Tungsten* (< 100 > axis) for low velocity channeled heavy ions and compared with earlier theoretical calculations and experimental results. This is shown in Fig.5.1 and Fig.5.2 respectively. Main motivation of this work has been to keep the problem analytical as far as possible so that applications to effects of defects and disorder [34] on this important quantity can be easily estimated. Of course, more detailed calculations using nonlinear density functional formalism [21,22] have been performed earlier which also yield Z_1 oscillations [19,30]. In those calculations, even after excessive computational efforts put for potential and charge density calculations, the effective electron density sampled in channeled particles is determined by equating the theoretical and experimental values of stopping for some specified Z\ (for example for *Silicon* < 110 > Z\ — 5 was chosen to implement the fitting [30]). Those calculations are ideally suited for degenerate electron gas in the limit of projectile velocity negligibly small compared to Fermi velocity so that projectile velocity dependence of oscillations does not appear in the problem. Our calculations are valid for projectile velocities above target electron velocities (i.e., Fermi velocity as well as outer orbital electrons contributing to stopping of well channeled projectiles). In fact all the experimental data on $Z1$\ oscillations available to date is in this velocity range ($v > v_F$). As discussed earlier [8-10] we assumed elastic scattering of free (loosely bound) electrons from the well channeled projectiles. The actual shell electron density is averaged along the channel in appropriate geometry and appropriate size effect of projectile is included. There is no scaling or best fitting done as far as final stopping power is concerned. The conduction electrons (like $6s$ in *Tungsten)* are assumed to contribute entirely as before. Apparent disagreement for some values of Z\ (e.g., Z\ - 24) is actually related with shifting of phase of the oscillations, with changes in relative velocity [28,29]. The

validity of the approximation of taking projectile velocity as relative velocity increases as v increases. Overall our calculations, inspite of being simplistic are reasonably accurate and useful. We feel that the data for heavy projectile ions ($Z_1 > 30$) is very sparse and further experiments are needed to study these oscillations for heavier ions. Moreover, as mentioned in *Chapter* 2, a systematic experimental study with respect to velocity dependence has never been undertaken, eventhough it is known at high velocities beyond maxima in stopping power vs velocity curve that the oscillation do not exist. Such interesting experiments are strongly suggested for channeling and random cases and we believe that we shall build relevant data in this region in near future and some progress has already been made in this direction [35].

References

[1] A. Teplova Ya, V. S. Nikolaev, I. S. Dmitriev and L. N. Fateeva *Sov. Phys. JETP.*, 15, 31, (1962).

[2] J. H. Ormrod and H. E. Duckworth *Can. J. Phys,* 41, 1424, (1963).

[3] J. H. Ormrod J. R. Macdonald and H. E. Duckworth *Can. J. Phys,* 43,275, (1965).

[4] P. Hvelplund and B. Fastrup *Phys. Rev,* 165, 408, (1968).

[5] L. Eriksson, J. A. Davies and P. Jespersgaard *Phys. Rev.*, 161, 219, (1967).

[6] F. H. Eisen *Can. J. Phys.*, 46, 561, (1968).

[7] A.P. Pathak *Radiat. Eff.*, 61, 1, (1982).

[8] J. S. Briggs and A. P. Pathak *J. Phys. C: Solid State Phys.*, 6, L153, (1973).

[9] J. S. Briggs and A. P. Pathak *J. Phys. C: Solid State Phys.*, 7, 1929, (1974).

[10] A. P. Pathak *J. Phys. F: Met. Phys.*, 4, 1883, (1974).

[11] 0. B. Firsov *Sov. Phys. - JETP,* 9, 1076, (1959).

[12] I. M. Cheshire, G. Dearnaley and J. M. Poate *Phys. Lett.* 27 A, 304, (1968).

[13] C. P. Bhalla and J. N. Bradford *Phys. Lett.*, 27 A, 318, (1968).

[14] A. H. El-Hoshy and J. F. Gibbons *Phys. Rev.* 173, 454, (1968).

[15] K. B. Winterborn *Can. J. Phys.*, 46, 2429, (1968).

[16] I. M. Cheshire and J. M. Poate *Atomic Collision Phenomena in Solids,* (eds. D. W. Palmer, M. W. Thompson and P. D. Townsend) (North Holland Publishing Co, Amsterdam) (1970), page 351.

[17] M. J. Puska and R. M. Nieminen *Phys. Rev.*, B 27, 6121, (1983).

[18] You - Nian Wang, Teng - Cai Ma and Yei Gong *Phys. Lett,l67* A, 287, (1992).

[19] M. Penalba, A. Arnau, P.M. Echenique *Nucl. Instrum. Methods.*, B 67, 66, (1992).

[20] V. Hari kumar and A. P. Pathak *J. Phys. Condens. Matter,* 5, 3163, (1993).

[21] P. Hohenberg and W. Kohn *Phys. Rev.,* B **136,** 864, (1964).

[22] W. Kohn and L. J. Sham *Phys. Rev.,* A **140,** 1133, (1965).

[23] E. Clementi and D.L. Raimondi *J. Chem. Phys.,* 38, 2686, (1963).

[24] E. Clementi, D.L. Raimondi and W.P. Reinhardt *J. Chem. Phys.,* 47, 1300, (1967).

[25] E. Clementi *Tables of Atomic Wave Functions* (IBM San Jose, California) (1965).

[26] H. S. W. Massey and E. M. S. Burhop *Electronic and Ionic Impact. Phenomena,* Vol. 1, (Oxford:Clarendon) (1969).

[27] A.P. Pathak *J. Phys. C: Solid State Phys, 7,* 3239, (1974).

[28] A.P. Pathak *Phys. Rev.,* B 22, 96, (1980).

[29] A.P. Pathak *Phys. Rev.,* B 22, 5544, (1980).

[30] P. M. Echenique, R. M. Nieminen, J. C. Ashley and R. H. Ritchie *Phys. Rev.,* A 33, 897, (1986).

[31] T. L. Ferrell and R. H. Ritchie *Phys. Rev.,* B 16, 115, (1977).

[32] R. Agnihotri and A.P. Pathak *Nucl. Instrum. and Methods.* B 67, 39, (1992).

[33] J. C. Slater *Quantum Theory of Atomic Structure,* (New York: McGraw-Hill) (1960) Page 210.

[34] A. P. Pathak *Phys. Rev., B 15,* 3309, (1977).

[35] N. Nath, O. P. Dahinwal, A. Bhagwat, D. K. Avasthi, V. Hari kumar and A. P. Pathak *Surface and Coatings Technology,* 66, 231, (1994).

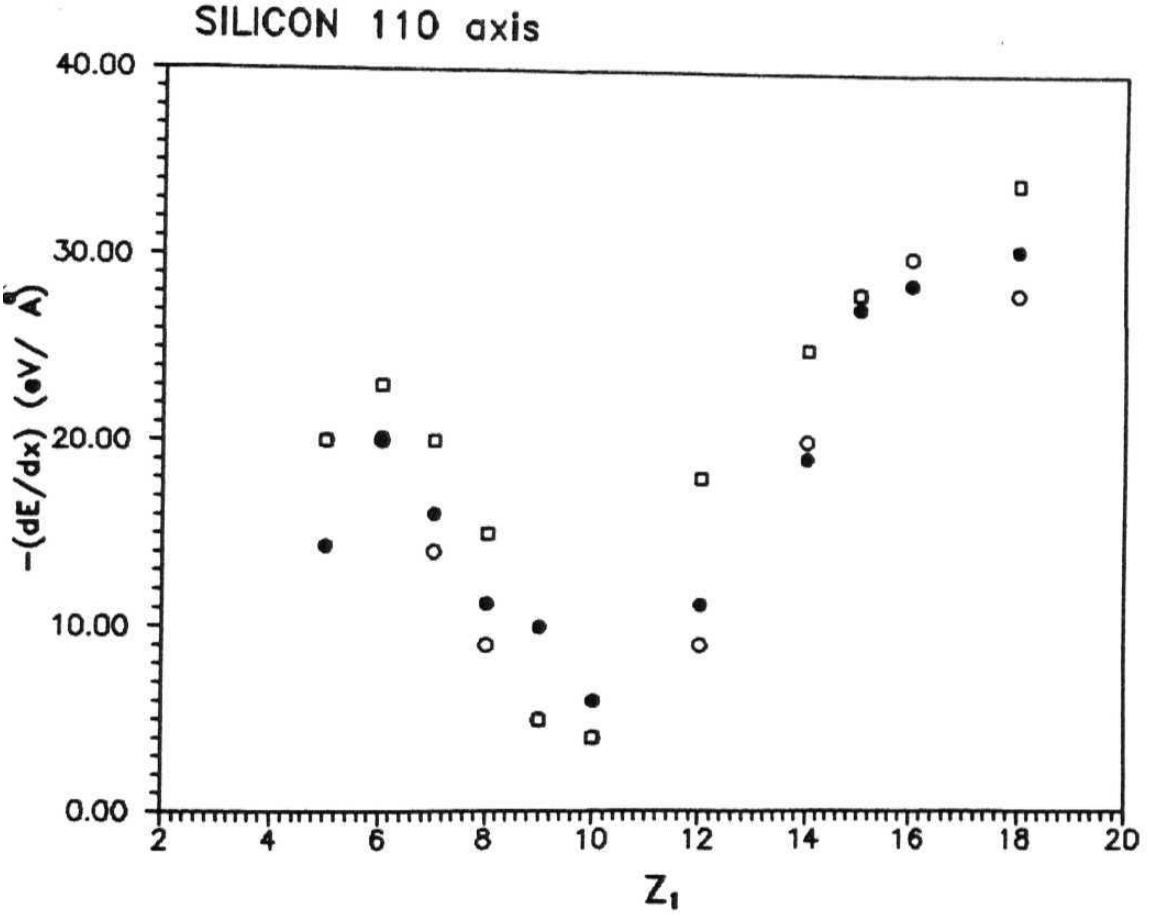

Fig 5.1: The stopping power of *Silicon* for heavy ions channeled along the < 110 > axis at a projectile velocity of 1.5×10^8 cms^{-1}, (□) represents the experiment of *Eisen* (Ref. 6.), (○) represents the calculation of *Briggs* and *Pathak* (Ref. 9.) and (●) represents the calculations using the *shell model charge density.*

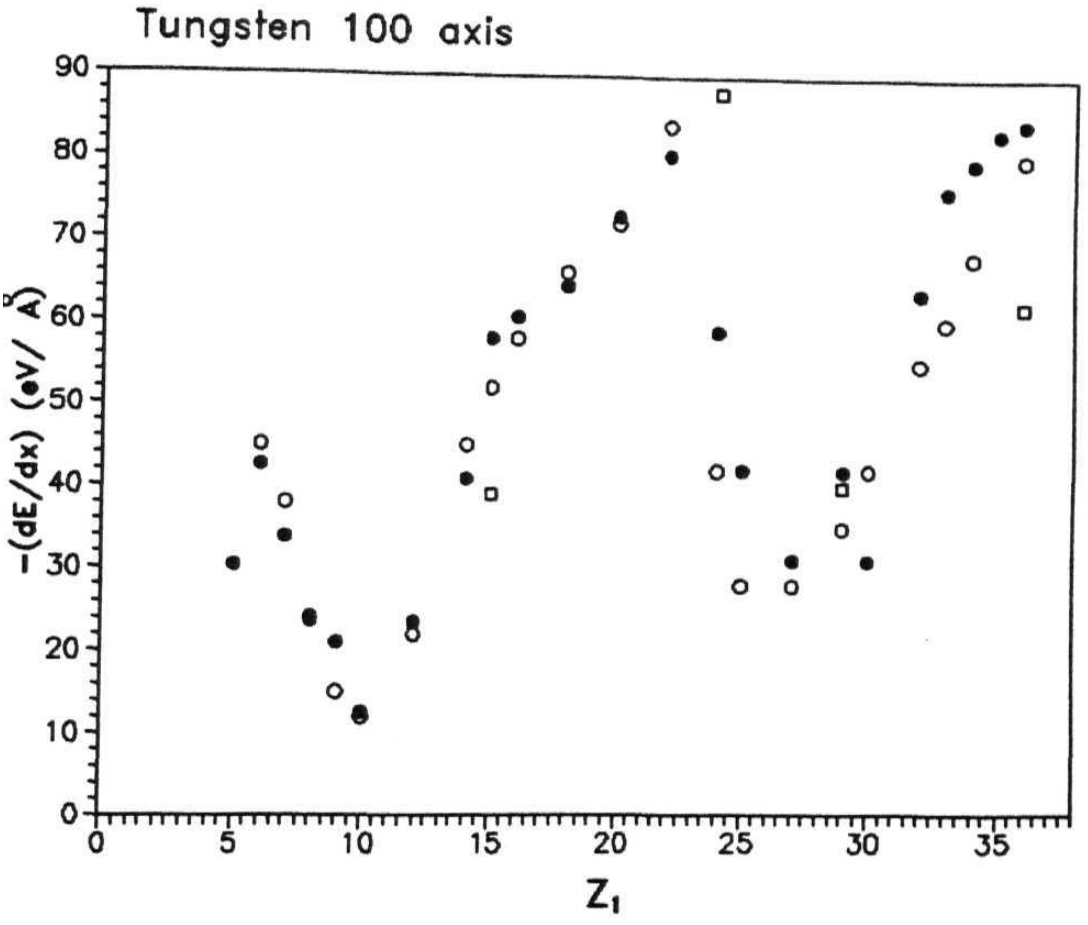

Fig 5.2: The stopping power of *Tungsten* for heavy ions channeled along the < 100 > axis at a projectile velocity of 1.5×10^8 cms^{-1}; (□) represents the experiment of *Eriksson et. al.* (Ref. 5.), (○) represents the calculation of *Pathak* (Ref. 10.) and (●) represents the calculations using the *shell model charge density.*

Chapter 6

STRAINED LAYER SUPERLATTICES

6.1 INTRODUCTION

Semiconductor Superlattices are one dimensional periodic structures consisting of ultra thin layers with period less than electron mean free path. This concept was proposed by *Esaki and Tsu* [1] at the end of sixties. Soon after the fabrication of superlatttices, their tremendous applications in the semiconductor technology were realized worldwide. The built in strain in these multilayers was considered as a constraint and hindrance in making good quality lattice matched Superlattices until *Osbourn* proposed that *Strained Layer structures* might display new electronic and optical properties not seen in the unstrained - consistent materials [2]. Strained Layer Superlattices (SLS) are layered structures of alternating composition of materials having not too large (~0.1 to 2.0 %) lattice mismatch [3,4]. This small lattice mismatch is accommodated by biaxial (compressive and tensile) strains in the plane of the layers and each layer acquires a perpendicular lattice constant due to strain accommodation. Thus for sufficiently thin layers misfit defects or dislocations are not generated. Due to these alternating tetragonal distortions along the growth direction, inclined crystal planes and rows undergo abrupt tilt (AV>) at each interface [5]. The unusual electronic and optoelectronic properties of *Strained Layer Superlattices* **(SLS)** have opened up possibilities to fabricate a new category of electronic and optoelectronic devices, which have wide ranging applications in many frontier areas

of science and technology. The ability to tailor the energy band gap in SLS's is one of the properties which is utilised in the manufacture of photodetectors and quantum well lasers. The presence of defects deteriorate the performance of these semiconductor devices, so it is important to characterize strain and strain relief mechanisms in the structures. Rutherford back scattering analysis along with channeling [6] measurements are extensively used for this purpose. Since channeled particles do not approach the atomic-nuclei, a substantial reduction in the scattering yield occur, whenever a particle is channeled. The presence of misfit defects or dislocations and the changes in the direction of the crystal rows or planes at the interfaces will give rise to dechanneling due to scattering. Reviews of the characterization and application of *Strained Layer Superlattices* are given in [7-10].

The *Catastrophic Dechanneling Resonance* is one of the methods extensively used to obtain strain in these strained layer structures. Catastrophic Dechanneling Resonance occurs when the half wavelength (A/2) of oscillatory motion of a planar channeled ion beam matches the path length per layer (s) of the SLS. This leads to sudden increase in the dechanneling after certain depth. Study of this resonance gives the information on the strains present in SLS. The complementary phenomena of *Resonance Channeling* [11] occurs when the path length per layer (5) matches the wave length (A) of planar channeled ion beam ie A = *s*. The dechanneling is minimum in this case. The experimental study on charged particle (α particle) channeling along the inclined (110) crystal plane of GaAs0.09P0.91/GaP superlattice under conditions of catastrophic dechanneling has been reported during last ten years or so [5,11-14]. Moliere planar potential [6,15,16] based on Thomas Fermi model has been mostly used for theoretical estimates in these studies. Here we have used a shell model potential [16] which is free from statistical nature of Moliere potential and takes into account of the detailed atomic shell structure of the target material (SLS).

Earlier we have successfully used the same Shell model charged density for energy loss (channeled case) calculation and in the next chapter the relevant results for *channeling radiation* will be presented [16-18]. This gave us motivation to use this shell model potential, in this exciting field of SLS's also. For comparison purpose, we have included results obtained using Biersack's Universal planar potential [19], which is refined version of Thomas Fermi potential, more frequently used in low energy stopping power studies [20]

Basic principles of *Strained Layer Superlattices* are outlined in section 6.2. The theory of planar channeling and various types of potentials used in this comparative study are discussed in section 6.3. The CDR analysis using a numerical program is outilined in section 6.4. The results obtained using Shell and Biersack's Universal potentials are also compared with Moliere planar potential in this section. Conclusion is given in the last section.

6.2 BASIC PRINCIPLES OF SLS

Superlattices are multilayered structures of alternate composition of materials having same crystal structure but with slightly different lattice parameter. Semiconductors belonging to *Diamond* or *Zinc blende* type crystal structures have four bonds oriented along the four tetrahedral directions. (ie, each bond has an angle of 109.5° with neighbouring bond) [21]. We can qualitatively represent such four bond crystal as square array of atoms in two dimensions. This is shown in Fig 6.1.*a*. For the lattice matched superlattices this four fold bonding sustain and the epilayer and substrate have the same lattice parameter. If the growth temperature is high enough to have sufficient thermal energy, the deposition of epilayer atom onto the substrate surface allows them to easily locate the potential minima corresponding to substrate lattice. Let a^0_{epi} and a^0_{sub} be the unstrained

lattice constants, h_{epi} and *fraub* be the unstrained thicknesses of the epitaxial layer and substrate respectively, the inplane lattice constant $a^{\|}$ can be written as

$$\begin{aligned} a^{\|} &= \frac{a^{o}_{epi} h_{epi} + a^{o}_{sub} h_{sub}}{h_{epi} + h_{sub}} \\ &\approx a^{o}_{sub} \end{aligned} \tag{6.1}$$

In SLS case, where the epilayer atoms are constrained to the substrate interatomic spacing in the plane of the interface,. the unit cell will distort tetragonally inorder to preserve its volume per unit cell and all the atoms retain fourfold bonding. If the unit cell of the epitaxial layer is smaller than that of the substrate it must be stretched in the inplane direction and its height will decrease. This process is known as *Poisson effect* and is illustrated in Fig. 6.1.6. The superlattice layers alternate between compressive and tensile biaxial strain and each layer acquires a distinct perpendicular lattice constant $a^{\perp}_{b}$ and $a^{\perp}_{a}$. due to strain accommodation. According to *Poisson ratio*, layers under biaxial compressive stress will have an $a^{\perp}$ • value larger than the equilibrium lattice parameter a_{sub} and those under biaxial tensile stress a smaller $a^{\perp}_{sub}$ value [5]. As a consequence of these alternating tetragonal distortions along the growth direction, , inclined crystal planes and rows undergo alternating tilts $\Delta\psi$ at each interface. Along the growth direction the crystal rows are straight and channeling behaviour is similar to that of single crystals. However, along inclined directions the alternating tilts between layers have tremendous influence on the channeling behaviour (shown in Fig. 6.1.*c*). Since the $\Delta\psi$ is of the order of critical angle for channeling of high energy ions, dechanneling increases with depth along these inclined direction [5].

The tilt angle between layers $\Delta\psi$ is given by

$$\begin{aligned} \Delta\psi &= \arctan \frac{a^{\perp}_{epi}}{a^{\|}} - \arctan \frac{a^{\perp}_{sub}}{a^{\|}} \\ &\approx \frac{a^{\perp}_{epi} - a^{\perp}_{sub}}{2\, a^{\|}} \end{aligned} \tag{6.2}$$

Thus the tilt angle is directly related to the difference in the tetragonal distortions between layers and is a measure of relative strain between SLS layers [5]. Significant elastic energy is stored in the structure and it increases linearly with substrate thickness. If the thickness of the SLS exceeds a critical thickness h_c, deformation of structure occurs in order to relax the strain energy accommodation in the system. In this situation four fold bonding can not be maintained along the interface and an occasional atom is left with only three bonds. This process introduces slipped regions into the crystal, bounded by line defects known as *misfit dislocations* and is shown in Fig.6.1.*a*.

6.3 PLANAR CHANNELING IN SLS

The equation of motion of a planar channeled particle in a crystal is given by [13]

$$\frac{d^2x}{dz^2} + \frac{1}{2E_z}\frac{dY_2(x)}{dx} = 0 \tag{6.3}$$

where *x* and *z* are the transverse and longitudinal displacement of channeled particle (This is shown in Fig. 6.2.*a*.) respectively and x is measured from the midpoint between the planes. E_z is the longitudinal energy and almost equals to the incident energy E (ie $E_z = E$). $Y_2(x)$ is the averaged continuum model planar potential given by [13]

$$Y_2(x) = Y(l-x) + Y(l+x) - 2Y(l) \tag{6.4}$$

where Y(x) is the planar potential and / = $d_p/2$, where d_p is the interplanar space. Here last term is a normalization factor so that $Y_2(x)$ is zero at the midpoint between planes.

The total transverse energy $E\pm$ is conserved and is given by [13]

$$E_\perp = E(\frac{dx}{dz})^2 + Y_2(x) \tag{6.5}$$

where dx/dz= ψ is the incident angle. From this we get

$$dz = \sqrt{E}\frac{dx}{\sqrt{E_\perp - Y_2(x)}} \tag{6.6}$$

which yields after integration, the wave length of particle trajectory as a function of transverse energy as

$$\lambda = 4\sqrt{E}\int_0^a \frac{dx}{\sqrt{E_\perp \sim Y_2(x)}} \tag{6.7}$$

Here a is the amplitude of motion defined by $Y_2(a) = E\pm$. The comparison between various potentials is much easier and lucid in the wave length function analysis.

In Figs.6.3.*a* and 6.3.6 the Moliere, Shell and Biersack's Universal average planar potentials (hard spring type potentials) are plotted as a function of distance from the centre of channel. Shell potential gives a slightly lesser value compared to Moliere and Biersack's Universal planar potentials. Near the plane both Universal and Shell potentials give values ,which lie below Moliere planar potential [11]. In other words Moliere planar potential is the strongest hard spring type potential discussed above. This is more evident from Fig. $6.4(a, b, \mathrm{c})$. Here A is a monotonically decreasing function of amplitude and transverse energy (characteristic of channeling potentials), which means the closer a positive particle moves to a plane the harder it is pushed away by the positive nuclei of lattice atoms. Therefore, for a given energy $E = 1.2$ MeV and incident angle ψ_o, the dechanneling will be maximum for shell and least for the Moliere potential. This can be seen in all the dechanneling fraction versus depth graphs shown in Figs. 6.6, 6.8 and 6.9.

The equation of motion for a planar channeled particle in a *SLS* is given by [3,12] (shown in Fig. 6.2.6.)

$$\frac{d^2x}{dz^2} + \frac{1}{2E_z}\frac{d}{dx}Y_2(x) = \sum_{j=1}^{n}(-1)^j\ \Delta\psi\ \delta(z - js) \tag{6.8}$$

where *n* is the number of layers. It may be noted that for the case of $\Delta\psi = 0$, the equation (6.8) reduces to the equation of motion for a perfect single crystal (equation6.3). The Delta function gives an impulse of magnitude $\Delta\psi$ to *dx/dz* at each interface located at $z = js$ with first impulse in the *-dx/dz* direction (by convention). Integrating the

equation from js^- to js^+ gives [13]

$$\psi(js^+) - \psi(js^-) = (-1)^j \Delta\psi \tag{6.9}$$

6.4 CATASTROPHIC DECHANNELING RESONANCE

The main cause of Catastrophic Dechanneling Resonance (CDR) is that a large fraction of **planar** channeled particles are simultaneously focussed onto channel wall under these resonance conditions [12]. Maximum dechanneling occurs in this case. CDR condition is achieved experimentally by changing the beam energy until the effective wavelength matches the superlattices period (A = 2s) as shown in Fig.6.2.*b*. Effective wavelength of planar channeled particle motion can be experimentally determined from the oscillations in the back scattered yield as a function of a depth [5].

We have studied the depth and angular dependence of CDR as a function of incident angle (ψ_o), strain tilt angle ($\Delta\psi$) and minimum impact parameter (r_c). The minimum impact parameter r_c defines the cut off distance for a channeled trajectory and if **a** particle approaches a plane within a distance r_c of that plane, it is considered to be dechanneled. We have calculated the dechanneling profile of 1.2 MeV ^4He particles in $GaAs_{0.09}P_{0.91}$ / *GaP (s* = 48.2 nm, layer thickness = 34 nm) for various incident angles ψ_o = —0.133°, 0.0°, 0.133° , tilt angles $\Delta\psi$ = 0.143°, 0.153°, 0.163° and minimum impact parameters r_c = $1.15a_T$,$1.25a_T$ and $1.13a_T$ respectively. This particle energy corresponds to resonance conditions discussed above.

The trajectory of a planar channeled particle is simulated numerically by integrating equation (6.8), for each incident angle (ψ_o) and initial longitudinal displacement (z_o). The trajectory calculations were carried out for 200 incident particles spaced uniformly between the planes (i.e., varying the initial transverse displacement x_o from $-d_p/2$ to $+d_p/2$). When a particle crosses the first interface ($z = s, j = 1$) there should be a

change in ψ by an amount equal to $-\Delta\psi$. At second interface ($z = 2s, j = 2$), this amount should be $+\Delta\psi$ because of opposite tilt. We have used this criterion (equation 6.9) for checking the program for various values of $\Delta\psi$ and ψ. All numerical calculations were carried out at Microvax II system with the help of IMSL Math/Library^{TM}.

There is a strong asymmetry in the incident angle dependence of CDR. When the incident angle is varied from $\sim\psi_o$ to ψ_o, the focussing of the channeled particles onto the channeling wall is advanced and the dechanneling depth is shifted to shallower depth (the angle ψ_o $(-\psi_o)$ is defined as towards (away) from the second layer direction). This asymmetry in the incident angle can be understood qualitatively from the phase plane analysis based on *modified harmonic model* discussed below [3,22].

Let ψ_M be the *critical angle* for channeling, and x_c be the *critical distance* defined such that $r_{min} = d_p/2 - x_c$. Since the *transverse energy* is conserved, *critical transverse energy* $E_{\perp,c}$ can be written as

$$E\,\psi_M^2 \;=\; Y_2(x_c) \tag{6.10}$$

Equation (6.5) can be simplified if the potential is approximated by a simple harmonic potential, $Y_2(x) \propto x^2$, giving

$$\frac{(dx/dz)^2}{\psi_M^2} \;+\; \frac{x^2}{x_c^2} \;=\; r_p^2 \tag{6.11}$$

In the modified - harmonic model all particles have the same wavelength (equation 6.7) because of the harmonic nature of the potential and motion of a particle in the phase plane is on a circle of radius r_p with co-ordinates $(2x/x_c, (dx/dz)/\psi_M)$ as shown in fig 6.5 [3,22]. (For simplicity the *critical distance* x_c on the phase circle was shown as $d_p/2$). Unit circle (see Fig. 6.5) corresponds to *critical transverse energy* for particles to remain channeled [12]. A uniform incident beam of particles is represented by a horizontal line

5 on a diagram of normalized transverse momentum (angle) versus normalized lateral position in the channel. This assumption is possible because in *harmonic approximation* the wavelength is independent of transverse energy [3]. For larger incident angles $(+\psi_o)$, the line will be placed higher above the *x - axis* and for negative incident angles the line will be placed below the *x -axis.* This line rotates as the channeled beam penetrates the crystal, and undergoes a vertical increase at each interface according to sign and magnitude of the tilt $\Delta\psi$ [10]. Since the *path length per layer* s is half the wavelength (A) of the beam (See Fig. 6.2.6.), while penetrating each layer the beam changes its direction. At the interface the crystal plane also changes it direction by $\pm\Delta\psi$ with respect to the sign of the incident angle. Thus, the angle of the channeled particles relative to the crystal planes increases at each interface until they become sufficiently large so that continuum potential can no longer restrict the motion of the particles with in the plane and consequently dechanneling of the particles occur. Since the outer circle corresponds to the maximum transverse energy for which particles remain channeled, the complete dechanneling situation corresponds to the shifting of line *S* completely outside the circle (shown in Fig. 6.5.)

The calculated trajectories for 1.2 MeV ^4He channeled in a SLS for incident angles $\psi_o = -\Delta\psi/2$ and $\psi_o = +\Delta\psi/2$ respectively are also shown in Fig 6.5. It is evident from the Fig.6.5 that there is a delay in depth for catastrophic dechanneling of one layer for $\psi_o = -\Delta\psi/2$ case. Since the starting line in the *phase plane* is below the origin for particles incident at an angle $\psi_o = -\Delta\psi/2$, its evolution out of the circle at each interface trails that of particles incident at an angle $\psi_o = +\Delta\psi/2$ by exactly one layer.

Moving the incident angle to increasingly larger negative values shifts the line *S* lower on the unit circle and there by delays the focusing of the channeled particle into the planar wall [12].

This incident angle asymmetry is shown in Fig.6.6*a*, 6, c. for ψ_o = —1.33°, 0.00° and

0.133° respectively. When the angle is increased from -0.133° to 0.133°, the dechanneling at a given depth is increased. The dechanneling fraction calculated using Moliere, Shell and Universal planar potentials compare well with experimental results. Specially the depth at which the abrupt rise in dechanneling (a characteristic of CDR) matches with experimental points. When the angle is decreased from +0.133° to —0.133°, this marked increase in dechanneling fraction diminishes.

It is evident from above mentioned *phase-plane analysis*, if one reduces the incident direction ψ_o by $\Delta\psi$ it delays the depth of the *CDR* by one layer. Let $D_c(\psi_o)$ denote the depth of the *CDR*, then

$$D_c(\psi_o) - D_c(\psi_o - \Delta\psi) = -1 \tag{6.12}$$

and hence

$$\frac{\Delta D_c(\psi_o)}{\Delta\psi} = \frac{-1}{\Delta\psi} \tag{6.13}$$

Thus the *CDR* depth versus incident angle should have an average slope $-1/\Delta\psi$ and thus be a measure of strain in the *Strained Layer superlattices.*

Using the phase plane analysis we can calculate the CDR depth as a function of incident angle ψ_o. It can be shown that the jumps in the *CDR* depth at interface *j* occur at the corresponding incident angle ψ_o such that [22]

$$j - 1 = \psi_c/\Delta\psi(A - \psi_o/\psi_m) \tag{6.14}$$

Where $A = [1 - ((1 - \chi_c)d_p/2x_c)^2]^{1/2}$ and χ_c is the dechanneling level. The *Catastrophic Dechanneling depth* increases when the angle of incidence is varied from $-\psi_o$ to $+\psi_o$ and is shown explicitly in Fig. 6.7. The calculations were done for the dechanneling depth corresponding to a dechanneling level $\chi_c = 0.85$ (i.e. 85 % of the particles were

dechanneled at this depth). Thus slope of the line in Fig. 6.7. which is calculated using *modified harmonic approximation* (equation (6.14)) is equal to the reciprocal of tilt angle $\Delta\psi$. This model allows rapid evaluation of results without the extensive numerical calculations. The staircased structure shown for *CDR* depth calculations using *Moliere*, *Biersack's Universal* and *Shell planar potentials* contains both strain and potential information and to a first approximation, the slope of the straight line passing through these staircased structure is equal to the reciprocal of the strain tilt angle $\Delta\psi$. The *CDR* depth calculations using Shell, Moliere and Biersack's Universal planar potentials are in good agreement with experimental results shown in Fig.6.7.

For larger minimum impact parameter r_c only few particles remain channeled, because the effective channel width is decreased. The parameter $|d_p/2-b.a_T|$ determines the width of the channel, where 6 is a variable (1.15, 1.25 and 1.35 in the present case) and a_T is the Thomas Fermi screening radius. So it is not surprising that dechanneling at a given depth is largest for highest value of r_c i.e., for r_c=1.35 a_T. (shown in Fig.6.8). Similar situation exists for other values of tilt angles. For higher values of the tilt angles, transverse energy acquired at the interface is large and that results in sharp rise in dechanneling fraction. This is shown in Fig.6.9.

There is no concrete analytical method to find energy corresponding to catastrophic dechanneling. The incident angle versus average yield $(\bar{x})$ is plotted on a graph and the energy corresponding to the maximum average yield is taken as the catastrophic dechanneling energy [14] (Shown in Fig.6.10.). x is defined to be the average yield between second and fourth interfaces, because in this region, maximum dechanneling occurs. The incident energy corresponding to CDR is analytically calculated using Moliere, Shell and Biersack's Universal potential (calculations have been done for ^4He ion beams incident along the (110) direction of the top layer of $GaAs_{0.17}P_{0.83}$ /GaP,where s = 45.2nm and d_p — 1.93$\mathring{A}$) Calculations using Moliere planar potential correctly predicts the energy value

corresponding to catastrophic dechanneling ($E = 1.2MeV$).Moliere calculations show dechanneling fractions are very sensitive to incident energy and there is a sudden rise in dechanneling fraction near $E = 1.2MeV$.For both Shell and Biersack's Universal planar potentials there is a gradual variation in *x* versus *E* graph. For Shell planar and Biersack's Universal planar potentials, analytical calculations predict energy corresponding to CDR at 1.3 MeV. The dechanneling fraction is very sensitive to the incident energy and the type of potential used in the calculations.

6.5 CONCLUSION

It has been already experimentally verified that the *Catastrophic Dechanneling Resonance* effect can be used to measure strain in *Strained Layer Superlattice.* Sensitivity of this ion channeling effect is due to the fact that the tilt angle $\Delta\psi$ is of the order of critical angle for channeling ψ_c [22]. The *CDR* technique is the most sensitive of the ion channeling techniques for strain measurements. Typically, the values of the tilt angle, $\Delta\psi$, can be determined within an accuracy of as great as 0.01°, which corresponds to strains of 0.02%. [10]. Since the half wavelength (A/2) of the planar channeled particles are of the order of 50 *nm* and must be made equal to path length per layer s, *CDR* technique is more suited for thick layers [10].

We have calculated the CDR dependence on various parameters using Moliere, Shell and Biersack's Universal planar potentials. The choice of the shell potential was due to its non statistical nature, and the signature of detailed atomic structure target material is inherent in the Shell model. We hope this will give more physically acceptable results in the defect studies in SLS, which we plan to undertake shortly. For the defect studies in SLS more parameters should be incorporated into the Shell model. Moreover the location of the atoms in SLS structure also becomes significant in this case.

References

[1] L. Esaki and R. Tsu *IBM. J. Res. Develop* 14, 61, (1970).

[2] G. C. Osbourn *J. Appl. Phys.* 53, 1586, (1982).

[3] W. K. Chu, J. A. Ellison, S. T. Picraux, R. M. Biefeld and G. C. Osbourn *Phys. Rev. Lett.*, 52, 125, (1984).

[4] A. P. Pathak and P. K. J. Balagari *Appl Phys. Lett.*, 48, 1075, (1986).

[5] S. T. Picraux, R. M. Biefeld, W. R. Allen, W. K. Chu and J. A. Ellison *Phys. Rev. B,* 38, 11086, (1988).

[6] A. P. Pathak, *Radiat. Eff.*, 61, 1, (1982).

[7] *Synthetic Modulated Structures* Eds. Leroy L. Chang and B. C. Giessen, (Academic Press Inc, New York), (1985).

[8] *Physics and Applications of Quantum Wells and Superlattices, Nato AS1 series* B **170,** Eds. E. E. Mendez and K. von Klitzing, (Plenum Press New York) (1987).

[9] *Strained Layer Superlattices: Physics, Semiconductors and semimetals,* 32, ed. Thomas P. Pearsall, (Academic Press Inc, New York) (1991).

[10] *Strained Layer Superlattices: Material Science and Technology, Semiconductors and semimetals,* 33, ed. Thomas P. Pearsall, (Academic Press Inc, New York) (1990).

[11] W. R. Allen, W. K. Chu, S. T. Picraux, R. M. Biefeld and J. A. Ellison *Phys. Rev. B,* 39, 3954, (1989).

[12] S. T. Picraux, W. R. Allen, R. M. Biefeld, J. A. Ellison and W. K. Chu *Phys. Rev. Lett,* 54, 2355, (1985).

[13] J. A. Ellison, S. T. Picraux, W. R. Allen and W. K. Chu *Phys. Rev. B,* 37, 7290, (1988).

[14] W. K. Chu, W. R. Allen, S. T. Picraux and J. A. Ellison *Phys. Rev. B,* 42, 5923, (1990).

[15] G. Moliere *Z. Naturforschung,* A 2, 133 , (1947).

[16] V. Hari kumar and A. P. Pathak *phys. stat.sol. b,* **177,** 269, (1993).

[17] V. Hari kumar and A. P. Pathak *J. Phys. Condens. Matter,* 5, 3163, (1993).

[18] V. Hari kumar and A. P. Pathak *phys. stat. sol b,* **182,** 51, (1994).

[19] D. J. O'Connor and J. P. Biersack *Nuclear Instrum. Methods,* B 15, 14, (1986).

[20] J. F. Ziegler, J. P. Biersack and U. Littmark *Stopping and Ranges of Ions in Matter* Vol. 1, eds., J.F. Ziegler (Pergamon Press, New York), (1984).

[21] J. C. Bean *Science,* **230,** 127, (1985).

[22] S. T. Picraux, W. K. Chu, W. R. Allen and J. A. Ellison *Nuclear. Instrum. Methods,* B 15, 306, (1986).

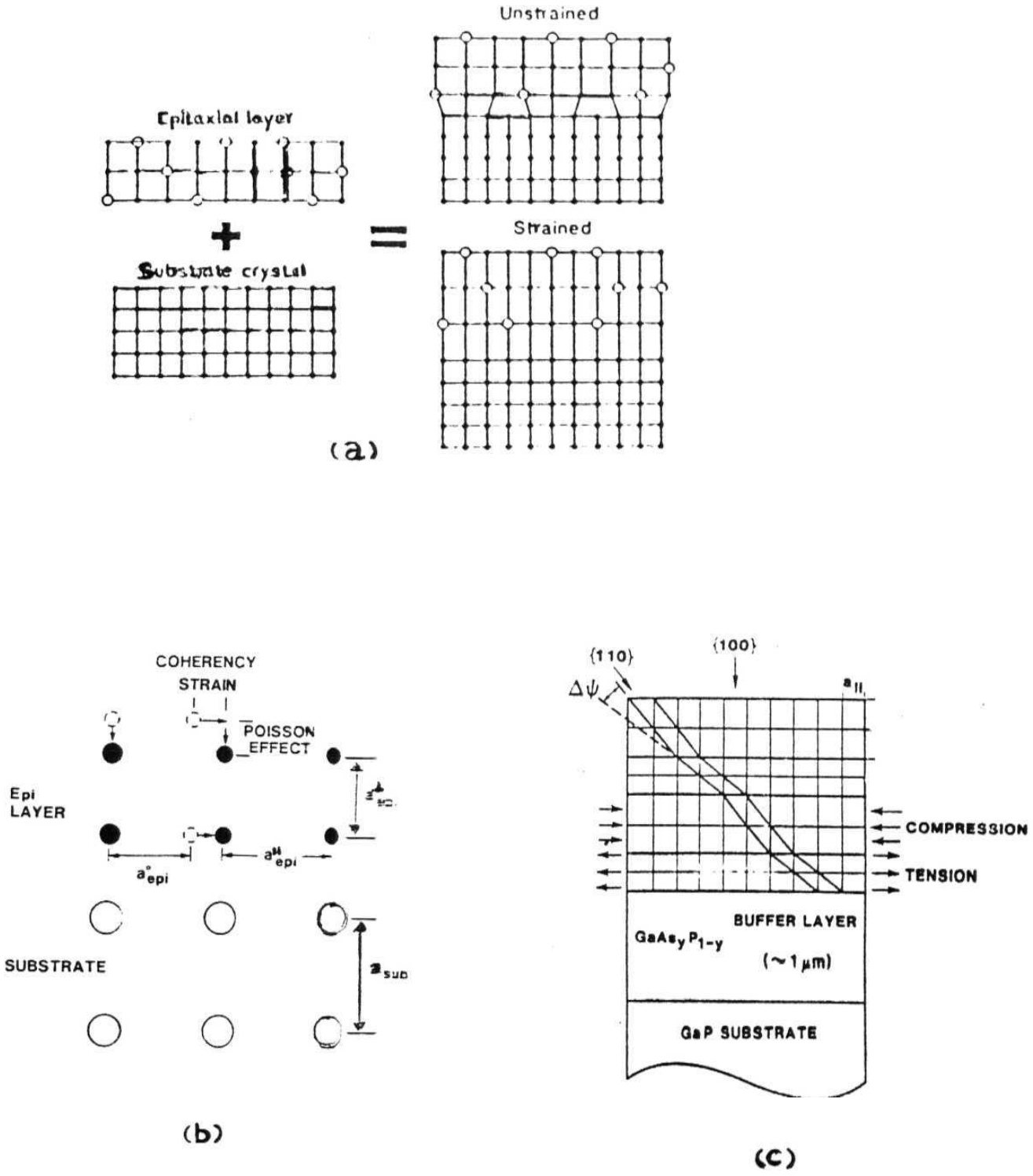

Fig 6.1: (a). Alternate mode of *Semiconductor epitaxy* (Ref (21)). (b) Atom positions for a *Strained epitaxial* feyer on a thick substrate fflwtratiiig the coherency *$train* and *Poisson effect* (Ref (10)). (c) Schematic diagram of a *SLS* with lattice distortion due to lattice mismatch between layers emphasised (Ref (5)).

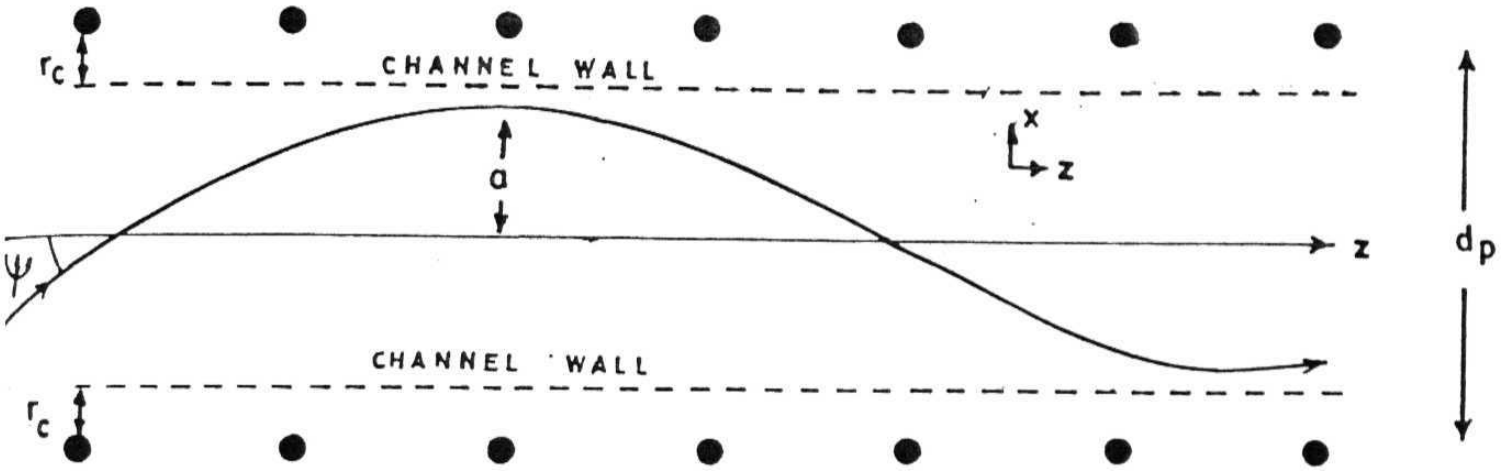

(a)

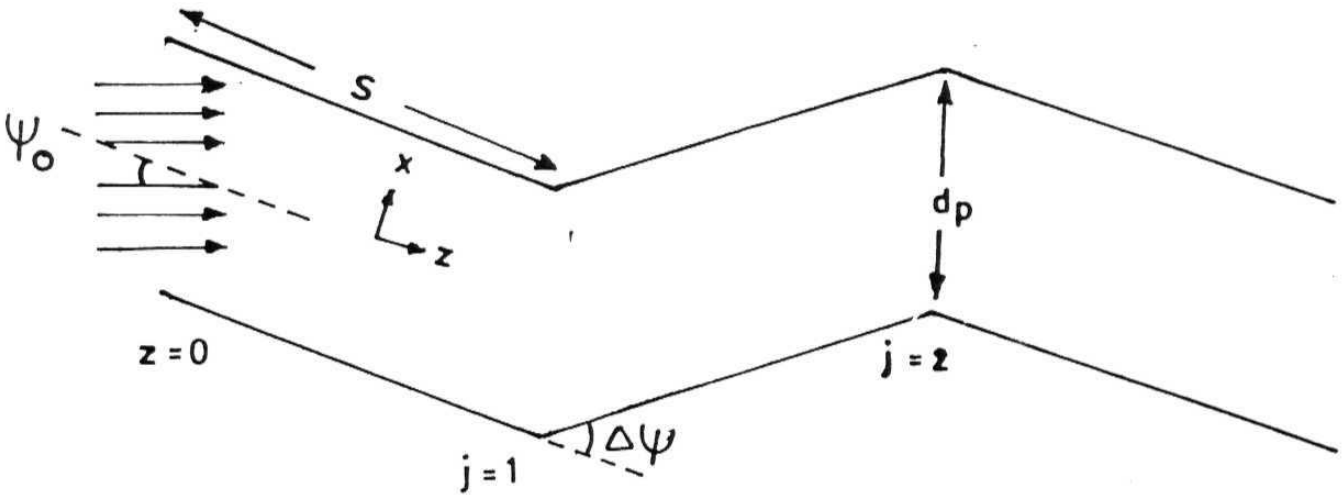

(b)

Fig 6.2: (a). **Trajectory** of a planar **channeled particle.** d_p is the interplanar **spacing,** r_c is the minimum impact parameter for **channeling ,** ψ it the incident angle and a is the amplitude of motion of a channeled **particle.** (b). Schematic diagram of (**110)** planar channel of a Strained Layer Superlattices (SLS). $\Delta\psi$ is the **tilt** angle and s is the path length per layer of the SLS.

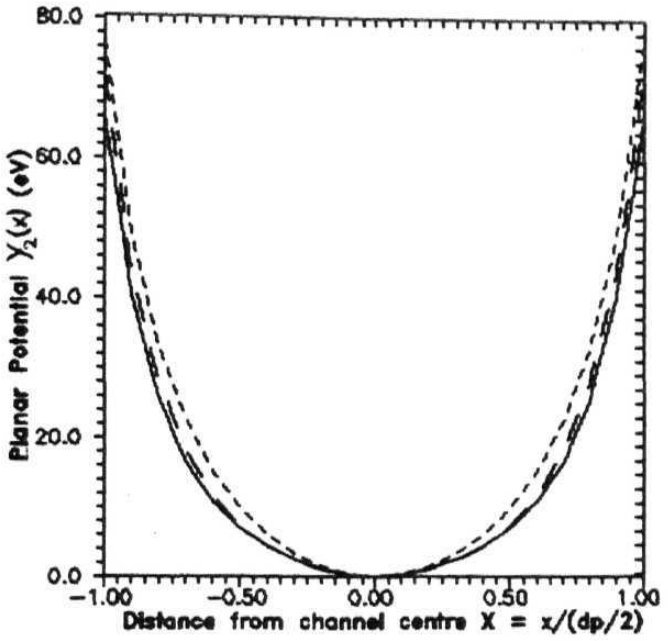

(a)

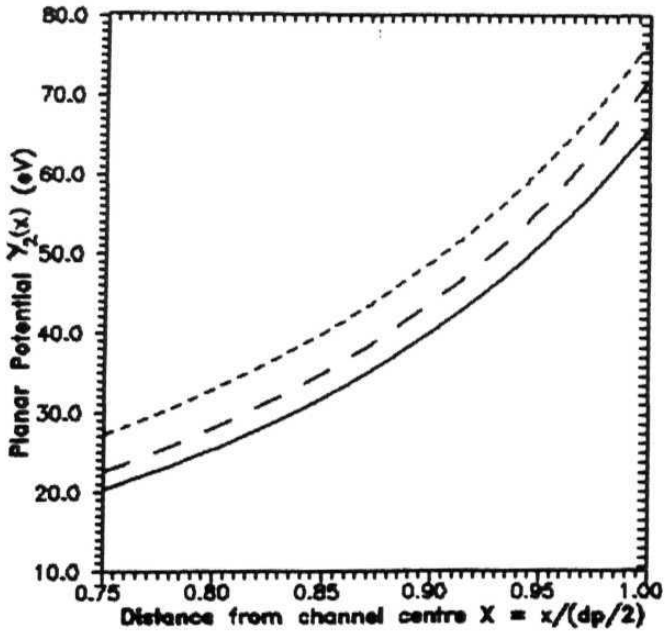

(b)

Fig 6.3: (a)Moliere (*dotted curve*), Shell (*solid curve*) and Biersack's Universal (*dashed curve*) planar potentials for channeling of 1.2 MeV ^{4}He ions incident along (110) plane of $GaAs_xP_{1-x}/GaP$ with x = 0.075. (b). Enlargement of the figures near the (110) plane.

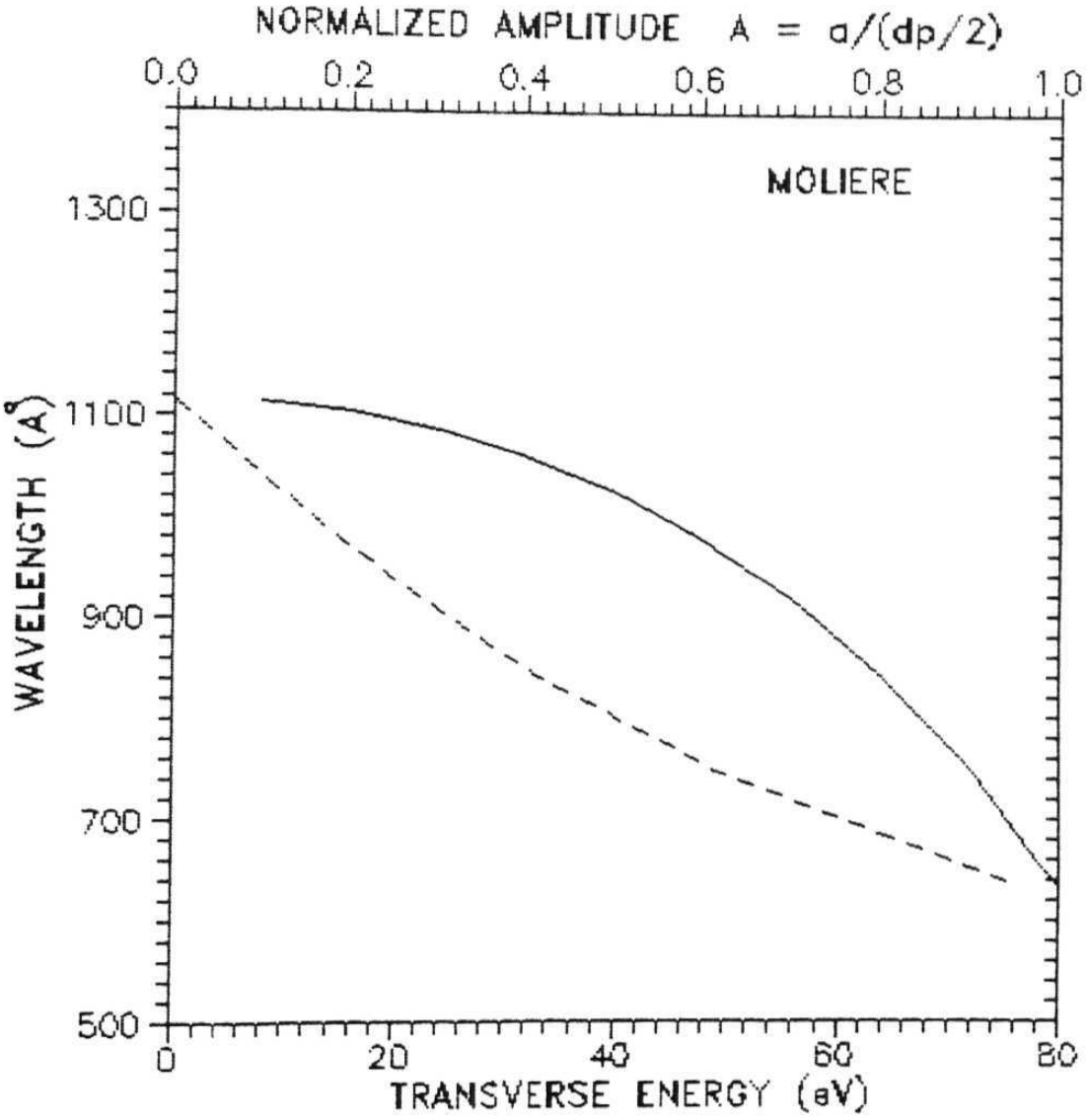

Fig 6.4.(a): **Wave length for 1.2 MeV ^{4}He in (110) $GaAs_xP_{1-x}/GaP$ as a function of normalised amplitude (*solid curve*) and as a function of transverse energy (*dashed curve*) for *Moliere planar potential.* Here wavelength is in Å units and transverse energy is in *electron volts.***

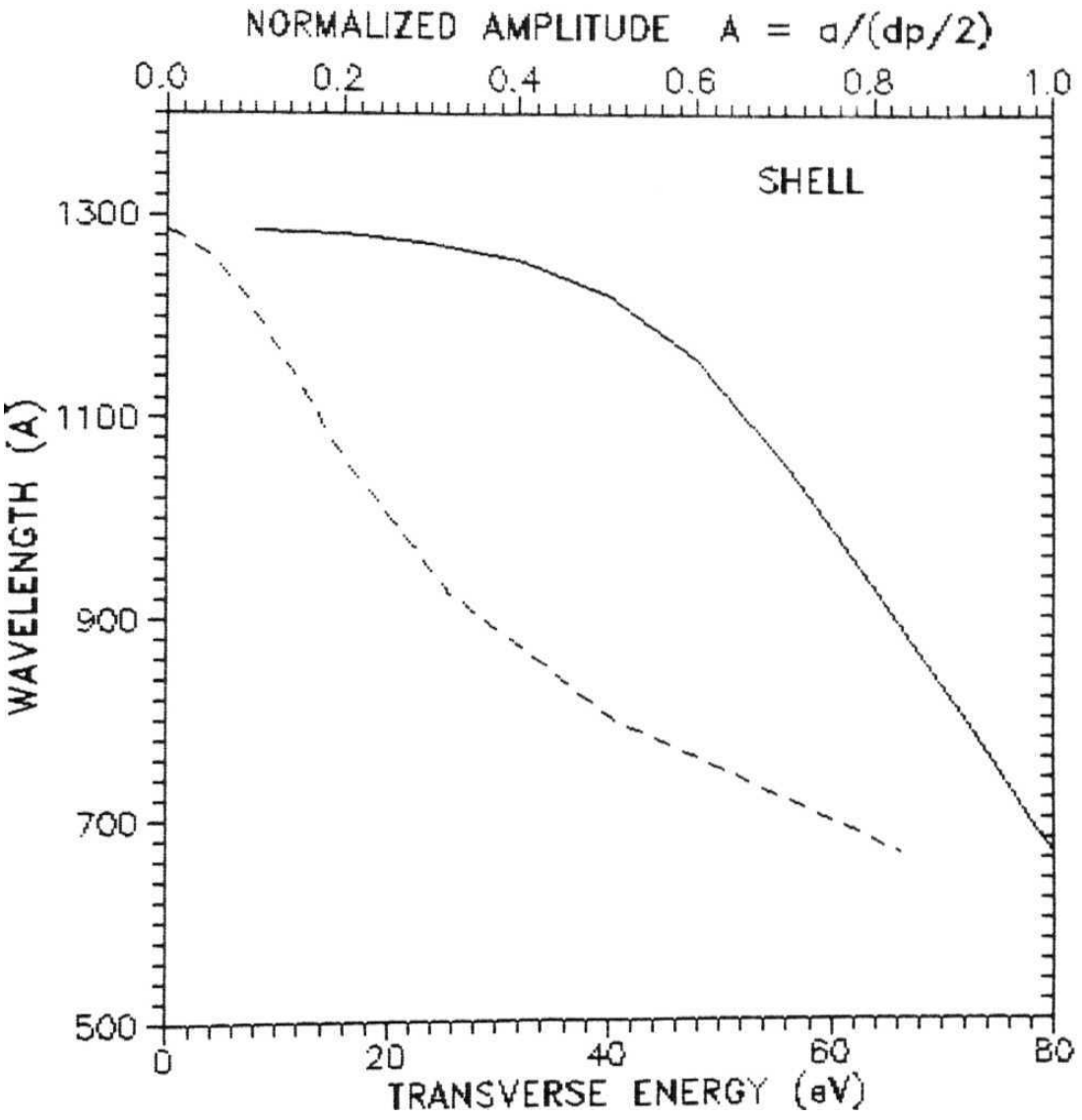

Fig 6.4.(b): **Wave length for 1.2 MeV ^{4}He in (110) $GaAs_xP_{1-x}/GaP$ as a function of normalised amplitude (*solid curve*) and as a function of transverse energy (*dashed curve*) for *Shell planar potential.* Here wavelength is in Å units and transverse energy is in *electron volts.***

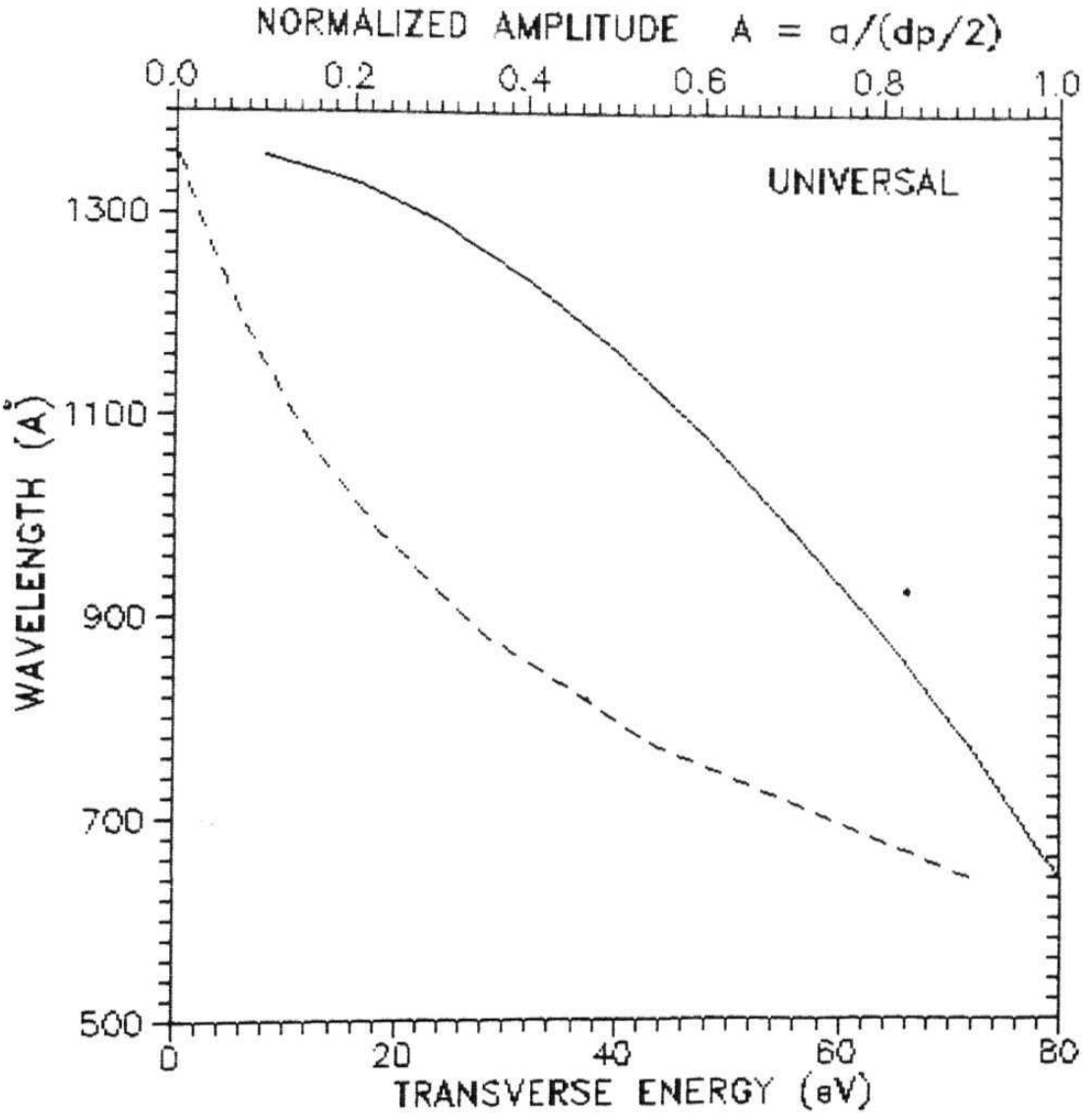

Fig 6.4.(c): **Wave length for 1.2 MeV ^4He in (110) $GaAs_xP_{1-x}/GaP$ as a function of normalised amplitude (*solid curve*) and as a function of transverse energy (*dashed curve*) for *Biersack's Universal planar potential.* Here wavelength is in Å units and transverse energy is in *electron volts.***

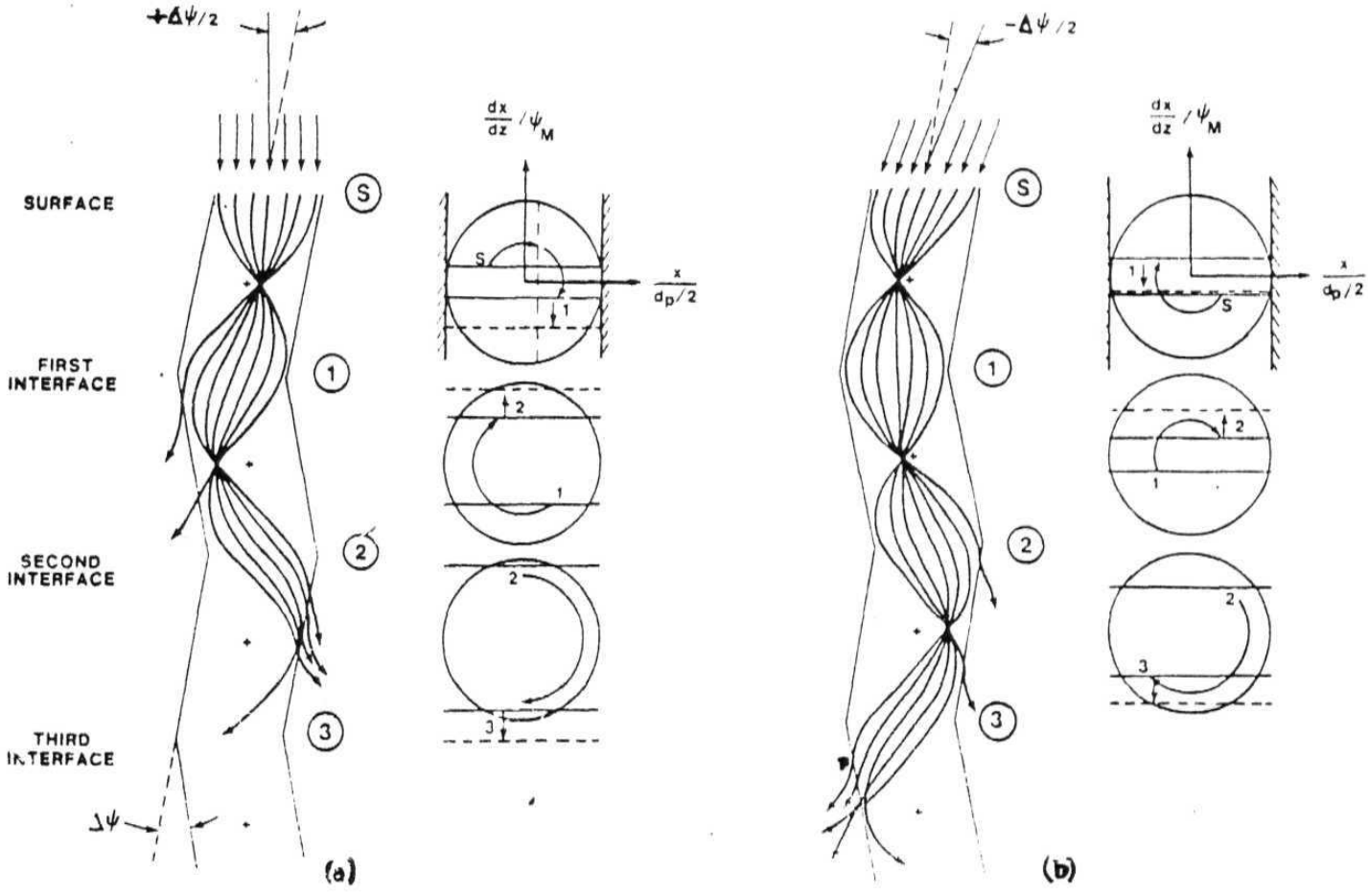

Fig 6.5: The calculated trajectories for 1.2 *MeV* ^4He in an *SLS* for two different incident angles, (a) for $\psi_o = +\Delta\psi/2$ and (b) for $\psi_o = -\Delta\psi/2$ (Ref. 12)

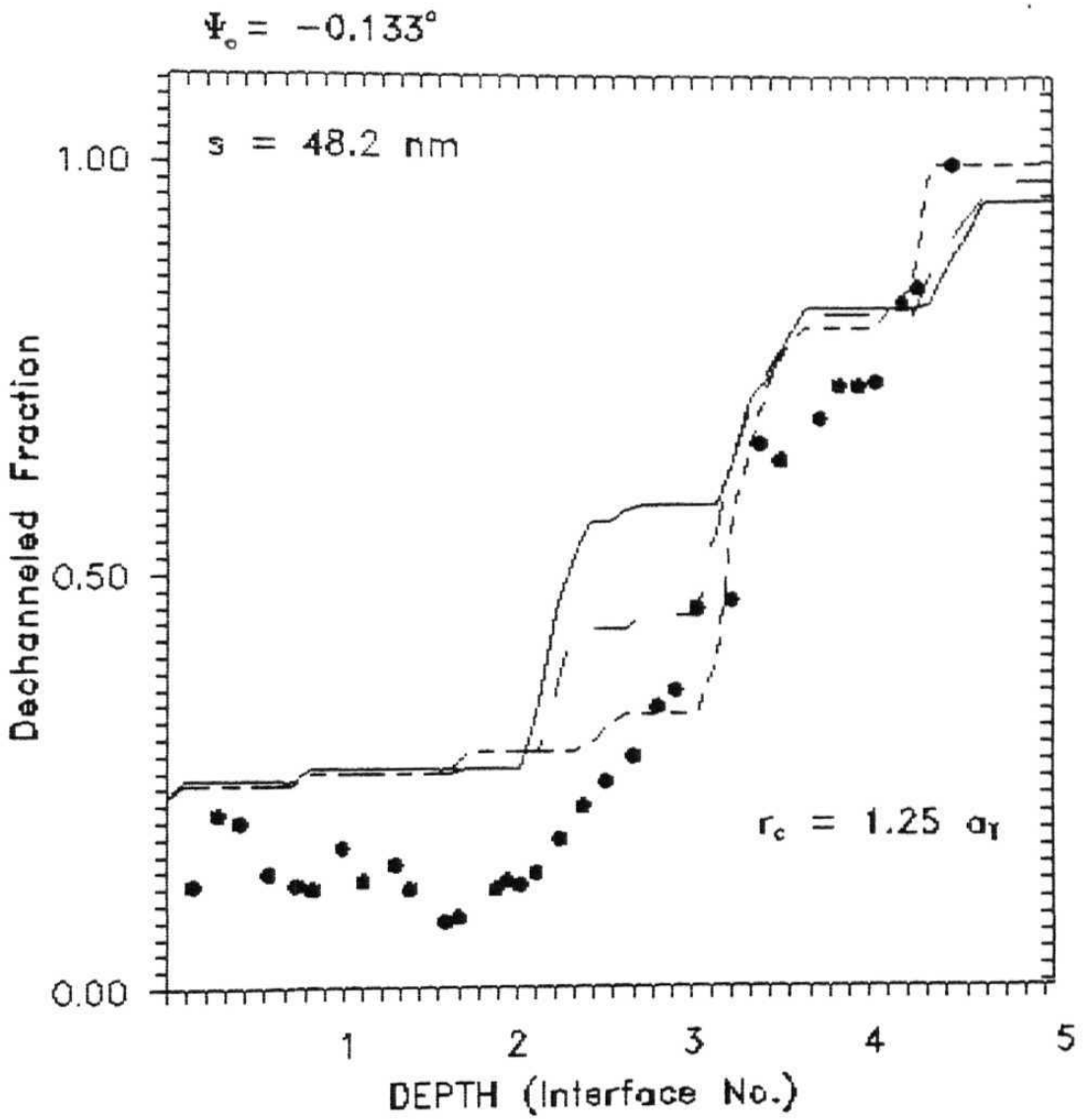

Fig 6.6 (a): **Calculated dechanneling depth profiles for a *Catastrophic Dechanneling Resonance* [CDR] (E = 1.2 MeV) using *Moliere* (*dotted line*), *shell* (*solid line*) and *Biersack's Universal* (*dashed line*) planar potentials. These calculations have been done for $r_c = 1.25a_T$ at $\psi_0 = -0.133°$. *Solid circles* represent experimental points.**

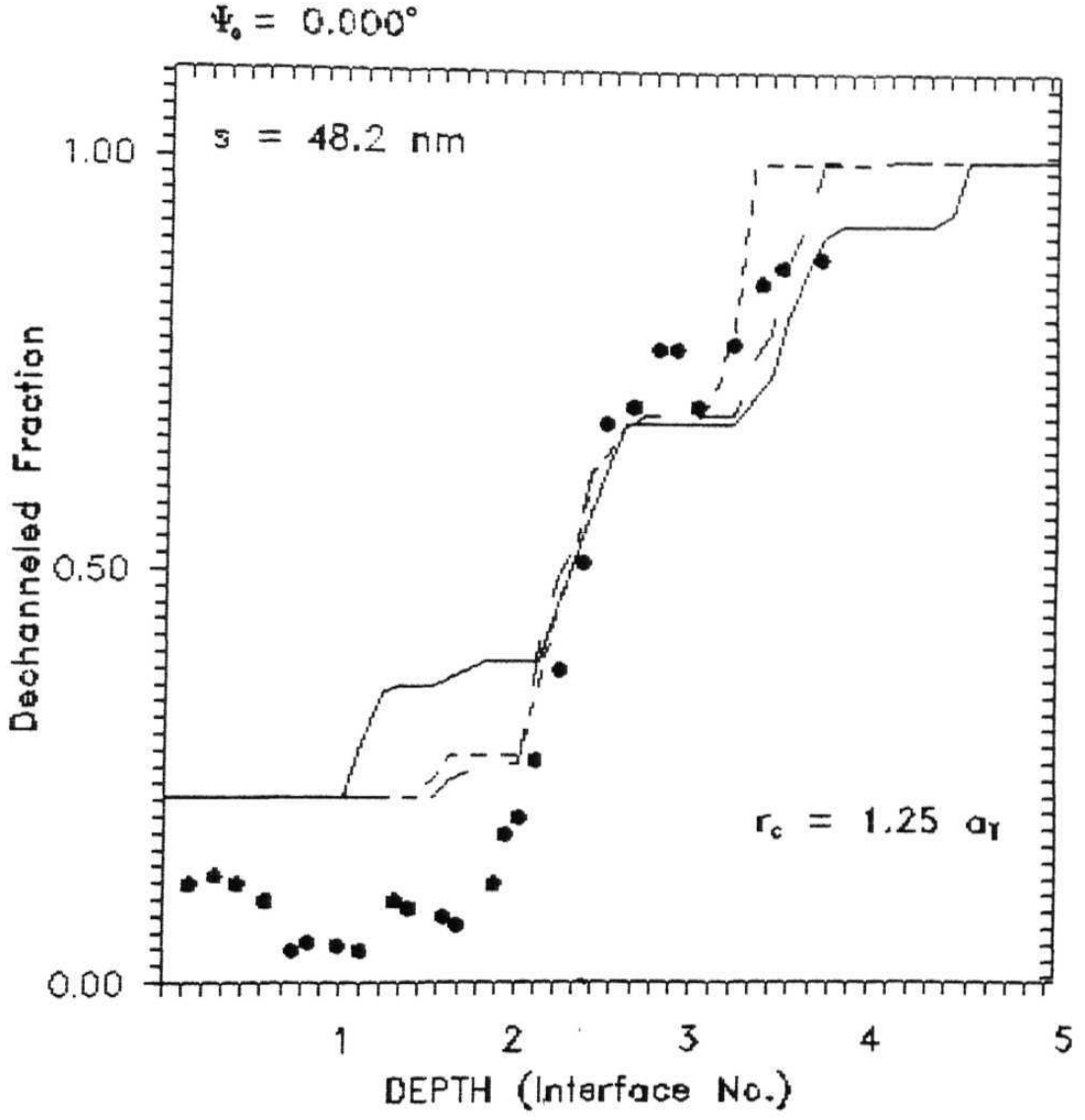

Fig 6.6 (b): **Calculated dechanneling depth profiles for a *Catastrophic Dechanneling Resonance* [CDR] (E = 1.2 MeV) using *Moliere* (*dotted line*), *shell* (*solid line*) and *Biersack's Universal* (*dashed line*) planar potentials. These calculations have been done for $r_c = 1.25a_T$ at $\psi_o = 0.0°$. *Solid circles* represent experimental points.**

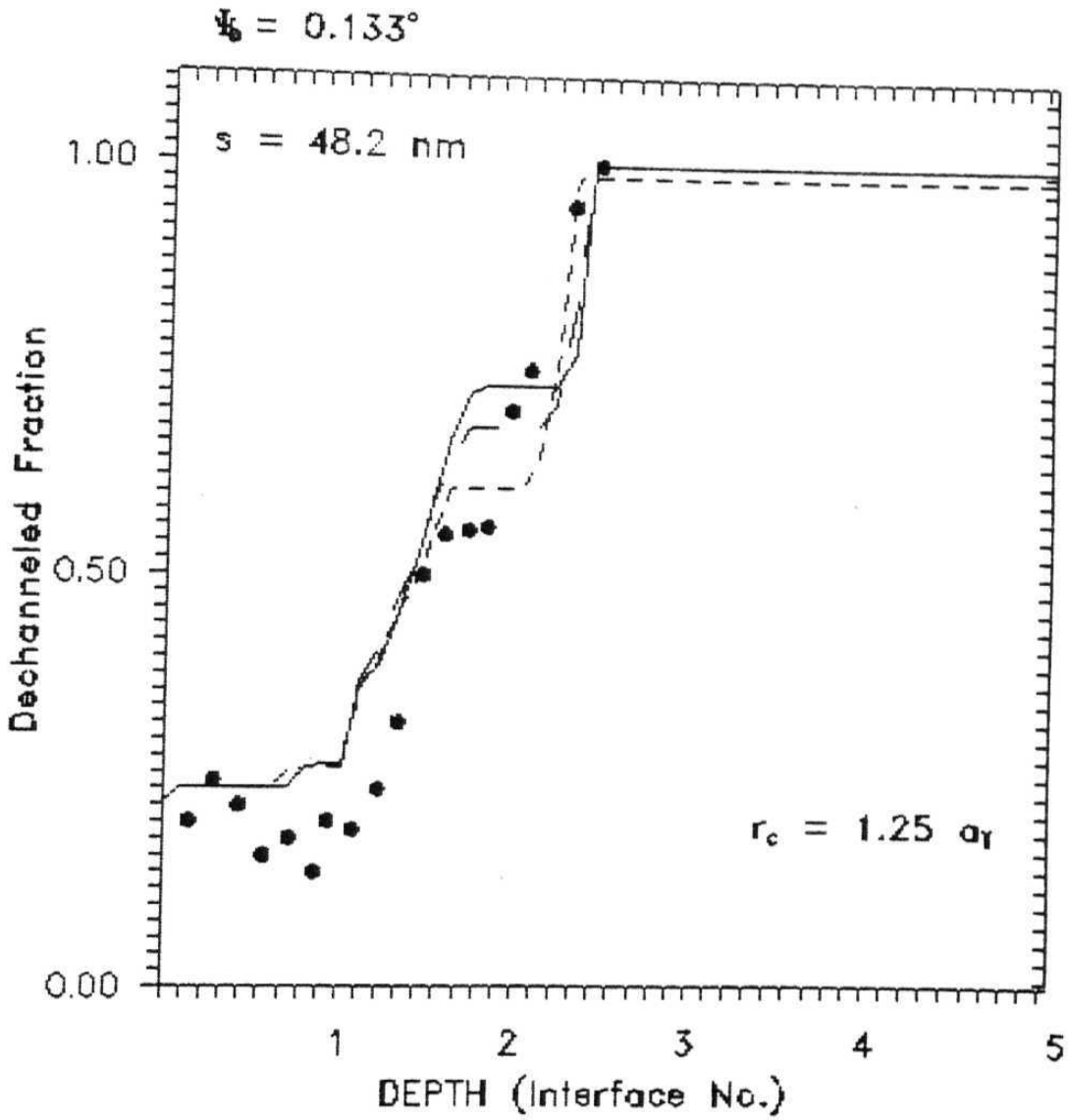

Pig 6.« (c): **Calculated dechanneling depth profiles for a *Catastrophic Dechanneling Resonance* [CDR] (E = 1.2 MeV) using *Moliere* (*dotted line*), *shell* (*solid line*) and *Biersack's Universal* (*dashed line*) planar potentials. These calculations have been done for $r_c = 1.25a_T$ at $\psi_o = 0.133°$. *Solid circles* represent experimental points.**

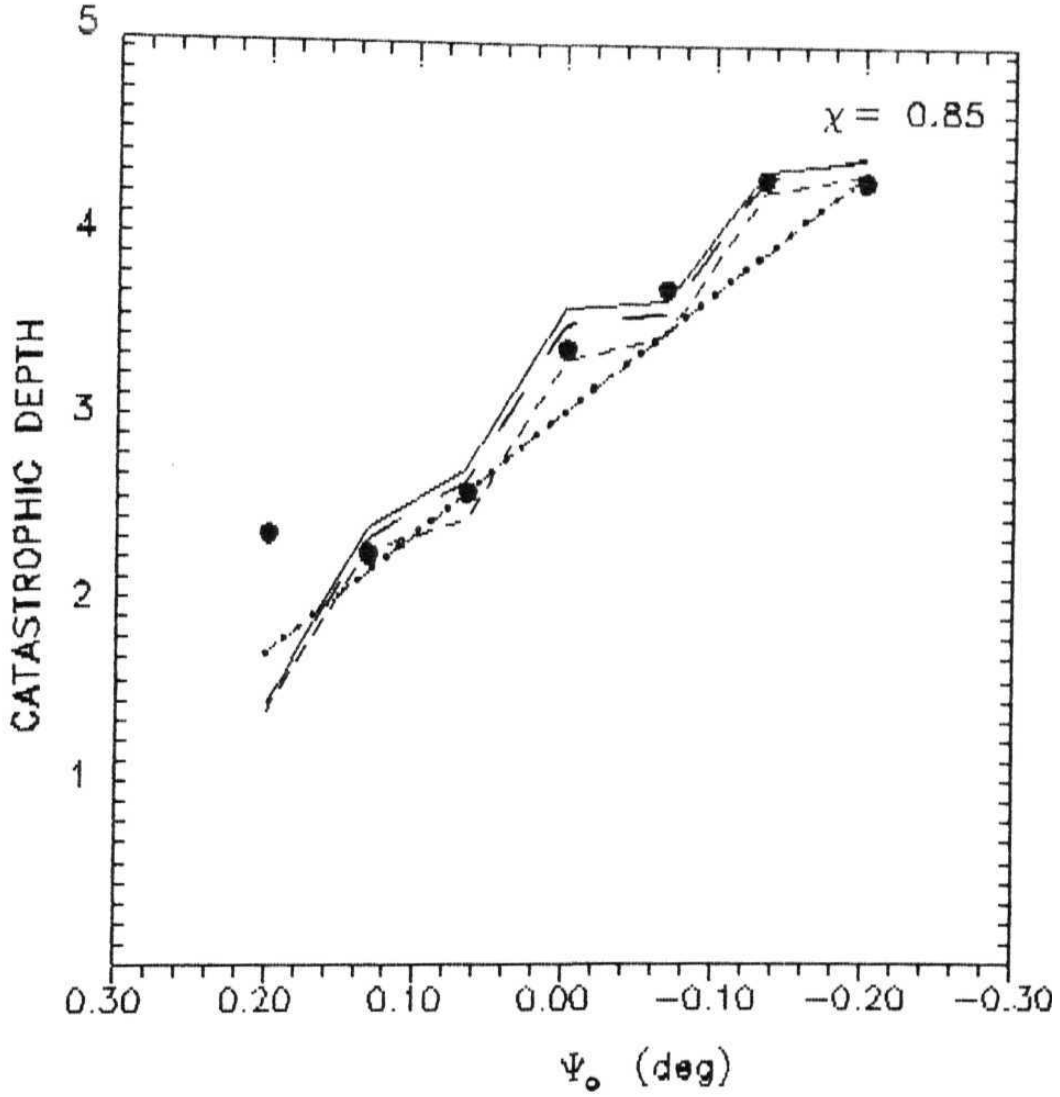

Fig 6.7: ***Catastrophic Dechanneling depth*** **(85 % dechanneled) versus** ***incident angle*** ψ_o **for measured and calculated** ***tilt angle*** **between layers** $\Delta\psi = 0.153°$ **(Ref. 10). (** ***dotted curve*** **) represents calculations using** ***Moliere planar potential,*** **(** ***solid curve*** **) represents calculations using** ***shell planar potential,*** $(\cdot - \cdot)$ **represents calculations using** ***modified harmonic model*** **(** ***dashed curve*** **) represents calculations using** ***Universal planar potential,*** **(** ***solid circles*** **) represents experimental points.**

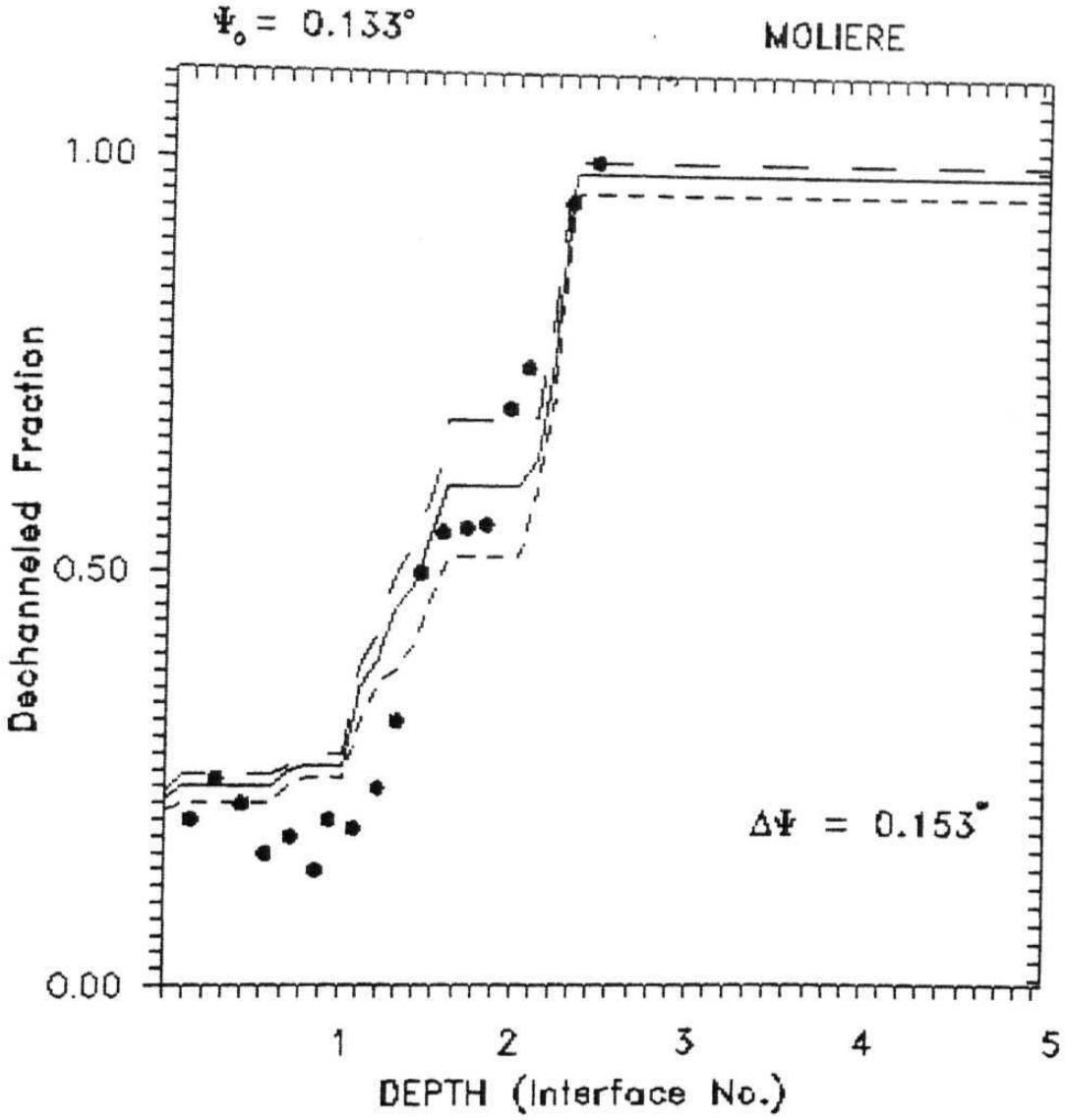

Fig 6.8 (a): Dechanneled fraction for *CDR* for $\psi_0 = 0.133°$ and $\Delta\psi = 0.153°$ impact parameters $r_c = 1.15a_T$ (*dotted curve*), $1.25a_T$ (*solid curve*) and $1.35a_T$ (*dashed curve*) using *Moliere planar potential*. *Solid circles* represent experimental points.

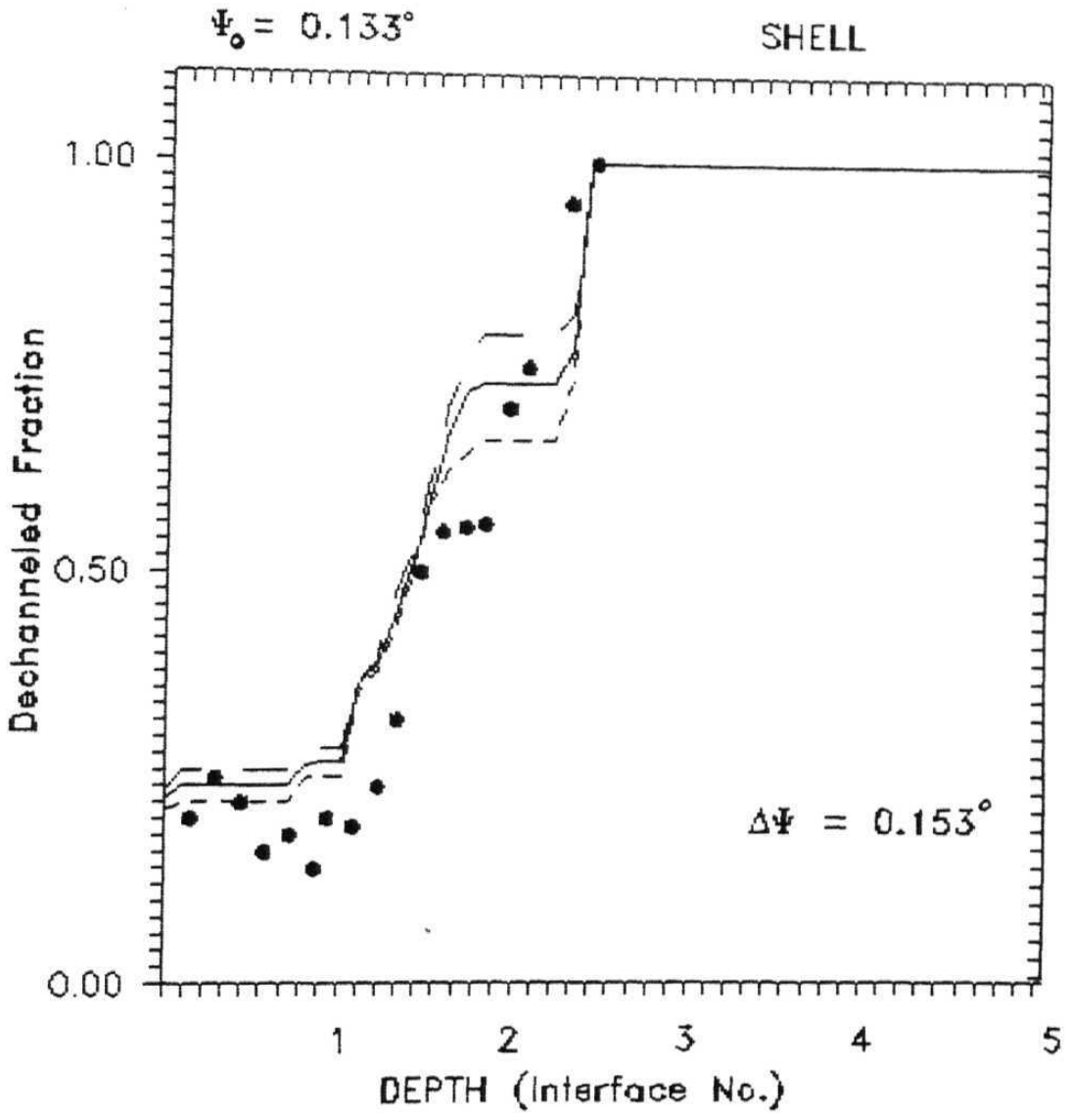

Fig 6.8 (b): **Dechanneled fraction for *CDR* for $\psi_0 = 0.133°$ and $\Delta\psi = 0.153°$ impact parameters $r_c = 1.15a_T$ (*dotted curve*), $1.25a_T$ (*solid curve*) and $1.35a_T$ (*dashed curve*) using *Shell planar potential*. *Solid circles* represent experimental points.**

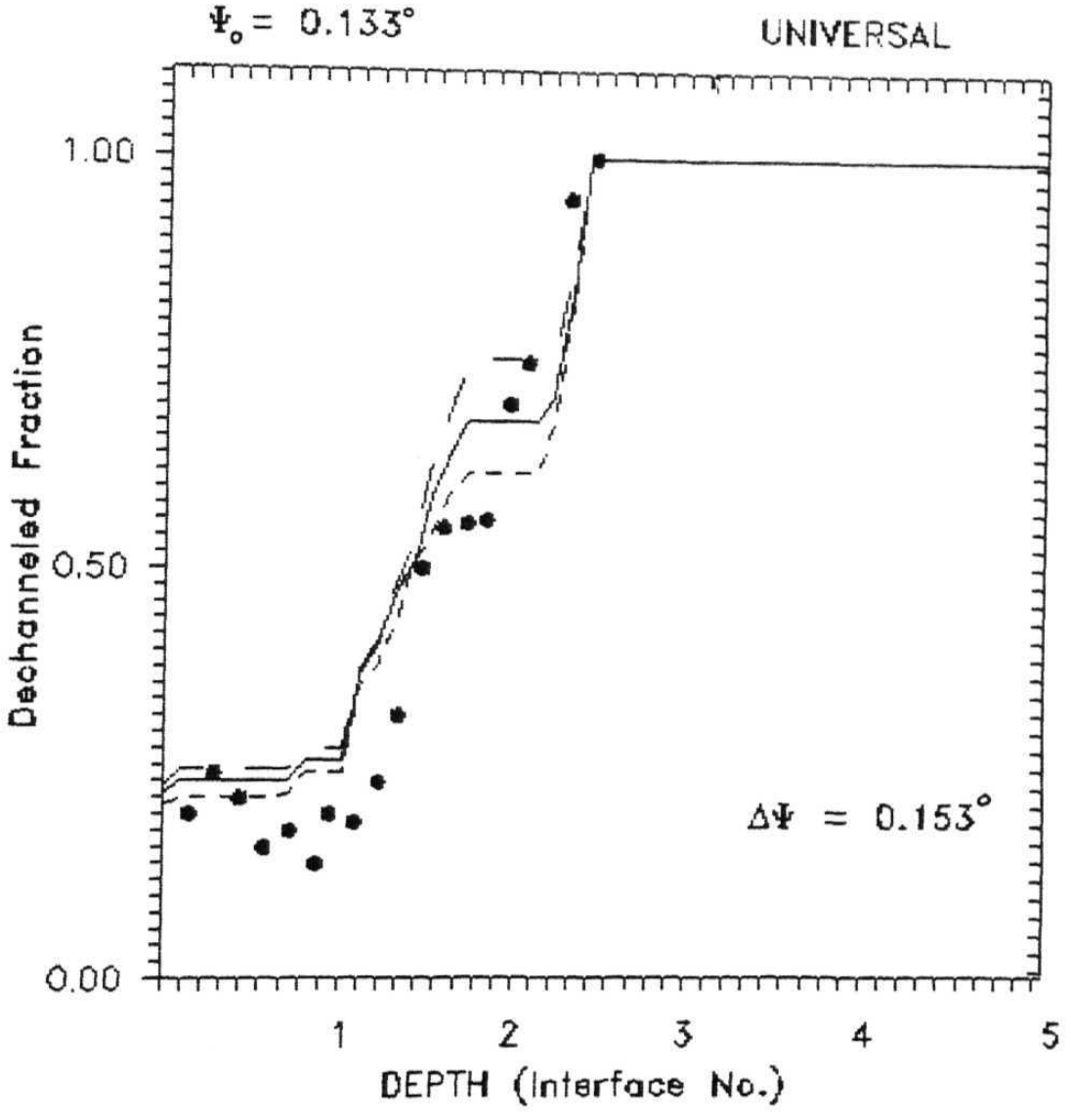

Fig 6.8 (c): Dechanneled fraction for *CDR* for $\psi_o = 0.133°$ and $\Delta\psi = 0.153°$ impact parameters $r_c = 1.15a_T$ (*dotted curve*), $1.25a_T$ (*solid curve*) and $1.35a_T$ (*dashed curve*) using *Universal planar potential. Solid circles* represent experimental points.

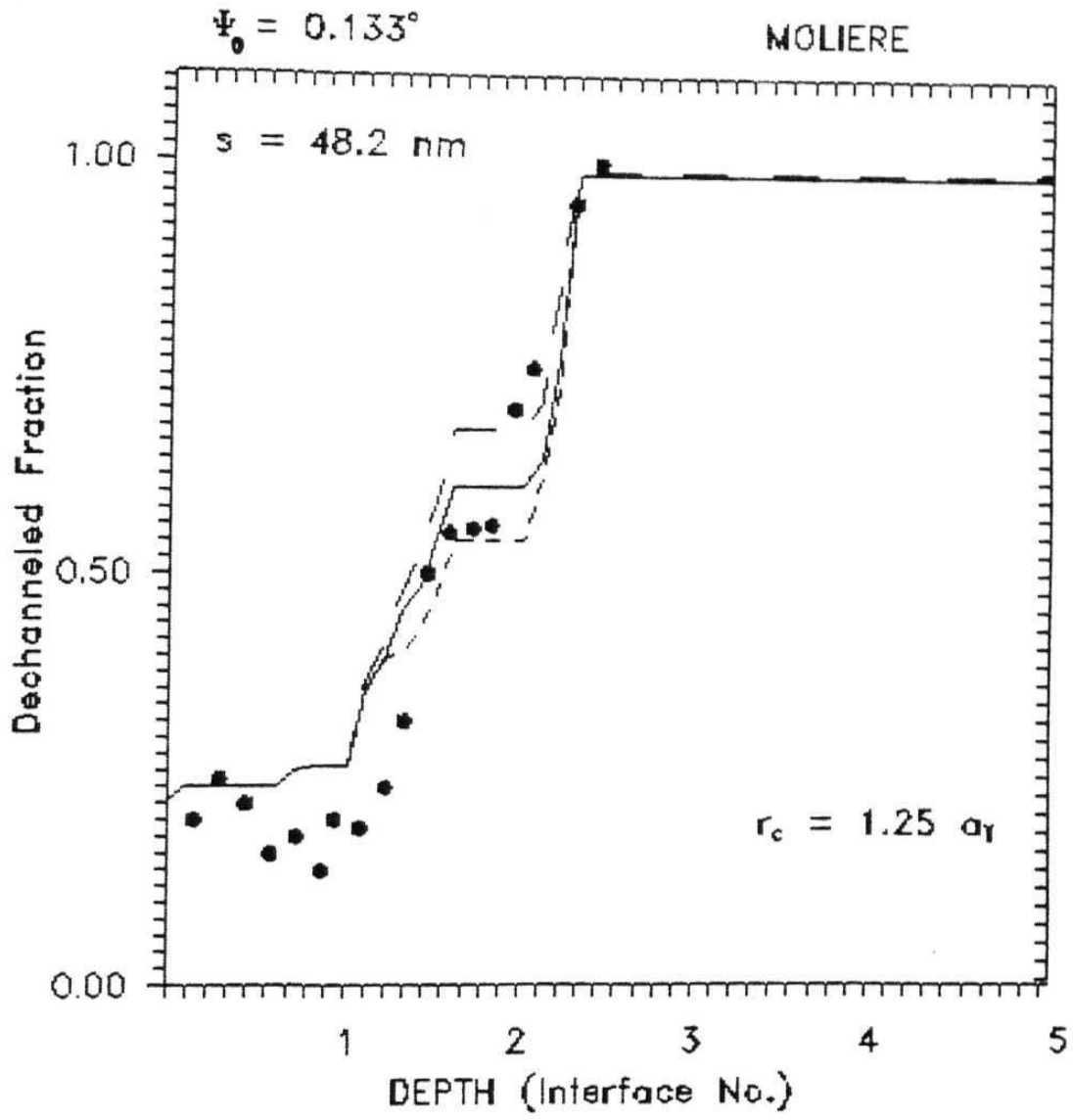

Fig 6.9 (a): **Calculated dechanneling depth profiles for *CDR* for $\psi_0 = 0.133°$ and $r_c = 1.25a_T$ for various strain tilt angle $\Delta\psi = 0.143°$ (*dotted curve*), $0.153°$ (*solid curve*) and $0.163°$ (*dashed curve*) using *Moliere planar potential. Solid circles* represents experimental points.**

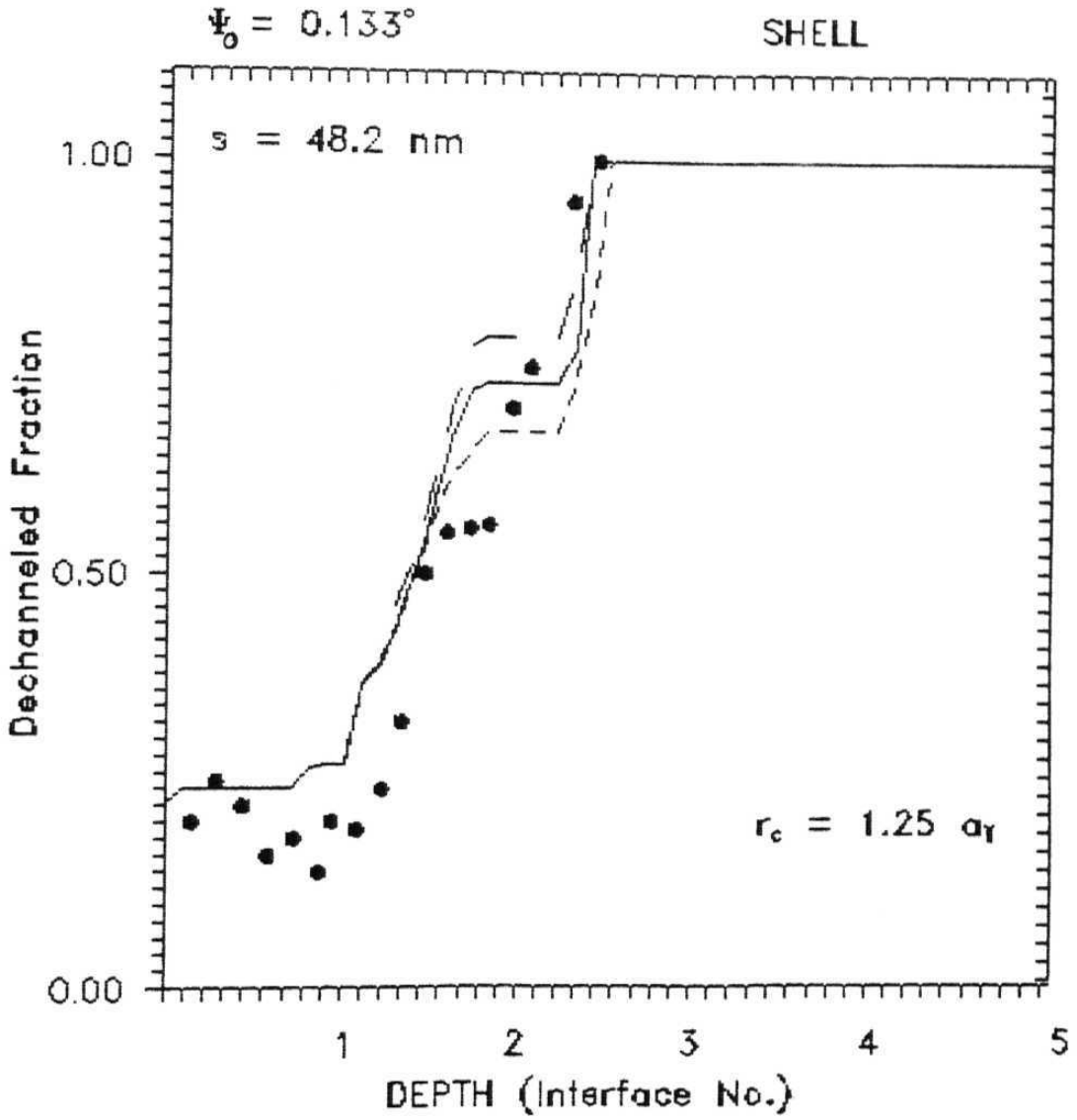

Fig 6.9 (b): **Calculated dechanneling depth profiles for *CDR* for $\psi_o = 0.133°$ and $r_c = 1.25a_T$ for various strain tilt angle $\Delta\psi = 0.143°$ (*dotted curve*), 0.153° (*solid curve*) and 0.163° (*dashed curve*) using *Shell planar potential. Solid circles* represents experimental points.**

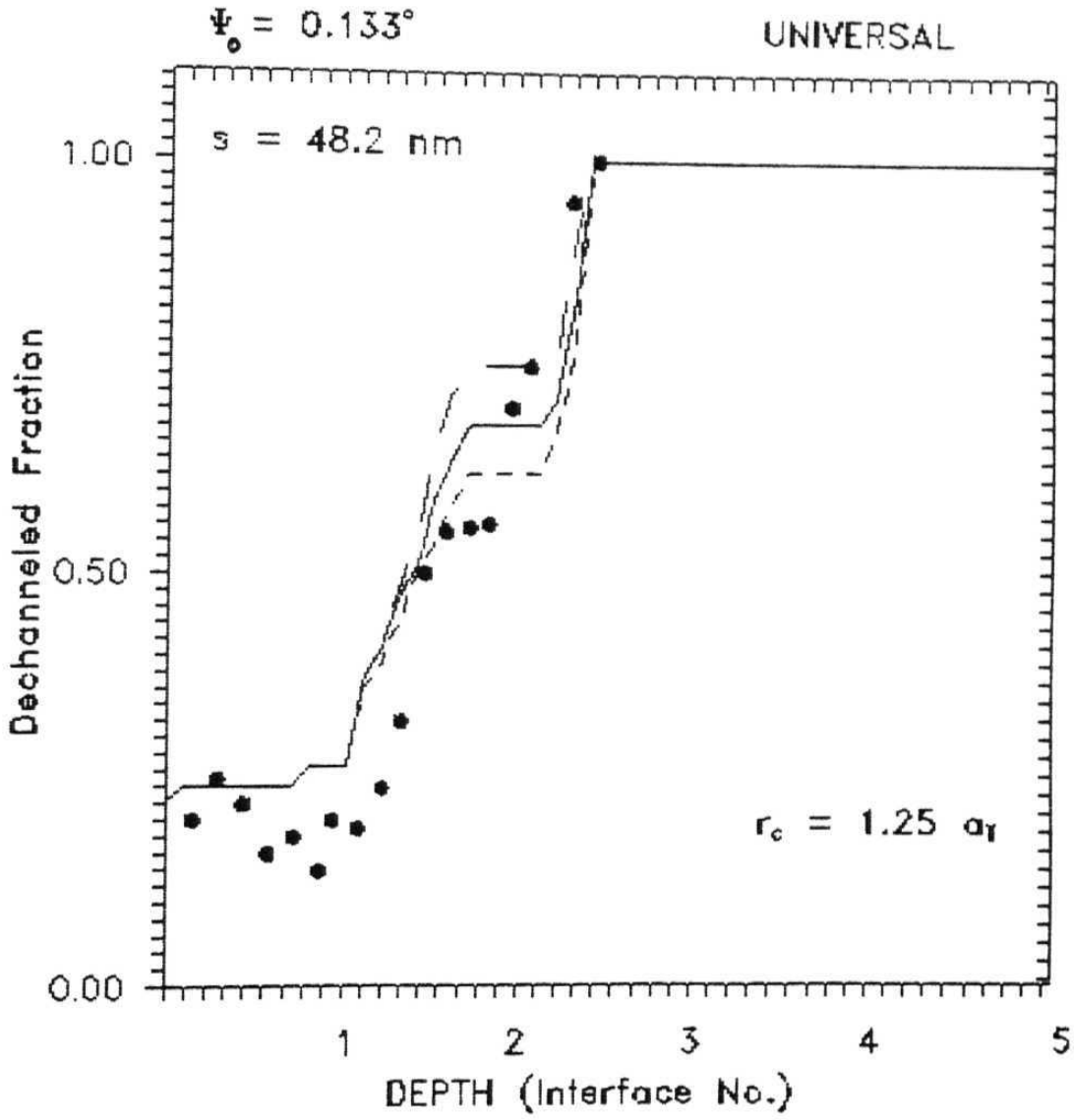

Fig 6.9 (c): **Calculated dechanneling depth profiles for *CDR* for $\psi_o = 0.133°$ and $r_c = 1.25a_T$ for various strain tilt angle $\Delta\psi = 0.143°$ (*dotted curve*), $0.153°$ (*solid curve*) and $0.163°$ (*dashed curve*) using *Biersack's universal planar potential. Solid circles* represents experimental points.

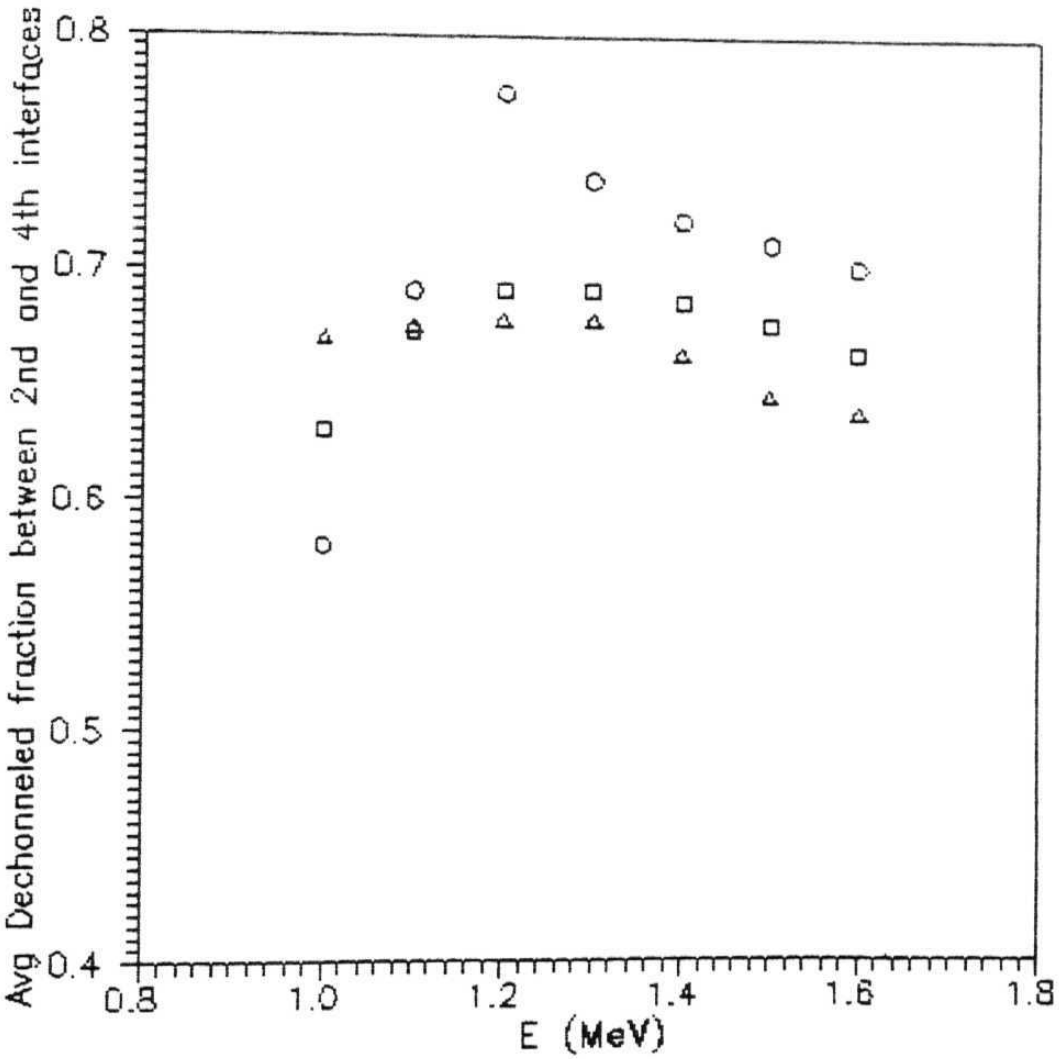

Fig 6.10 Average yield $\bar{x}$ calculated using *Moliere* (o), *Shell* (Δ) and *Biersack's Universal* (□) planar potentials are plotted as a function of *incident energy E*.

Chapter 7

CHANNELING RADIATION

7.1 INTRODUCTION

When charged particles propagating through a medium get accelerated or deccelerated through various physical processes, electromagnetic radiation is emitted. This is a well known fact in *electrodynamics theory.* As mentioned in *Chapter* /, the longitudinal motion of a channeled particle [1,2] is assumed to nearly free particle type motion (neglecting energy losses for short longitudinal distance, compared to particle energy) and only the transverse motion of particles is governed by the continuum transverse potential. The channeled particles execute to and fro oscillatory motion in the transverse space and are accelerated and deccelerated in the process resulting in emission of electromagnetic radiation. Quantum mechanically, the bounded transverse motion in the field of continuum potential is quantized and the spontaneous transition among these levels result in the emission of relevant energy as electromagnetic radiation. The calculated transverse oscillation frequencies ω_o and the corresponding energies are generally very low and the observation of channeling radiation seemed to be impossible because the radiations due to other mechanisms (like *Bremsstrahlung)* are stronger and hence dominate in the same energy range. Later, towards the end of *seventies*, *Kumakhov* realized that when a relativistically fast charged particle is channeled in a crystal, the longitudinal relativistic motion results in Lorentz contraction along the axes or planes so that the strength of

continuum potential is enhanced by a factor γ ($\gamma = 1 / \sqrt{1 - (v^2/c^2)}$). Since the emitted electromagnetic radiation is to be observed in the laboratory frame, the radiation frequency is Doppler shifted in the forward direction by a factor 2γ , so overall enhancement in the frequency, of the order of $2\gamma^2$ results for forward emission [3,4]. Where v is particle velocity and c is velocity of light. The observed frequency is given by $\omega = 2\ \gamma^2\ \omega_o$, where ω_o is the original frequency due to spontaneous transition among the discrete eigenstates supported by the continuum planar or axial potential of the crystal. Experimental verifications of *Kumakhov*'s prediction were followed promptly by the observation of channeling radiation from 56 and 28 *MeV* positrons [5] and electrons [6] channeled along the major crystallographic axis and planes of *silicon* single crystal respectively. Electrons and positrons are of practical interest as projectiles in channeling radiation experiments because classically the the instantaneous radiated power is proportional to acceleration which in turn is inversely proportional to mass of the projectile. Since the potential minima for electrons are at the centre of atomic strings or planes, channeled electrons have maximum probability for hard collision with atoms, contrary to positrons case. The planar potential for positrons can be approximated to harmonic type and frequency is almost independent of amplitude, so the energy levels are equidistant. Due to the negative charge of the electrons they cross the atomic planes during their motion, this results in anharmonic interaction between the electrons and atomic plane which gives nonequidistant energy levels and broad range of oscillation frequencies in the spectrum.

Eventhough channeling radiation occurs at higher energies, the transverse motion of particles can be still described by the usual non-relativistic *Schrödinger* equation. This is because the critical angle ψ_c is inversely proportional to the square root of incident particle energy and consequently the transverse energy $E\psi_c^2$ remains non-relativistic even at high energies. Several theoretical methods using classical and quantum mechanical

treatments for channeling radiation were made and reported during last 15 years or so [8-14].

Most of the initial efforts on channeling radiation work have been towards its application as coherent source as well as to characterize the properties of crystal and channeled particle [15]. The photon energy can be tuned by changing the particle energy. The planar channeling radiation is linearly polarized. At high relativistic particle energies, the observed channeling radiation in the forward direction consists of hard *x rays* or 7 rays concentrated inside a narrow cone of half angle $1/\gamma$. The radiation characteristics (frequency, line width etc) are also functions of crystal structure in addition to particle parameters. It is possible to investigate the imperfections in the crystals, to study various processes like defect formation which results in the dechanneling of channeled particles. So it is important to know the details about the radiation characteristics of channeling radiation emitted from a crystal and we have calculated the characteristics of the radiation emitted from relativistic positrons and electrons channeled along the (110) plane in *Silicon* single crystals using Shell planar potential and discussed in section 7.2 and 7.3 respectively. The effects of dislocations on channeling radiation is discussed in section 7.4 and the applications of channeling radiation are outlined in the last section.

7.2 CHANNELING RADIATION FROM RELATIVISTIC POSITRONS

The positrons move between the crystallographic planes with small amplitude of oscillation and the potential due to the two planes is given by [16,17]

$$Y_2(x) = Y(l - x) + Y(l + x) \qquad (7.1)$$

where / is given by / = $d_p/2$ and x is measured from the halfway point between two planes. We have numerically evaluated equation (7.1) using shell planar potential and curve fitted it to a fourth order polynomial of the form, $Y_2^{poly}(x) = Y_2(0) + (1/2)\ k_1\ x^2$

+ (1/4) k_2 x^4. The coefficients k_1 and k_2 (both are in atomic units) are given by k_1 = 0.354918, k_2 = 0.026305 respectively. Using harmonic approximation for potential and keeping only upto quadratic term the channeling radiation frequency is given by

$$\omega = 2\,\gamma^2\sqrt{\left(\frac{k_1}{m_o\gamma}\right)} \tag{7.2}$$

where m_o is the rest mass of positron. The finite line width due to slightly different energies of the radiation because of the anharmonic effect is calculated using perturbation theory [15] and is determined in terms of a parameter ϵ and is proportional to n_{max}, where $n_{max}$is the maximum number of bound states supported by transverse continuum potential. The transitions are calculated using first order perturbation theory, (This number corresponds to n_{max} = 11 , ϵ = 0.00885612 for γ = 111 and n_{max} = 10, ϵ = 0.00937775 for 7 = 99) .

$$\hbar\omega_{n,n-1} = \frac{\hbar\omega_o}{1-\beta\cos\theta}\,(1+n\epsilon) \tag{7.3}$$

For forward emission *9 = 0* and ϵ is given by

$$\epsilon = \frac{3\,\hbar\,k_2}{4\,k_1^{3/2}\sqrt{m_o\gamma}} \tag{7.4}$$

The spectral peaks were calculated for 56 *MeV* and 50 MeV positrons channeled along (110) plane of *Silicon* single crystal and is compared with experimental results. This is shown in *Table* 7.1..

7.3 CHANNELING RADIATION FROM RELATIVISTIC ELECTRONS

The planar potential experienced by an electron is attractive and can be approximated to a form [17-19]

$$Y(y) = Y_o\,exp(-k|y|) + A$$

where y is the distance from the plane, k is the effective screening length, and A is a constant added, so that energy can be fixed to zero at the midway point between two planes. Solving the *Schrodinger equation* using the above mentioned potential, we get the wave function.

$$\psi_p(y) = J_{\nu_p}\left(Q_o \, exp\left(\frac{-k\,|y|}{2}\right)\right) \tag{7.6}$$

where J_{ν_p} is the *Bessel function* of the first kind and of order ν_p , Q_o and ν_p are respectively given by

$$\begin{aligned} Q_o &= \sqrt{\frac{8\, m_o\, \gamma\, |Y_o|}{k^2\, \hbar^2}} \\ \nu_p &= Q_o \sqrt{\frac{E_p - A}{Y_o}} \end{aligned} \tag{7.7}$$

where m_o is the rest mass of electron, $\hbar$ is the planck constant, E is the energy eigenvalue associated with ψ_p. The continuity condition for both odd and even parity states are imposed as

$$J_{\nu_p}(Q_o) = 0 \quad odd \quad state \tag{7.8}$$

$$\frac{d}{dy} J_{\nu_p}(Q_o) = 0 \quad even \quad state \tag{7.9}$$

The odd and even parity states are derived from (7.8) and (7.9) respectively and the photon energy can be calculated using the relation

$$\hbar\omega_{obs} = 2\,\gamma^2\,\Delta E_p \tag{7.10}$$

where ΔE_p is the difference in eigenvalue for the transition of interest . Equation (7.5) can not provide a good approximation to the potential function when thermal vibration of atoms are considered .The eigen values are calculated using equation (7.5) and the first order perturbation theory has been used to correct these eigen values to account for thermal vibrations of atoms which is dominant near the region y = 0 (i.e close to planes).

The shell planar potential is therefore curve fitted to a function of the form [18]

$$Y(y) = Y_o exp(-ky) + A; \quad for \quad u_1 \leq |y| \leq \frac{d_p}{2} \tag{7.11}$$

$$Y(y) = Y_1 y^2 - B; \quad for \quad |y| \leq u_1 \tag{7.12}$$

where u_1 is the root mean square displacement due to the thermal vibrations. In actual practice the shell planar potential was curve fitted to the function of the form Y_o $exp(-k|y|)$(this is shown in Fig 7.1) and the constant *A* added afterwards so that energy can be normalized to zero at the midway point between two planes. In order to find the value of the parameter *B* we convoluted the fitted potential to write [20]

$$Y_c(y) = \frac{Y_o \, exp(k^2 \, u_1^2/2)}{2}\left(exp(-k|y|) \;\; erfc\left[\frac{1}{\sqrt{2}}\left(ku_1 - \frac{y}{u_1}\right)\right] + exp(k|y|) \;\; erfc\left[\frac{1}{\sqrt{2}}\left(ku_1 + \frac{y}{u_1}\right)\right]\right) \tag{7.13}$$

where $Y_c(y)$ is the convoluted potential and $erfc(y)$ is the complementary error function given by

$$erfc(y) = \frac{2}{\sqrt{\pi}} \int_y^\infty exp(-t^2) \; dt \tag{7.14}$$

The value of convoluted potential for $y = 0$ is taken to be the value of the parameter B, and since the values of parameters Y_o , A, B are known ,the value of the parameter Y_1 can be found out by equating the potential given in (7.11) and (7.12) at $y = u_1$. The spectral peaks were calculated (*Table 7,2*) using equations (7.8) (7.9) and (7.10) respectively for shell planar potential for both 56 *MeV* and 28 *MeV* electrons channeled along (110) direction of silicon single crystal using *IMSL MATH/LIBRARY*™', *IMSL MATH/LIBRARY Special functions*™ and cross checked with *Mathematica*™ software package, and is compared with experimental results. Corresponding eigenvalues were calculated and are shown in Fig.7.2. Here we have used the following values for the parameters Y_o ,*k,A,Y*\ and *B*. Y_o = -27.539568 eV, k = 25.24414 nm^{-1},A =2.440461 eV,Y_1 = 184.55627 × 10^2 eV/nm^2 and B = 21.387006 eV.

7.4 EFFECTS OF DISLOCATIONS

As mentioned in the section 7.1, the channeling radiation can be used to study imperfections in the crystal. The presence of defects in crystals affects channeling phenomena in general and channeling radiation in particular. The effects are of two types. The obstruction effects like those created by point defects, stacking faults etc and distortion effects like those resulting from dislocations. Here we present the study of effects of dislocations on channeling radiation from 56 *MeV positrons* channeled along < 110 > axial channel of *Silicon* single crystals using *Shell axial potential* taking into account the geometry of the < 110 >.

Around a dislocation the atomic rows and planes exhibit curvature which will alter the trajectory of the channeled particle and can dechannel the particle altogether if the curvature is large enough to modify the trajectory.The distortion produced due to the presence of dislocation axis decreases as one moves away from the dislocation axis. So the curvature in channel decreases as its distance *d* from the dislocation axis increases. **Ail** the particles passing through regions where the centrifugal force $2E\pm /R$ (due to distortion) is greater than the restoring force due to the continuum potential will be dechanneled. The axial potential due to all six strings surrounding an < 110 > axial channel of *Silicon* is given by

$$U(r') = U(R_o - r') + U(R_o + r') + 2U(\sqrt{R_o^2 + r'^2 + R_o r'}) + 2U(\sqrt{R_o^2 + r'^2 - R_o r'}) \quad (7.15)$$

where R_o is the radius of the channel, r' is measured from the channel axis and the cross section of < 110 > axial channel has been approximated by a regular hexagon. Thus R_o **is simply taken** as distance between channel axis and one of the strings of regular **hexagon. This is** curve fitted to a polynomial of the form

$$U_S^{poly}(r) = U_o(p_o + p_2 r^2 + p_4 r^4) \quad (7.16)$$

where r' has been replaced by r .The *Schrodinger* equation for transverse motion of a positron channeled along < 110 > axial channel is a two - dimensional harmonic oscillator equation with potential given by equation (7.15). The observed channeling radiation frequency for perfect crystal case is given by [5]

$$\omega_{obs} = 2\,\gamma^{3/2}\sqrt{\frac{2\,U_o\,p_2}{m_o}} \tag{7.17}$$

where m_o is the rest mass of positron. Our calculations are based on *Constant curvature model* (shown in Fig. 7.3.) for dislocation affected channel proposed by *Pathak* [23,24]. The dislocations are assumed to introduce a continuous and constant curvature with radius of curvature R in the channel which is given by

$$R = \frac{2\,\pi^2\,d_o^2}{b\,\cos^3\phi} \tag{7.18}$$

where ϕ is the angle between channel axis and plane perpendicular to the dislocation axis. The half length z_c of curved part of dislocation affected channels situated at a distance d_o from the dislocation of *Burgers* vector b are given by [24],

$$z_c = \frac{\pi\,d_o}{\cos\phi} \tag{7.19}$$

Here we assume that particles are still outside the dechanneling cylinder [25,26] so that the ions do not get dechanneled but their state of motion is appreciably modified due to the curvature of the channels [24]. The assumption of constancy of curvature is valid only for those channels which are not too close to dislocation core. Thus for an initially (i.e., before encountering the dislocation affected channel) well channeled particle the equation of motion becomes [21]

$$m\,\ddot{r} + \frac{dU_S^{poly}}{dr} - \frac{2\,E}{R} = 0 \tag{7.20}$$

second order equation which after integration gives

$$\dot{r} = \sqrt{\left(\frac{2}{m}\right)\left[\,U_S^{poly}(0) - U_S^{poly}(r) + \left(\frac{2E}{R}\right)r\,\right]} \tag{7.21}$$

Because of the additional centrifugal force in the transverse direction,the equilibrium axis shifts from r — 0 to $r = r_o$ given by

$$\frac{2\ E}{R} - \frac{dU_S^{poly}}{dr}\Big|_{r=r_o} = 0 \tag{7.22}$$

The maximum oscillation amplitude r_m gained by particle is given by

$$U_S^{poly}(r_m) - \frac{2\ E}{R}\ r_m = U_S^{poly}(0) \tag{7.23}$$

Substituting the potential (equation 7.16) in equation (7.22) and (7.23), we get cubic equations for r_o and r_m as

$$\begin{aligned} r_o^3 + \frac{p_2}{2p_4}\ r_o - \frac{E}{2\ p_4\ R\ U_o} &= 0 \\ r_m^3 + \frac{p_2}{p_4}\ r_m - \frac{2E}{p_4\ R\ U_o} &= 0 \end{aligned} \tag{7.24}$$

These equations can be solved analytically [27] and positive roots are given by

$$\begin{aligned} r_o &= 2\sqrt{\frac{p_2}{6p_4}}\ sinh\left[\frac{1}{3}\ sinh^{-1}\left(\frac{3\ E\ \sqrt{6p_4}}{2\ R\ U_o\ p_2\ \sqrt{p_2}}\right)\right] \\ r_m &= 2\sqrt{\frac{p_2}{3p_4}}\ sinh\left[\frac{1}{3}\ sinh^{-1}\left(\frac{3\ E\ \sqrt{3p_4}}{R\ U_o\ p_2\ \sqrt{p_2}}\right)\right] \end{aligned} \tag{7.25}$$

For initially well channeled particles the oscillation amplitude r_{amp} gained in *harmonic approximation,* after crossing the dislocation affected channel is given by [24]

$$r_{amp} = \frac{4\ R_o^2\ E\ b}{3\ \pi^3\ d_o^2\ U_o} \tag{7.26}$$

The corresponding change in the period is obtained from the equation of motion in the transverse space

$$\frac{1}{2}m\dot{r}^2 + U_S^{poly}(r) = U_S^{poly}(r_{amp}) \tag{7.27}$$

The period of oscillation for transverse motion is then

$$T = 4 \int_o^{r_{amp}} \frac{dr}{\dot{r}} \tag{7.28}$$

The observed channeling radiation frequency is given by

$$\begin{aligned} \omega_{obs}^d &= \frac{4\pi\gamma^2}{T} \\ &= \omega_{obs} \sqrt{\left[\frac{p_2 + 2r_{amp}^2 p_4}{p_2}\right]} \frac{\pi}{2F\left(r_{amp}/\sqrt{2\, r_{amp}^2 + (p_2/p_4)}\right)} \end{aligned} \tag{7.29}$$

where F is the complete elliptic integral of the first kind. Fractional increase in channeling radiation frequency is given by

$$f = \frac{\omega_{obs}^d - \omega_{obs}}{\omega_{obs}} \tag{7.30}$$

we have calculated the fractional increase in channeling frequency using shell model axial potential for $(r_{amp} = R_o/2)$ and $(r_{amp} = R_o/4)$ and obtained the values 0.286 **and** 0.042 respectively. This means that frequencies increase due to concentration of dislocation.

To the best of our knowledge, the only experiment of this kind, ie, study of crystal defects using channeling radiation was reported by *Park et.al* [28]. The experiment was done in *Diamond* cyrstals and the effects of dislocationlike structures (along (100) planar direction) have indicated an increase in channeling radiation peak frequencies from positrons. The concentration of dislocations was too high in type I diamond crystals. Most of the positrons are dechanneled at high dislocation concentration, moreover at these high dislocation concentrations they interact with each other and one sees formation of dislocation loops. The model presented above is for single noninteracting dislocation, ofcourse the results are quantitatively in right direction namely increase in channeling radiation frequency as observed experimentally. But quantitative comparison

is not possible at this stage. We suggest an experiment of channeling radiation in single crystals with moderate dislocation density of the order of 10^9 / cm^2.

The other area in which channeling radiation can be used as a tool to study the crystal defects and strains is *Semiconductor Superlattices* in general and *Strained Layer Superlattices (SLS)* in particular. As discussed in the last chapter *Catastrophic Dechanneling Resonance* is one of the methods in ion channeling experiments used extensively for this purpose. It has been already theoretically predicted that [29,30] the channeling radiation peak frequency decreases by a factor of $\cos\Delta\psi$ and line width decreases by a larger factor $\cos^2\Delta\psi$ in *SLS* (where $\Delta\psi$ is the tilt at the interface and is a measure of strain). The theory is based on the experimental fact [31] that due to the tilt at successive interfaces, the continuum planar potential is weakened as evidenced by the decrease in the width of channeling dips. Hence if the strains in *SLS*'s become too large (due to increase in layer thickness), they relax to create dislocations resulting in increase of channeling radiation frequencies and line widths. Therefore, one can immediately conclude from channeling radiation experiments, whether or not the misfit defects have been created at the interfaces.

7.5 CONCLUDING REMARKS

The application of channeling phenomena to get monochromatic (and possibly coherent) radiation has essentially revived the interest in coherent radiation sources and their application in Solid State, Nuclear and Atomic Physics [12]. Presently the use of channeling radiation is only of speculative nature [32] and the most exciting and challenging task is **the** realization of the possibility to some how induce a population inversion mechanism to cause the the channeled electrons or positrons to get pumped to higher transverse energy levels. If this can be achieved, either by using a part of the emitted radiation to

re-excite the transverse energy levels or any other way, one can produce a coherent *x my* or 7 ray laser source, tunable by varying the channeled particle energy [30]. As mentioned earlier the radiation characteristics are dependent on the crystal structure, one has to characterize the properties of crystals and study the paramater like *channeling length* [33] etc inside a crystal. Systematic accumulation of channeling radiation data on variety of crystal species has already been reported [33-35]. One can expect that very soon *Channeling Radiation techniques* will emerge as potential alternative to EPR and electron microscopy techniques for the determination of structure and properties of both imperfect and perfect crystals.

References

[1] J. Lindhard *Kgl. Danske. Videnskab. Mat. Fys. Medd.,* 34, No.14, (1965).

[2] A. P. Pathak *Radiat. Eff.*, 61, 1, (1982).

[3] M. A. Kumakhov *Phys. Lett.*, 57, 17, (1976).

[4] M. A. Kumakhov *phys. stat. sol. b,* 84, 41, (1977).

[5] M . J. Alguard, R. L. Swent, R. H. Pantell, B. L. Berman, S. D. Bloom and S. Datz *Phys. Rev. Letters*, 42, 1148, (1979).

[6] R. L. Swent, R. H. Pantell, M. J. Alguard, B. L. Berman, S. D. Bloom and S. Datz *Phys. Rev. Letters*, 43, 1723, (1979).

[7] A. P. Pathak *Phys. Rev,* B 31, 1633, (1985).

[8] M. A. Kumakhov and R. Wedell *phys. stat. sol. b*, 84, 581, (1977).

[9] R. Wedell *phys. stat. sol. b,* 99, 11, (1980).

[10] V. V. Beloshitskii and F. Komarov *Physics. Rep.,* 93, 117, (1982).

[11] J. U. Andersen, E. Bonderup and R. H. Pantell *Ann. Rtv. Nucl. Part. Sci.*, 33, 453, (1983).

[12] A. W. Saenz and H. Uberall (Eds), *Coherent Radiation Sources,* (Springer - Verlag, Berlin), (1985).

[13] R. A. Carrigan Jr., J. A. Ellison (Eds) *Relativistic Channeling,* (NATO AS1 Series Vol. B 165) (Plenum, New York), (1987).

[14] M. A. Kumakhov and R. Wedell *Radiation of Relativistic Light Particles during Interaction with Single Crystals,* (Spektrum Verlag, Berlin), (1991).

[15] R. H. Pantell and M .J. Alguard *J. Appl Phys.*, 50, 798, (1979).

[16] V. Hari kumar and A. P. Pathak *Proc. Internat. Conf. Synchrotron Radiation Sources,* Eds. S. S. Ramamurthi, G. Singh and D. Angal, CAT Indore (India), Page 402, (1992).

[17] V. Hari kumar and A. P. Pathak *phys. stat. sol. b*, **182,** 51, (1994).

[18] R. H. Pantell and R. L. Swent *Appl. Phys Letters*, 35, 910, (1979).

[19] V. Hari kumar and A. P. Pathak *Proc. DAE Solid State Phys. Symp. Tirupati (India)* , 35 C, 163, (1992).

[20] B. R. Appleton, C. Erginsoy and W. M. Gibson *Phys. Rev*, **161,** 330, (1967).

[21] A. P. Pathak and P. K. J. Balagari *J. Appl. Phys*, 60, 955, (1986).

[22] V. Hari Kumar and A. P. Pathak *AIP Conference Proceedings* , **286,** Eds. Vipin Srivastava, Anil. K. Bhatnagar and Donald. G. Naugle (AIP Press, New York), page 255, (1994).

[23] A. P. Pathak *Phys. Rev.*, B 13, 4688, (1976).

[24] A. P. Pathak *Phys. Lett.* ,57 A, 467, (1976).

[25] Y. Quere *Phys. Lett,* **26** A, 578, (1968).

[26] Y. Quere *phys. stat. sol.*, 30, 713, (1968).

[27] J. P. Mckelvey *Amer. J. Phys.* , 52, 269, (1984).

[28] H. Park, R. H. Pantell, R. L. Swent, J. 0. Kephart, B. L. Berman, S. Datz and R. W. Fearick *J. Appl. Phys.*, 55, 358, (1984).

[29] A. P. Pathak and P. K. J. Balagari *J. Appl Phys.* , 48, 1075, (1986).

[30] A. P. Pathak *Atomic and Molecular Physics*, Ed. A. P. Pathak, (Narosa, New Delhi), page 165, (1992).

[31] S. T. Picraux, L. R. Dawson, G. C. Osbourn and W. K. Chu *Nucl. Instrum. Methods*, **218,** 57, (1983).

[32] A. H. S0rensen and E. Uggerhøj *Nature*, 325, No.22, 311, (1987).

[33] J. 0. Kephart, R. H. Pantell, R. L. Berman, S. Datz, H. Park and R. K. Klein *Phys. Rev,* B 40, 4249, (1989).

[34] J. 0. Kephart, R. L. Berman, R. H. Pantell, S. Datz, R. K. Klein and H. Park *Phys. Rev.*, **B**44, 1992, (1991).

[35] H. D. Dulman, R. H. Pantell, J. 0. Kephart, B. L. Berman, H. Park, S. Datz, R. K. Klein, R. L. Swent and Z. -H. Bian *Phys. Rev,* B 48, 5818, (1993).

Spectral feature of planar channeled positrons

Table - 7.1

Crystal plane	Beam energy (MeV)	γ	*Energy of emitted channeling radiation (keV)*		
			E (exp) [5]	E(calc) [15]	E (calc) (present)
110	50	99	36.5 ± 1	33 to 38	32.2 to 34.9
110	56	111	42.5 ± 0.05	38 to 44	38.2 to 41.6

Spectral peaks for planar channeled electrons

Table - 7.2

Crystal plane	Beam energy (MeV)	γ	*Energy of emitted channeling radiation (keV)*		
			E (exp) [6]	*E (Present Results)*	
				with out Thermal correction	with Thermal correction
110	56	111	128	150	121
			94	87	90
			68	71	67
			52	54	55
			42	45	43
	28	56	40	46	39
			25	25	26

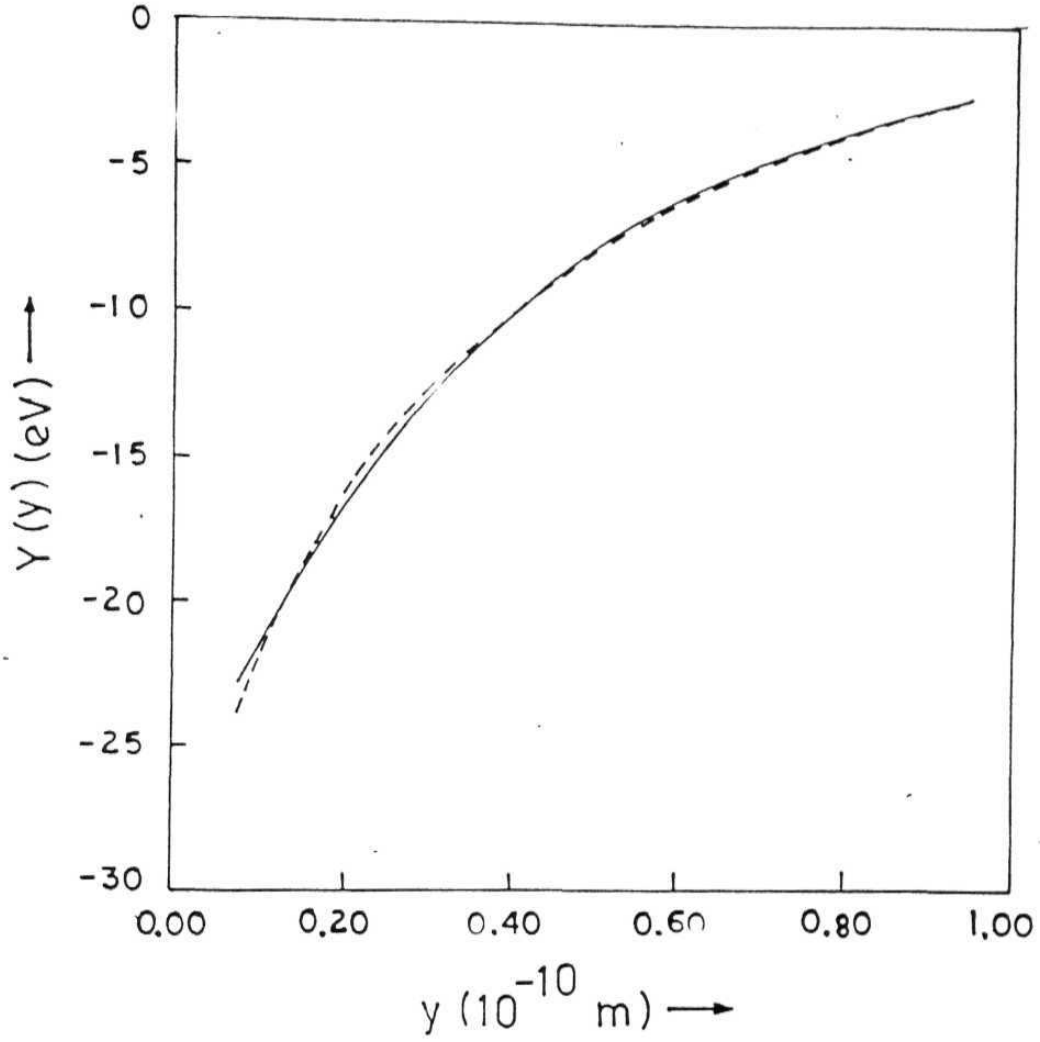

Fig 7.1: The *dashed curve* represents the *shell planar potential* and the *solid curve* represents the *shell planar potential fitted to the form* $Y_o\ exp(-k|y|)$ *in the region* $|y| \leq d_y/2$

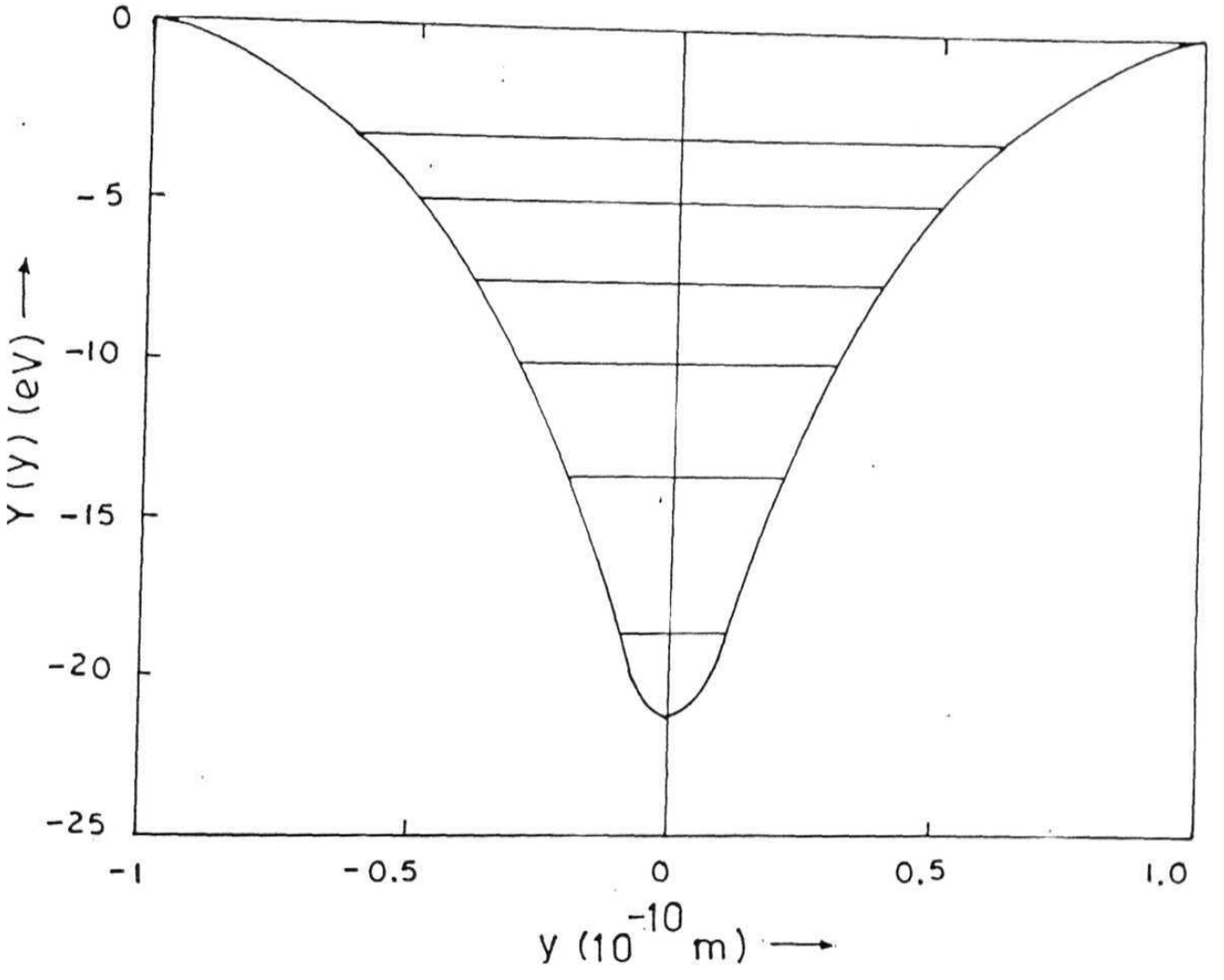

Fig 7.2: *The curve represents the* **shell planar potential** *curve fitted to a function of the form* $Y = Y_o\, exp(-ky) + A$, *the* **eigenvalues** *of this function are shown by horizontal lines.*

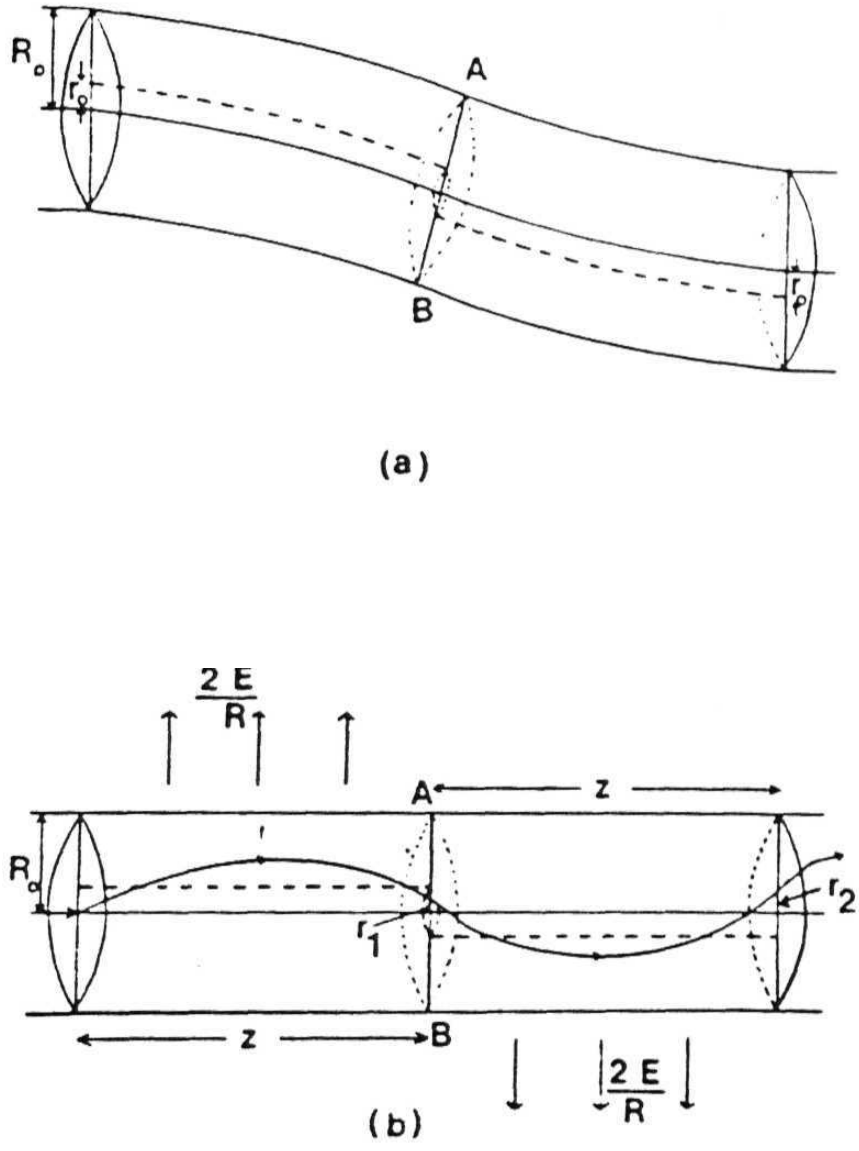

Fig 7.3: **(a)** *A typical channel at some finite distance d_0 from a dislocation.* **(b)** *The model channel replacing the actual channel of the part* **(a)**, *and showing the co-ordinates used in the text. Here R_0 is the distance between the axis of the channel and one of the strings, r_0 is the equilibrium position about which the particle will oscillate and r_1 and r_2 are the positions at which the particle arrives after traversing the first and second parts of the channel, respectively (i.e. left and right to* **AB**, *respectively).* **(Ref [24])**

Chapter 8

CONCLUSION

8.1 SUMMARY OF THESIS

Beginning part of this thesis deals with energy loss measurements in the interesting velocity **range near** the maxima of stopping power versus velocity curve. These measurements were restricted to random situations due to non-availability of *goniometer at* Palletron in *Nuclear Science Centre (N.S.C.), New Delhi.* Corresponding theoretical calculations using different models were performed and compared with experimental results. However, **the major** portion of the work reported in this thesis is mainly concerned with the theoretical calculations on energy losses (random and channeling cases), channeling radiation and effects of dislocations/strains on channeling phenomena. The interatomic potential used in all these calculations is based on the Shell structure potential constructed by using spherically symmetric orbitals obtained by using *Clementi*'sself consistent orbital exponents. These results are compared with those obtained by using other *Thomas Fermi* type potentials. In most of the cases results obtained using shell structure potential are in good agreement with experimental data and the degree of agreement is of the same order as obtained using other statistical type potentials.

The statistical type potentials are useful choice for a rough estimation of the interactions involving heavier atoms, because, when the size of the atom increases its number **of shells and number of** electrons also increase. The accuracy of statistical models also

improves with the increase in number of electrons. At the same time, the computer time needed to handle the shell potentials increases enormously where as it remains more or less constant for statistical potentials. We will elucidate the above mentioned comment with an example of the time of run taken for trajectory simulations of ^4He ions in $GaAs_xP_{1-x}/GaP$. For 200 incident particles with ψ_o = 0.133°, r_c = $1.35a_T$ and $\Delta\psi$ = 0.153°, Shell potential calculations took 27 *hours*, 3 *minutes* and 19 *seconds* (27 : 3 : 19). For Moliere and Biersack's Universal cases, the computation times were just 0:19: 42 and 0 : 20 : 22 respectively. Eventhough the computation time is more in shell potential case, this potential gives a better physical picture of the interactions involving the target and probe beam.

Channeling and its applications were discussed in *chapter 1.* We have done electronic energy loss measurements (random case) using *Elastic Recoil Detection Analysis (ERDA)* method at the *N.S.C., New Delhi, India.* The unique features of *electronic energy loss* measurements using *ERDA* method were discussed in the second chapter. Most of the interatomic potentials used in the *channeling* studies are either of statistical nature or obtained using numerical iteration methods. We have developed *Shell model* charge densities and corresponding *Shell model* potentials which have analytical forms and carry information on detailed distribution of electrons in the atom. We strongly feel that these *shell model potentials* give better physical picture compared to the other *Thomas Fermi* Statistical type potentials. The Shell model potentials were compared with other statistical type potentials and were discussed in *chapter 3.* The calculations using *Shell model charge density* in the position dependence of electronic stopping power in planar and axial cases gave good comparison with the experimental results. This is discussed in *chapter 4.* In *chapter* 5, the Z_1 oscillations in the electronic stopping powers of elements are discussed on the basis of *Briggs-Pathak theory* and shell model charge density is used to calculate the electronic stopping powers of *Silicon* and *Tungsten* for ions ranging from

Z_1 = 6 to Z_1 — 35. Results are in good agreement with experimental data. This gave us the motivation to study various problems like *channeling* in Strained Layer Superlattices and *Channeling Radiation* in semiconductors using the corresponding *Shell continuum potentials.* The results are compared with other theoretical models and experimental results. As expected the calculations using *Shell model potenitals* gave good agreement with experimental results. These calculations were discussed thoroughly in *chapter 6* and *chapter* 7 respectively. Both *Shell model charge densities and potentials* were derived in a phenomenological form which can be used as a potential alternative for numerical computer simulation methods.

8.2 COMMENTS ON POSSIBLE FUTURE WORK

In *chapter 2* we have made only an introduction to our series of ongoing research project of electronic energy loss measurements at *N.S.C., New Delhi, India.* The projectile energy has been chosen in such a manner that the velocity is of the order of 1.0 — 3.0 atomic units of velocity. Only very few experimental data values are available in this low velocity region. As mentioned earlier, it has been theoretically predicted that in the velocity region of 2 — 3 atomic units, the oscillations in the electronic stopping power will damp out. In the future experimental runs, we will cover the energy values corresponding to low velocity region and projectile belonging to the range (Z_1 = 8 — 29), for which we didn't have the data sofar. We also plan to perform channeling experiments, once goniometer becomes available at palletron in *N.S.C. New Delhi.* A theoretical model for random electronic stopping power taking into account of shell structure of target atom is to be developed. The transition from channeling to random case involves breaking of *continuum* approximation and close encounter processes cannot be completely neglected in random situations.

In *Strained Layer Superlattices (SLS)* the tilt at the interfaces were represented by *Dirac Delta function.* Then replacing the *Dirac Delta function* by a smooth function is on the cards and this will tremendously improve the scope of getting an analytical solution to the problems of effects of defects on channeling in *SLS.*

It has been already stated before that many theoretical predictions are not experimentally verified. For example, Only very few experimental data are available for the electronic stopping power region for $1 - 3$ atomic unit of velocities. The other area where the experimental data are very sparse is the possibility of using *Channeling radiation* in the defects and dislocation studies in *Strained layer Superlattices.* Setting up of channeling facility at *Indira Gandhi Centre For Atomic Research, Kalpakkam, India IGCAR* is presently at the preliminary stage, where 400 *KeV* and 2 *MeV* accelerators have already been installed for material science applications. There is also a possibility of installation of channeling facility at *NSC.* Once these channeling facilites become operational, we can do many interesting *channeling* experiments in the areas of *energy loss measurements*, *channeling radiation* and *defect studies in Strained Layer Superlattices*, and verify many of the theoretical predictions.

LIST OF PUBLICATIONS

Papers published in journals

1. 'Shell Structure Potential for Channeling in Solids', by V.Hari kumar and A.P.Pathak *physica status solidi (b),* 177, 269, (1993).

2. 'Z_1 Oscillations in Stopping power of Silicon and Tungsten fox Low Velocity Channeled Heavy Ions', by V.Hari kumar and A.P.Pathak *J.Phys.Condens.Matter,* 5, 3163, (1993).

3. 'Planar Channeling Radiation from Relativistic Elections and Positrons in Silicon' by V.Hari kumar and A.P.Pathak *physica status solidi (b),* 182, 51, (1994).

4. 'Stopping Power of Mylar for ^{16}O and ^{48}Ti Ions', by N.Nath, O.P.Dahaniwal, A.Bhagwat, D.K.Avasthi) V.Hari kumar and A.P.Pathak *Surface and Coatings Technology,* 66, 231, (1994).

5. 'Double Screening Problem in Dechanneling by Point Defects' by A.M.Siddiqui, V.Hari kumar and A.P.Pathak *physica status solidi (b),* 185, 77, (1994).

6 'Stopping Power of Mylar and Carbon', by V.Hari kumar, A.P.Pathak, N.Nath, S.K.Sharma, A.Bhagwat and D.K.Avasthi *Radiation Effects and Defects in Solids,* 132, 211, (1994).

Papers accepted/communicated for publication in journals

1. 'Charged Paricle Probes to Semiconductor Superlattice' by A.P.Pathak and V.Hari kumar *Nuclear Instruments and Methods in Physics Research B.* (in press)

2. 'Study of Catastrophic Dechanneling Resonance in Strained Layer Superlattices using Shell Structure Potential', V. Hari kumar and A. P. Pathak (communicated to *J.Phys.Condens.Matter.*).

Papers published in Conference/Symposium **Proceedings**

1. **V.Hari** kumar, **A.P.Pathak, R.Agnihotri,** Proceedings of DAE Solid State Physics Symposium **1991, Varanasi. (Vol 34C,** page 157)

2. V.Hari kumar aad **A.Pathak,** Proceedings of International Conference on Synchrotron Radiation Sources **1992,** Indore. (page 402).

3. V.Hari kumar and **A.P.Pathak,** Proceedings of DAE Solid State Physics symposium **1992,** Tirupati. (Vol SSC, page 163).

4. V.Hari kumar and A.P.Pathak, Proceedings of DAE Solid State Physics Symposium 1993, Bombay. (Vol 36G, Page 265).

5. V.Hari kumar and A.P.Pathak, American Institute of Physics **Conference Proceedings 286, Ordering** Disorder: Prospect and Retrospect in Condensed Matter Physics, Editors; Vipin **Srivastava,** Anil K. **Bhatnagar** and Donald G.Naugle (page 255).

6. **V.Hari kumar and** A.P.Pathak, **Proceedings of DAE** Solid State **Physics** Symposium 1994, Jaipur. (Vol 37C, page **185).**

7. Stopping Powers of ^{48}Ti, ^{56}Fe and ^{64}Cu ions (Energy Range 0.2 - 1.0 MeV/u) In **Carbon, S.K.Sharma,** Shyam kumar, N.Nath, A.P.Pathak, V.Hari kumar and D.K.Avasthi Proceedings of DAE Nuclear Physics symposium 1994, Bhubaneswar (Vol 37B, page 509).